REPUBLIC OF TÜRKİYE
YILDIZ TECHNICAL UNIVERSITY
GRADUATE SCHOOL OF SCIENCE AND ENGINEERING

OPTIMIZATION OF PROCESS PARAMETERS FOR OUT-OF-AUTOCLAVE THERMOPLASTIC COMPOSITE MANUFACTURING

Sevinç ORMAN

DOCTOR OF PHILOSOPHY THESIS

Department of Chemical Engineering

Program of Chemical Engineering

Supervisor

Prof. Dr. Belma ÖZBEK

Co-Supervisor

Dr. Mustafa DOĞU

February, 2025

REPUBLIC OF TÜRKİYE

YILDIZ TECHNICAL UNIVERSITY

GRADUATE SCHOOL OF SCIENCE AND ENGINEERING

OPTIMIZATION OF PROCESS PARAMETERS FOR OUT-OF-AUTOCLAVE THERMOPLASTIC COMPOSITE MANUFACTURING

A thesis submitted by Sevinç ORMAN in partial fulfillment of the requirements for the degree of **DOCTOR OF PHILOSOPHY** was approved by the committee on 27.02.2025 in the Department of Chemical Engineering, Program of Chemical Engineering.

Prof. Dr. Belma ÖZBEK Yildiz Technical University Supervisor	Dr. Mustafa DOĞU Mir Arastirma ve Gelistirme Inc. Co-supervisor

Approved By the Examining Committee

Prof. Dr. Belma ÖZBEK, Supervisor
Yildiz Technical University _____

Prof. Dr. Kutlu ÜLGEN, Member
Boğaziçi University _____

Prof. Dr. Elçin YILMAZ, Member
Yildiz Technical University _____

Prof. Dr. Aliihsan KOCA, Member
İstanbul Technical University _____

Dr. Öğretim Üyesi Ekin KIPÇAK, Member
Yildiz Technical University _____

I hereby declare that I have obtained the required legal permissions during data collection and exploitation procedures, that I have made the in-text citations and cited the references properly, that I haven't falsified and/or fabricated research data and results of the study and that I have abided by the principles of the scientific research and ethics during my Thesis Study under the title of "Optimization of Process Parameters for Out-of-Autoclave Thermoplastic Composite Manufacturing" supervised by my supervisor, Prof. Dr. Belma ÖZBEK and co-supervisor, Dr. Mustafa DOĞU. In the case of a discovery of a false statement, I am to acknowledge any legal consequence.

Sevinç ORMAN

Signature

Dedicated to my daughter

ACKNOWLEDGEMENTS

I would like to express my deepest gratitude to all the individuals and institutions who contributed to the completion of this thesis. First and foremost, I sincerely thank my supervisor Prof. Dr. Belma ÖZBEK and my co-advisor Dr. Mustafa DOĞU for their invaluable guidance, constant support, and patience throughout this journey. Their mentorship has not only helped me acquire academic knowledge and skills but has also played a key role in shaping my understanding of the research process. I am also grateful to Prof. Dr. Kutlu ÜLGEN and Prof. Dr. Elçin YILMAZ for their valuable contributions and support during the research process.

I would like to extend my heartfelt thanks to my colleagues Hakan ÖZTÜRK, Gülşah ARSLAN, Kübra ATEŞ, Ezgi UÇAR, Reyhan ÖZBAŞ, Gizem ŞIDIM, Pınar KARBUZ, Osmancan ACET, Alihan ARSLAN, and Rüzgar AKSOY for their assistance in the laboratory work, and Burak OĞUZ for his support in analysis studies which were vital to the progress of my research.

My sincere thanks go to Mir Araştırma ve Geliştirme Inc. for their financial and logistical support, which provided me with the necessary resources to advance my research. The opportunities they provided have been instrumental in the development of my work.

Above all, I want to express my deepest gratitude to my daughter, who has been my greatest source of motivation. Her presence and love have given me strength and inspiration. She has made this experience even more meaningful.

Finally, I owe my deepest thanks to my family, friends, and my dear husband for their unwavering moral support, love, and encouragement throughout this challenging process. Their presence has been a source of strength and motivation.

Thank you all.

Sevinç ORMAN

TABLE OF CONTENTS

LIST OF SYMBOLS vii
LIST OF ABBREVIATIONS viii
LIST OF FIGURES ix
LIST OF TABLES xi
ABSTRACT xiii
ÖZET xv
1 INTRODUCTION 17
1.1 Thermoplastic Composites 17
1.1.1 Definition and General Properties 18
1.1.2 Applications of Thermoplastic Composites 21
1.2 Manufacturing Methods for Thermoplastic Composites 22
1.2.1 Hand Lay-up 24
1.2.2 Injection Molding 24
1.2.3 Thermoplastic Pultrusion 25
1.2.4 Thermoforming 25
1.2.5 Compression Molding 25
1.2.6 Autoclave Processing for Composites 26
1.2.7 Out-of-Autoclave Processes 29
1.2.8 Automated Composite Manufacturing: ATL and AFP 29
1.2.9 Filament Winding (FW) 34
1.3 Process Optimization by Response Surface Methodology (RSM) 45
1.4 Finite Element Analysis 49
1.4.1 Fundamental Principles of FEA 49
1.4.2 Applications of FEA in Composite Manufacturing 50
1.5 Motivation of the Thesis 50
2 MATERIALS AND METHODS 52
2.1 Materials 52
2.2 Method 53

2.3 Preliminary Studies on a Basic AFP 53
2.3.1 Heater Replacement 56
2.3.2 Scale-Up Studies 59
2.4 Process Optimization on Filament Winding (FW) 61
2.5 Autoclave Processing 66
2.6 Characterization Studies 68
2.7 Finite Element Method (FEM) 70
3 RESULTS AND DISCUSSIONS 73
3.1 Materials 73
3.2 Preliminary Studies on a Basic AFP 76
3.2.1 Heater Replacement 79
3.2.2 Scale-Up Studies 84
3.3 Process Optimization of Filament Winding (FW) 86
3.3.1 Segmented Mandrel 86
3.3.2 Solid Mandrel 95
3.3.3 Production at the Optimum Point of FW Process 111
3.4 Finite Element Method (FEM) 115
4 CONCLUSION 119
REFERENCES 121
PUBLICATIONS FROM THE THESIS 128

LIST OF SYMBOLS

X_C	Crystallinity
ρ_c	Composite Density
ρ	Density
ρ_f	Fiber Density
T_g	Glass Transition Temperature
ΔH_f	Heat of Fusion
T_H	Heater Temperature
T_m	Melting Temperature
P	Pressure
P_R	Roller Pressure
ρ_t	Theoretical Density
T	Temperature
V_V	Void Content
v	Winding Speed
W_r	Weight Percentage of Resin
W_f	Weight Percentage of Fiber

LIST OF ABBREVIATIONS

AFP	Automated Fiber Placement
ATL	Automated Tape Laying
ATP	Automated Tow Placement
CF	Carbon Fiber
CFRP	Carbon Fiber-Reinforced Plastics
DOE	Design of Experiments
DSC	Differential Scanning Calorimeter
FEM	Finite Element Method
FEA	Finite Element Analysis
FW	Filament Winding
GF	Gass Fiber
GFRP	Glass Fiber-Reinforced Plastics
ILSS	Interlaminar Shear Strength
OOA	Out-Of-Autoclave
PA66	Polyamide 6,6
PP	Polypropylene
PPS	Polyphenylene Sulfide
RSD	Relative Standard Deviation
RSM	Response Surface Methodology
SEM	Scanning Electron Microscope
TDS	Technical Data Sheet
TGA	Thermogravimetric Analyzer
TPC	Thermoplastic Composite

LIST OF FIGURES

Figure 1.1 Material forms of thermoplastic composites 19
Figure 1.2 Impregnation techniques of thermoplastic composites 23
Figure 1.3 Illustration of automated tow placement 30
Figure 1.4 The thermoplastic filament winding process 35
Figure 1.5 Various filament winding methos; (a) robotic, (b) coreless, and (c) spatial winding 36
Figure 1.6 Thermoplastic filament winding system (a) scheme, (b) process 37
Figure 1.7 Different heating methods used in FW and their thermal expansions. 39
Figure 1.8 Fundamental structure of a process or system 46
Figure 1.9 (a) A three-dimensional response surface graph, (b) contour plot 47
Figure 1.10 A Box-Behnken design for three factors 49
Figure 2.1 Methodology of the thesis 53
Figure 2.2 Lab-scale AFP system 54
Figure 2.3 The heater used in FW and AFP systems 56
Figure 2.4 Schematic of the AFP system used in this study 57
Figure 2.5 Schematic of filament winding system 59
Figure 2.6 Filament winding system (a) front view, (b) side view 59
Figure 2.7 The winding pattern created in CADWIND® software 60
Figure 2.8 Flowchart of the process optimization methodology 61
Figure 2.9 Segmented mandrel; (a) overview, (b) sectional view 64
Figure 2.10 Solid mandrel (a) design, (b) mounted on FW system 65
Figure 2.11 Compression test 65
Figure 2.12. Autoclave cycle of GF/PPS (V for vacuum in bar, P for pressure in bar, T for temperature in °C) 66
Figure 2.13. Autoclave cycle parameters of GF/PA66 (V for vacuum in bar, P for pressure in bar, T for temperature in °C) 67
Figure 2.14. Autoclave cycle parameters of GF/PP (V for vacuum in bar, P for pressure in bar, T for temperature in °C) 67
Figure 2.15 Composite structure and test sampling 68

Figure 2.16 The direction of the force in FEA for GF/PPS, GF/PP, and GF/PA66 composites by ANSYS ® 70

Figure 2.17 Finite element mesh of filament-wound composites (ANSYS ®) 71

Figure 3.1 Tensile test samples (a) before and (b) after the test 74

Figure 3.2 Temperature profile of the 1st layer laying during Experiment-1 80

Figure 3.3 Temperature profile of the 2nd layer laying during Experiment-1 81

Figure 3.4 Temperature profile of the 3rd layer laying during Experiment-1 81

Figure 3.5 Temperature profile of the 1st layer laying during Experiment-2 82

Figure 3.6 Temperature profile of the 2nd layer laying during Experiment-2 83

Figure 3.7 Temperature profile of the 3rd layer laying during Experiment-2 83

Figure 3.8 GF/PPS composite produced by filament winding process 85

Figure 3.9 Segmented mandrel; (a) gaps between pieces, (b) triangle edges 94

Figure 3.10 Filament-wound composites 95

Figure 3.11 Predicted vs. actual compressive loads of the composites 105

Figure 3.12 The effects of pressure and temperature on the compressive load of GF/PPS composites produced by FW 106

Figure 3.13 The effects of winding speed and temperature on the compressive load of GF/PPS composites produced by FW 107

Figure 3.14 The effects of pressure and winding speed on the compressive load of GF/PPS composites produced by FW 108

Figure 3.15 The effects of pressure and temperature, on the compressive load of GF/PP composites produced by FW 109

Figure 3.16 The effects of winding speed and temperature on the compressive load of GF/PP composites produced by FW 109

Figure 3.17 The effects pressure and winding speed on the compressive load of GF/PP composites produced by FW 110

Figure 3.18 Side view of GF/PP composite 114

Figure 3.19 Side view of GF/PPS composite 115

Figure 3.20 Reaction force of PP composites 116

Figure 3.21 Reaction force of PPS composites 116

Figure 3.22 Reaction force of PA66 composites 117

LIST OF TABLES

Table 1.1 Comparison of thermoset and thermoplastic polymers.....18

Table 1.2 Properties of some important fibers used to reinforce thermoplastics..20

Table 1.3 Different types of fiber reinforced composites and their applications in automotive.....22

Table 1.4 Different axes in FW.....40

Table 1.5 A three-variable Box-Behnken design.....48

Table 2.1 The properties of GF/PP, GF/PPS, and GF/PA66 composite tapes.....52

Table 2.2 The coded process parameters 54

Table 2.3 Box–Behnken experimental design used in the production of GF/PPS composite panels.....55

Table 2.4 Properties of the heater used in Filament Winding (FW) and 56

Table 2.5 Abbreviations used in the temperature investigation study 58

Table 2.6 Temperature change investigation studies 59

Table 2.7 Roller pressure and compaction force.....60

Table 3.1 Thermal properties of GF/PP, GF/PPS, and GF/PA66 tapes.....73

Table 3.2 Tensile test results of the composites produced by the autoclave process 74

Table 3.3 ILSS test results of the composites produced by the autoclave process 75

Table 3.4 Impact test results of the composites produced by the autoclave process 75

Table 3.5 Three-point bending test results of the composites produced by the autoclave process 76

Table 3.6 Experimental design of GF/PPS composites for process optimization in the AFP system 77

Table 3.7 Regression statistics of GF/PPS composites according to ILSS results78

Table 3.8 ANOVA results of GF/PPS composites according to ILSS results 78

Table 3.9 Regression statistics of GF/PPS composites according to impact test results 79

Table 3.10 ANOVA results of GF/PPS composites according to impact test results 79

Table 3.11 Maximum temperature in AFP laying during Experiment-1 80

Table 3.12 Maximum temperature in AFP laying during Experiment-2 82

Table 3.13 Filament winding process conditions and ILSS test results of GF/PPS composites..... 85

Table 3.14 Preliminary studies of GF/PPS composites 86

Table 3.15 Preliminary studies of GF/PA66 composites 87

Table 3.16 Preliminary studies of GF/PP composites..... 88

Table 3.17 Experimental design factors and levels of GF/PPS composites 88

Table 3.18 Box Behnken experimental design and compression test results of GF/PPS composites..... 89

Table 3.19 Experimental design factors and levels of GF/PP composites..... 90

Table 3.20 Box Behnken experimental design and compression test results of GF/PP composites..... 91

Table 3.21 Experimental design factors and levels of GF/PA66 composites 92

Table 3.22 Box Behnken experimental design and compression test results of GF/PA66 composites 93

Table 3.23 Box-Behnken experimental design for GF/PPS composites..... 96

Table 3.24 Box-Behnken experimental design for GF/PP composites..... 97

Table 3.25 Box-Behnken experimental design for GF/PA66 composites 98

Table 3.26 ANOVA results of GF/PPS experimental design 99

Table 3.27 ANOVA results of GF/PP experimental design 100

Table 3.28 ANOVA results of GF/PA66 experimental design..... 101

Table 3.29 Coefficient estimation of the quadratic model of GF/PPS experimental design 102

Table 3.30 Coefficient estimation of the quadratic model of GF/PP experimental design 102

Table 3.31 Sum of differences between predicted and actual compressive loads of GF/PPS composites..... 104

Table 3.32 DSC test results of the composites produced by FW..... 112

Table 3.33 Density and void content of the composites produced by FW at the optimum process conditions 113

Table 3.34 Comparison of compressive load results between Filament Winding (FW) experiments and Finite Element Analysis (FEA)..... 117

ABSTRACT

Optimization of Process Parameters for Out-of-Autoclave Thermoplastic Composite Manufacturing

Sevinç ORMAN

Department of Chemical Engineering
Program of Chemical Engineering
Doctor of Philosophy Thesis

Supervisor: Prof. Dr. Belma ÖZBEK
Co-supervisor: Dr. Mustafa DOĞU

The development and process optimization of composite materials plays a crucial role in the advancement of manufacturing techniques for high-performance structures in various industries. This research focuses on the process optimization of the filament winding for producing glass fiber-reinforced polypropylene (GF/PP), glass fiber-reinforced polyphenylene sulfide (GF/PPS), and glass fiber-reinforced polyamide 6,6 (GF/PA66). These materials were selected due to their diverse melting temperature and promising properties for aerospace, automotive, and other high-performance applications.

A Box-Behnken experimental design was employed to optimize the process parameters (heater temperature, roller pressure, and winding speed) and evaluate their effects on the compressive load of the composites.

Mathematical models were developed to quantify the impact of each parameter, and optimal processing conditions were identified across a wide temperature range. The results revealed that the optimized processes significantly improved the performance and reliability of filament winding for various thermoplastic

applications. Specifically, the study showed that GF/PPS composites achieved a compressive load of 3357 N, while GF/PP composites reached 2946 N under optimized conditions. However, the optimization of the filament winding process for GF/PA66 composites did not yield satisfactory results and requires further investigation.

Additionally, the study employed the Finite Element Method (FEM) to simulate the composite behavior and validate the filament winding process. The computational modeling provided a robust comparison with the experimental results from the compression tests, confirming the reliability of filament winding as an effective thermoplastic composite manufacturing technique.

Keywords: Filament winding, thermoplastic composites, glass fiber reinforced composites (GFRC), polypropylene (PP), polyphenylene sulfide (PPS), polyamide 6,6 (PA66), process optimization, Box-Behnken, finite element method (FEM)

ÖZET

Otoklav Dışı Termoplastik Kompozit Üretimi İçin Proses Parametrelerinin Optimizasyonu

Sevinç ORMAN

Kimya Mühendisliği Anabilim Dalı
Kimya Mühendisliği Programı
Doktora Tezi

Danışman: Prof. Dr. Belma ÖZBEK

Eş-Danışman: Dr. Mustafa DOĞU

İleri düzey yapısal uygulamalar için üretim tekniklerinin geliştirilmesinde kompozit malzemelerin proses optimizasyonu önemli bir rol oynamaktadır. Bu araştırma, cam elyaf takviyeli polipropilen (GF/PP), cam elyaf takviyeli polifenilen sülfid (GF/PPS) ve cam elyaf takviyeli poliamid 6,6 (GF/PA66) üretimi için elyaf sarma prosesinin optimizasyonuna odaklanmaktadır. Bu malzemeler, farklı erime sıcaklıkları ve havacılık, otomotiv ve diğer yüksek performanslı uygulamalar için gelecek vadeden özellikleri nedeniyle seçilmiştir.

Proses parametrelerini (ısıtıcı sıcaklığı, merdane basıncı ve sarma hızı) optimize etmek ve bu parametrelerin kompozitlerin basma yükü üzerindeki etkilerini değerlendirmek için Box-Behnken deneysel tasarımı kullanılmıştır.

Her parametrenin etkisi nicelendirilerek matematiksel modeller geliştirilmiş ve geniş bir sıcaklık aralığında optimum proses koşulları belirlenmiştir. Sonuçlar,

optimize edilen proseslerin, elyaf sarma işleminin çeşitli termoplastik uygulamalar için performansını ve güvenilirliğini önemli ölçüde artırdığını göstermiştir. Özellikle, araştırma, GF/PPS kompozitlerinin optimize edilen koşullar altında 3357 N'lik bir basma yüküne ulaştığını, GF/PP kompozitlerinin ise 2946 N'ye kadar çıktığını ortaya koymuştur. Ancak, GF/PA66 kompozitleri için elyaf sarma sürecinin optimizasyonu tatmin edici sonuçlar vermemiştir ve daha fazla inceleme gerektirmektedir.

Ayrıca, çalışmada, kompozit davranışını simüle etmek ve elyaf sarma sürecini doğrulamak için Sonlu Elemanlar Yöntemi (FEM) kullanılmıştır. Hesaplamalı modelleme, basma testlerinden elde edilen deneysel sonuçlarla güçlü bir karşılaştırma sunarak, elyaf sarmanın etkili bir termoplastik kompozit üretim tekniği olarak güvenilirliğini doğrulamıştır.

Anahtar kelimeler: Elyaf sarma, termoplastik kompozitler, cam elyaf takviyeli kompozitler (GFRC), polipropilen (PP), polifenilen sülfid (PPS), poliamid 6,6 (PA66), proses optimizasyonu, Box-Behnken, sonlu elemanlar yöntemi (FEM).

1
INTRODUCTION

1.1 Thermoplastic Composites

Composite materials combine the strengths of fibers and matrices to achieve properties unattainable individually [1]. Thermoplastics are distinguished by their toughness, recyclability, and chemical resistance, along with their ability to be reshaped at various temperatures without curing, unlike thermosets. However, their high viscosity poses challenges for composite processing [2], [3], [4], [5], [6].

Advancements in automation and material systems have made thermoplastic composites increasingly viable, offering faster processing, lower energy consumption, and improved efficiency compared to thermosets. Key benefits include an indefinite shelf life, recyclability, and reusability of production waste, aligning with sustainable practices. These properties drive their adoption in aerospace, automotive, and industrial applications [7].

Glass and carbon fiber-reinforced polymer composites have become the preferred materials for improving performance while reducing weight and costs in military aircraft, general aviation planes, transport aircraft, and space launch vehicles. Numerous organizations globally are exploring these advanced materials. Today's modern transport aircraft, such as the Boeing 787, Airbus A320-340, and A350-XWB, utilize high-performance composites for large structural parts like the fuselage, wings, and empennage. These components, made of laminated carbon fiber in a thermoset polymer matrix, are typically cured in autoclaves under precise temperature and pressure cycles to ensure exceptional quality [8].

1.1.1 Definition and General Properties

Composite materials consist of three main components: a matrix, reinforcement, and optional additives. The matrix provides structural integrity and facilitates stress transfer, while reinforcements, such as glass or carbon fibers, enhance the material's strength, crack resistance, and durability. Additives further improve the interphase properties between the matrix and the reinforcement. Polymer matrices are broadly classified into two categories: thermosetting and thermoplastic. A comparison of the properties of their properties are presented in Table 1.1. Thermoset polymers form rigid, three-dimensional structures upon curing. While they offer excellent structural stability, they are non-recyclable. In contrast, thermoplastic polymers are recyclable, tougher, and resistant to moisture and chemicals. However, their higher cost and increased processing expenses, due to the need for melting, are notable drawbacks.

Table 1.1 Comparison of thermoset and thermoplastic polymers [9]

	Thermosets	**Thermoplastics**
Advantages	• Low viscosity enables efficient fiber wetting • Forms strong and durable chemical bonds • Highly resistant to chemicals	• Fast and efficient processing • Recyclable and can be reshaped • Does not require curing • Resistant to moisture and harsh environments
Disadvantages	• Brittle and prone to cracking • Cannot be recycled nor reshaped • Requires curing	• High melt viscosity makes processing more challenging • Weaker adhesive bonding compared to thermosets
Construction method	• Resin transfer molding • Filament winding • Pultrusion	• Injection molding • Compression molding • Extrusion

As described in Figure 1.1, thermoplastic matrix composites are divided into two main categories: continuous and discontinuous fiber reinforced thermoplastics. Unidirectional tape, woven prepreg, and other forms such as braided prepregs are continuous fiber reinforced thermoplastics. Discontinuous fiber reinforced thermoplastics are further classified as long fiber reinforced thermoplastics (LFT) and short fiber filled thermoplastics. Both types undergo processes such as thermoforming, injection molding, compression molding, extrusion, etc. These operations result in the production of the end product [4].

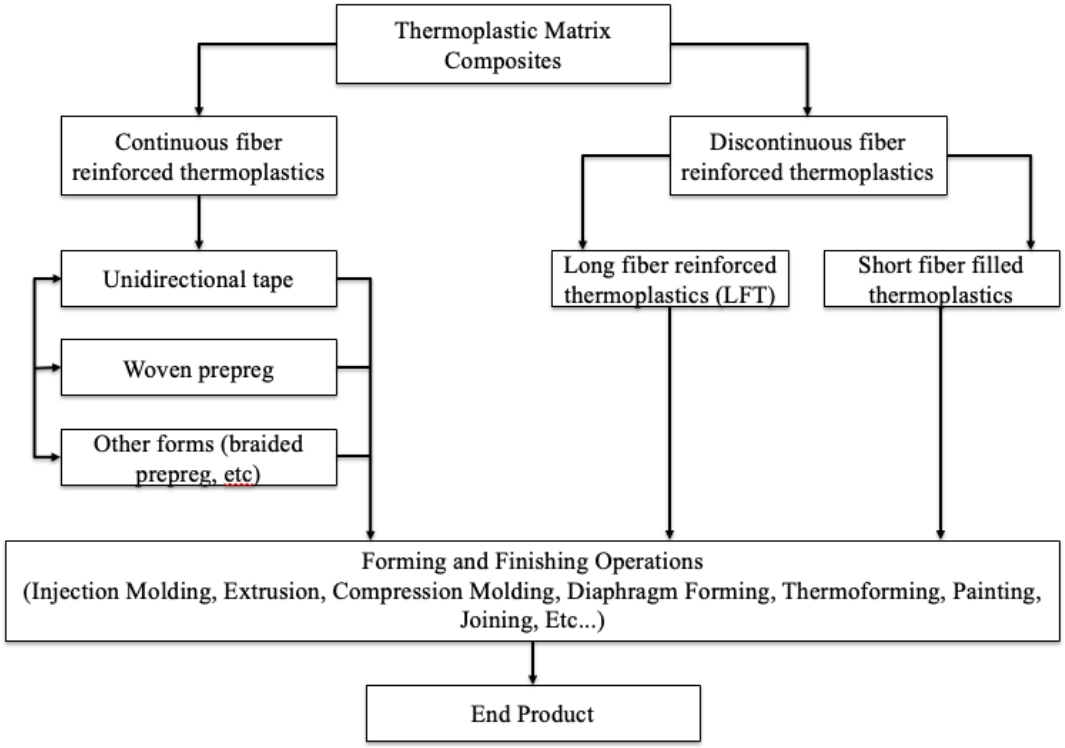


Figure 1.1 Material forms of thermoplastic composites [4]

Composites are favored for their corrosion resistance, thermal stability, and design flexibility. Despite challenges in achieving cost-effective surface finishes, they offer advantages in manufacturing, repair, and recyclability. Techniques like filament winding and molding have reduced fabrication costs, making composites an economical and sustainable choice for various applications [10].

Reinforcement fibers are crucial for providing strength and rigidity to composite materials, enabling them to withstand structural strain. Synthetic fibers, like glass fibers, dominate the market due to their high strength and impact resistance but lack recyclability. In contrast, natural fibers are eco-friendly, lightweight, and

biodegradable but have inconsistent quality, higher moisture absorption, and lower mechanical performance [11].

A fiber is a material characterized by a long axis that is significantly greater than its diameter, often described using its aspect ratio (length-to-diameter), which is typically greater than 100. A filament, the smallest unit of fibrous material, is produced through a single hole during the spinning process and is considered synonymous with fiber [12]. The properties of some important fibers used to reinforce thermoplastics are given in Table 1.2.

Table 1.2 Properties of some important fibers used to reinforce thermoplastics [4]

Material (Fiber)	**Tensile Modulus (GPa)**	**Tensile Strength (GPa)**	**Compressive Strength (GPa)**	**Density (g/cm^3)**
E-glass	70	1.5–2.5	-	2.5
S-glass	90	4.5	>1.1	2.46
Carbon P 100 (pitch-based)	725	2.2	0.48	2.15
Carbon M60J (PAN-based)	585	3.8	1.67	1.94
Nylon 6	1.0	0.1	0.1	1.14

Designing fiber-reinforced polymer composites is more complex than designing isotropic materials due to their anisotropic nature. The layered structure limits bonding strength and increases stress at free edges or holes, leading to potential damage. Factors like thickness variations, ply arrangement, and shear stresses must be carefully analyzed, making the design process more challenging [9].

Carbon fibers are essential materials in high-performance composite structures due to their superior mechanical properties. Carbon fibers combined with polymer matrices closely match the ideal engineering material's attributes of high strength, toughness, stiffness and low weight. They are elastic up to failure, creep-resistant, chemically inert in most environments, and have excellent damping properties.

However, carbon fibers also have limitations: they are brittle with low impact resistance, exhibit low strain to failure, and have compressive strengths lower than their tensile strengths. Additionally, they are significantly more expensive than glass fibers [12].

Glass fibers account for 90% of the global market for fiber-reinforced polymer composites and are widely used in industries such as aerospace, automotive, marine, and construction. Reinforcements can be in the form of particles, whiskers, or fibers. Fibers can be continuous or discontinuous, with continuous fibers typically bundled into aligned structures to enhance mechanical performance [1], [11], [12].

1.1.2 Applications of Thermoplastic Composites

In the automotive industry, composites such as carbon fiber reinforced plastics (CFRP) and glass fiber reinforced plastics (GFRP) enable significant weight reductions of 40–60% compared to metals like steel and aluminum while maintaining strength and stiffness. This weight reduction improves fuel efficiency and decreases CO_2 emissions, aligning with environmental regulations[11].

Over the years, the use of polymer matrix composites in automotive applications has grown, particularly in exterior and interior parts, which account for 65% of their usage. The market value of automotive polymer composites rose from USD 200 million in 2014 to an estimated USD 700 million by 2025, reflecting increasing demand [11]. Fiber-reinforced polymers (FRPs) are widely used for their superior strength, fatigue resistance, and reduced thermal expansion. Applications include braking systems, engine hoods, body stiffeners, and T-joints [10].

Advanced composites, incorporating carbon, glass, and silver fibers in metallic matrices, offer lightweight and durable solutions for automotive components like brake pads, chassis, bumpers, and engine cradles. Natural and synthetic fiber composites also serve diverse applications, such as door panels and seatbacks, leveraging their high strength-to-weight ratios and eco-friendly properties (Table 1.3) [10].

Table 1.3 Different types of fiber reinforced composites and their applications in automotive [10]

Composites	**Applications**	**Advantages**
Carbon Fiber Reinforced Polymer (CFRP)	Body panels, chassis parts, and interior elements	Improved fuel efficiency and overall vehicle performance
Glass Fiber Reinforced Polymer (GFRP)	Body panels, bumpers, etc.	Provides good strength and stiffness
Aramid Fiber Reinforced Polymer (AFRP)	Armour panels and protective elements	Excellent impact resistance

Polymeric composites also play a critical role in the aerospace industry, where components like rudders, fuselages, and landing gear doors benefit from their lightweight properties and superior fatigue resistance. Composites reduce the need for fasteners and simplify assembly, enhancing efficiency [1]. Common thermoplastics used in aerospace include PEEK, PPS, PEI, and PEKK, with PAEK family materials such as LM-PAEK offering improved flow and faster processability. Carbon/PEEK composites, for example, are used in Airbus A400 cockpit floors, while PPS composites are employed in Airbus A340-500/600 structures for their chemical resistance to aviation fluids [7].

1.2 Manufacturing Methods for Thermoplastic Composites

To achieve effective impregnation of reinforcements with thermoplastic polymers, various methods have been developed, which are broadly categorized into pre-impregnation and post-impregnation techniques [4].

- Pre-impregnation Methods: Fibers are wetted and impregnated with the polymer in a single step. Prepreg layers are then consolidated with heat and pressure to create the final composite part.
- Post-impregnation Methods: The polymer is added as a film, filament, or powder during shaping, allowing impregnation to occur simultaneously.

Figure 1.2 illustrates typical impregnation techniques of thermoplastic composites. The manufacturing process depends on the type and length of reinforcing fibers [4]:

- Short fibers (3 mm): Suitable for injection molding or glass mat thermoplastics (GMT).
- Long fibers (3–25 mm): Ideal for extrusion or compression molding.
- Continuous fibers: Used in processes like thermoforming, thermostamping, or pultrusion.

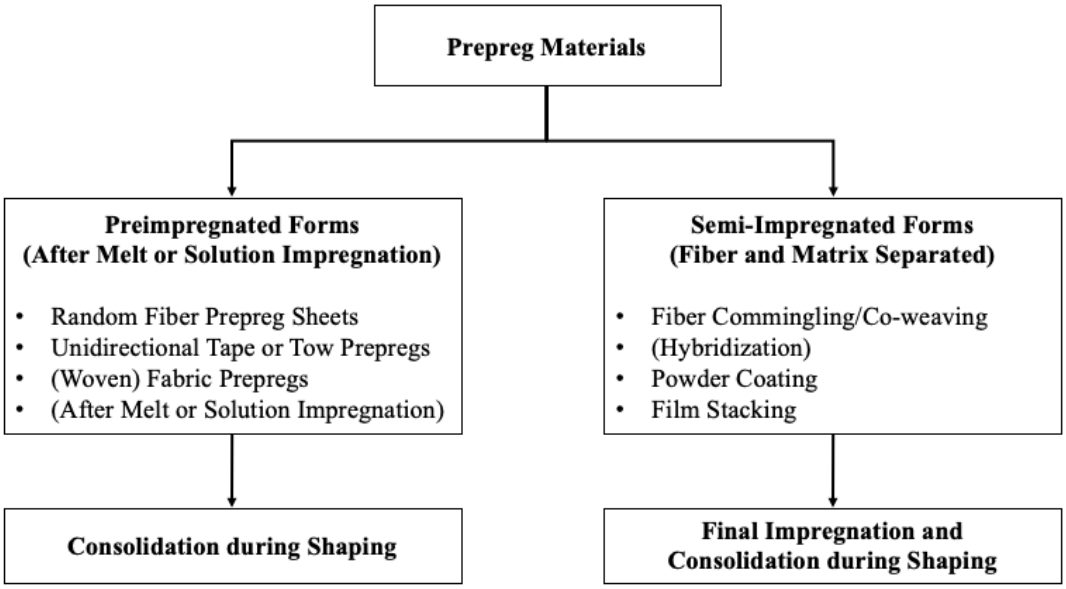


Figure 1.2 Impregnation techniques of thermoplastic composites[4]

The performance of thermoplastic composites is influenced by polymer type, reinforcement characteristics, and manufacturing techniques. Size, production volume, and cost dictate the choice of method, while innovations like resin transfer infusion (RTI) address challenges such as high melt viscosity, and ensuring uniform fiber impregnation under controlled conditions [9], [11].

The degree of crystallinity impacts properties:

- Higher crystallinity improves strength, chemical resistance, and creep performance but reduces ductility.
- Cooling rates play a crucial role: slow cooling promotes higher crystallinity, while rapid cooling minimizes it. For example, PEEK requires precise cooling to balance performance [7].

Post-processing techniques such as annealing or tempering redistribute crystallinity and relieve residual stresses. These processes are particularly valuable in automated

techniques like automated fiber placement (AFP) and tow placement (ATP), where repeated heating and cooling cycles can create uneven crystallinity [7].

1.2.1 Hand Lay-up

The hand lay-up process is one of the first and easiest methods used in composite manufacturing. In this technique, reinforcement materials such as prepregs (pre-cut and pre-impregnated fibers) are applied manually, layer by layer. These materials consist of fibers pre-impregnated with resin, bundled into tows, and arranged either as woven fabrics or as unidirectional plies.

During the lay-up process, each ply is manually shaped to match the required contour and carefully adhered to the previous layer or mold surface, ensuring no gaps between the layers. This meticulous approach results in highly compact and uniform laminates. The hand lay-up method is frequently employed in the production of glass fiber reinforced composites, especially for automotive applications [10].

1.2.2 Injection Molding

Injection molding is an efficient and widely used technique for manufacturing thermoplastic composites, particularly in high-volume industries such as automotive and appliances, because of its capability to manufacture highly detailed structures with precise geometry [12].

The process involves melting polymer compounds (e.g., pellets) in an injection chamber and injecting the molten material under high pressure into a closed mold cavity. After cooling and solidifying, the part is ejected, with cycle times ranging from 20 to 120 seconds depending on factors like part thickness and reinforcement content [4], [12].

Short fibers enhance properties like strength and electrical conductivity, enabling applications such as EMI shielding and ESD protection. Advantages include high production efficiency, material versatility, and low waste through recycling, although limitations include high tooling costs and lower mechanical performance compared to continuous fiber composites. Emerging techniques, such as over-molding, integrate thermoformed laminates with injection molding to create complex 3D structures for automated production [7], [12].

1.2.3 Thermoplastic Pultrusion

Pultrusion is a continuous manufacturing process where reinforcing fibers impregnated with a polymer are pulled through a die to create components with uniform cross-sections, such as rods and channels, making it widely used across industries [4]. While thermoset matrices dominate due to their low viscosity and established techniques, thermoplastic pultrusion is gaining attention for its advantages, including the ability to remelt the matrix for post-processing and faster production speeds [4].

However, thermoplastic pultrusion faces challenges like high melt viscosity, which complicates fiber impregnation and affects product quality, though advancements such as theoretical models have improved process efficiency and adoption [4]. The process involves melting prepreg tapes, shaping them under heat and pressure in a die assembly, and cooling them to consolidate the composite structure, with critical steps like melting, flow, crystallization, and solidification impacting final quality [4].

1.2.4 Thermoforming

Thermoforming is a versatile, cost-effective process for manufacturing large thermoplastic components with wall thicknesses ranging from 0.5 to 5 mm. It involves heating a thermoplastic sheet and forming it over a male mold or into a female mold under low pressure. Mold materials commonly include aluminum alloys, wood, or polymer composites.

Techniques like vacuum forming, drape forming, plug-assisted forming, and air-slip forming enable the production of complex, curvilinear parts. Thermoforming is widely used in aerospace, automotive, and packaging industries due to its adaptability, scalability, and potential to reduce manufacturing costs, particularly in large-scale production [4], [7].

1.2.5 Compression Molding

Compression molding is a widely used method for forming thermoplastic composites by consolidating materials under heat and pressure in a hot press. Commonly processed materials include unidirectional prepreg tapes, commingled fabrics, and woven graphite cloth, often stacked in alternating layers before consolidation [7].

The process minimizes fiber attrition, ensuring high reinforcement aspect ratios and improved impact resistance, strength, and stiffness. It is ideal for large components with consistent mechanical performance, requiring lower molding pressure compared to injection molding [4].

Emerging techniques like Continuous Compression Molding (CCM) enable the production of complex profiles with low porosity, making them suitable for aerospace applications [7]. Additionally, hybrid methods like press-forming combine molding and shaping into one operation, further streamlining production [7]. Compression molding is extensively applied in automotive and aerospace industries for parts like body panels, hoods, and structural components, offering versatility, cost efficiency, and durability [10].

1.2.6 Autoclave Processing for Composites

Autoclave processing is a widely used method for manufacturing high-performance fiber-reinforced plastic composites, particularly for large and complex structures. This technique involves stacking prepreg layers into the desired shape, often combined with additional structural materials like honeycomb cores and stiffeners.

The assembly is covered with layers of breather and bleeder cloths, sealed in a vacuum bag, and placed in an autoclave—a temperature and pressure-controlled vessel. The vacuum system and autoclave work together to remove air, compact the laminate and cure the resin through a predefined thermal cycle. After curing, the part is removed, debagged, and prepared for secondary processes [13]. A thermoplastic autoclave process consists of three main stages: laying of prepregs**,** packaging, and pressuring at the correct temperature cycle- known as the autoclave cycle**.**

1. Prepreg Laying: Prepreg laying is critical to achieving accurate test results and the desired composite quality. The orientation of the prepregs must be precise and consistent (e.g., 0°, 90°, or ±45°). Deviations exceeding ±5° in the intended orientation significantly reduce mechanical properties, preventing the composite from achieving the required strength values. Additionally, welding zones must be placed outside the usable part. If the welding zones remain within the composite, they lead to structural flaws and decrease the material's overall strength.

2. Packaging: The packaging process is essential for maintaining vacuum integrity and ensuring even temperature distribution.

- Vacuum Leakage: Special care must be taken to prevent vacuum leaks during packaging. Leaks, especially in the material's melting zone, hinder proper vacuum application and result in air gaps within the composite, which are considered major defects and render the product unusable.
- Vacuum Blanket Placement: Proper placement of the vacuum blanket is crucial. Misalignment leads to non-homogeneous airflow, causing polymer flow irregularities and preventing the removal of air bubbles from the composite.

3. Autoclave Cycle: The autoclave cycle involves several critical parameters—vacuum, pressure, and temperature—to ensure full consolidation of the composite material.

- Vacuum: A vacuum pressure of approximately 1 bar is maintained throughout the cycle, with a minimum allowable reduction of 0.8 bar. The vacuum is particularly critical during the material's transition from melting to solidification, ideally maintaining the maximum vacuum in this range (approximately 100°C above the material's Tg).
- Pressure: Pressurization must be gradual, at a rate of 0.5 bars/min, to avoid damaging the material. The pressure is generally set to 2 bars for thermoplastic composites, increasing incrementally as the melting point is approached. When the resin melts, the pressure is maintained at the maximum level to ensure full consolidation. At the end of the cycle, pressure is released gradually at the same rate (0.5 bars/min) to prevent part distortion.
- Temperature: Heating is performed at a controlled rate of 5°C/min until the temperature is approximately 20°C above the melting point. The composite is then held at this temperature for 15–30 minutes under maximum pressure and vacuum to achieve complete consolidation. Cooling follows, and this step must also be carefully controlled to ensure proper crystallization. The temperature is reduced below the material's Tg before pressure is released, and the composite is demolded.

Key challenges in autoclave processing include:

1. Cure Cycle Optimization: Determining the appropriate temperature, pressure, and time to produce void-free, fully cured, and distortion-free components efficiently.
2. Residual Stress Management: Residual stress, caused by resin movement and thermal gradients during curing, can lead to warping, resin-rich/poor regions, and dimensional inaccuracies.
3. Pressure Distribution: Ensuring uniform pressure is crucial to avoid void formation, especially in sandwich panels prone to surface dimpling and core buckling.

Traditionally, addressing these challenges required trial-and-error modifications to tooling, material, and process cycles, which is both costly and time-consuming. Therefore, modern advancements focus on intelligent process control and computational modeling [13].

While autoclave technology has remained mostly unchanged for decades, advancements in modeling and simulation are streamlining development, making the process more efficient and cost-effective. Innovations are expected to lead to better tooling, thermally efficient autoclaves, and improved control systems. Autoclave processing will likely remain the preferred choice for applications requiring high-quality, high-performance components with minimal part counts [13].

Despite its effectiveness, autoclave processing has several critical drawbacks, including [13].

- Lengthy processing cycles (often over 8 hours)
- High-pressure requirements
- Significant upfront investment
- High energy consumption due to inefficiencies in heating large-scale tools and inert gases
- Batch processing limitations, which restrict scalability

1.2.7 Out-of-Autoclave Processes

Out-of-autoclave (OOA) manufacturing methods are emerging as a viable replacement, offering cost-effective and efficient solutions. These methods combine advanced automation techniques, such as Automated Tape Laying (ATL), Automated Fiber Placement (AFP), and Liquid Composite Molding (LCM), with innovative heating systems like infrared, induction, laser, or Quickstep technologies. OOA systems address many of the limitations of autoclave processing by significantly reducing energy use, shortening cycle times, and lowering costs, while still delivering high-quality composites suitable for aerospace applications [14].

Additionally, advancements in low-performance composite manufacturing have reshaped the composites industry by reducing production costs and broadening accessibility. These innovations are driving a gradual transition from traditional autoclave systems to more agile OOA approaches, enabling efficient and reliable composite production across various sectors [14].

1.2.8 Automated Composite Manufacturing: ATL and AFP

Automated Tape Placement (ATL) and Automated Fiber Placement (AFP) are revolutionary technologies in composite manufacturing, widely employed in aerospace and automotive industries for producing lightweight, high-performance components. While both techniques share the goal of automating the layup process, their distinct approaches cater to varying complexities and scalability requirements. ATL is optimized for creating large, flat laminates using wide prepreg tapes (75–300 mm), while AFP is designed for precise placement of narrower tows (6.35–12.7 mm), enabling fiber steering and placement on complex geometries [15].

As illustrated in Figure 1.3, ATL consolidates wide tapes onto substrates using heated rollers and precise tension control, typically followed by autoclave curing, making it ideal for large-scale components like wing skins and fuselage sections. AFP, on the other hand, enables in-situ consolidation during the layup process, applying heating and pressure via advanced systems like diode lasers and ultrasonics to bond layers without additional curing steps. This capability makes AFP particularly suited for complex geometries, such as stringers and curved aerospace components [4], [7], [15].

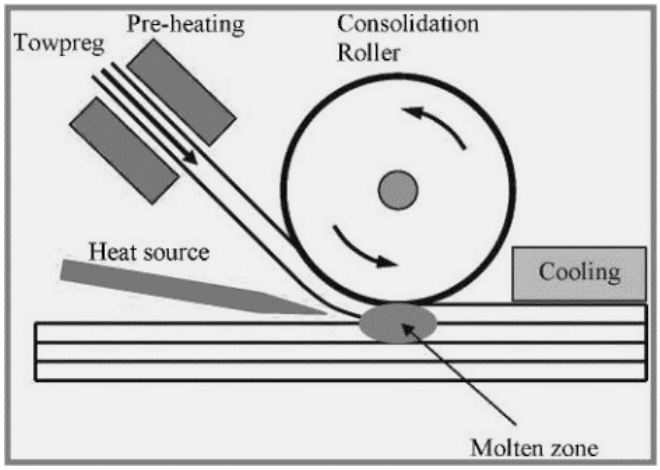


Figure 1.3 Illustration of automated tow placement [4]

Thermoplastics are increasingly used in AFP due to their recyclability and repairability, offering significant advantages over thermosets, including the elimination of autoclave steps. However, challenges like high processing temperatures and slower speeds required for effective surface contact persist. Despite these limitations, thermoplastic AFP has achieved consistent industrial success, with advancements in process modeling and complementary technologies further enhancing its efficiency and applicability [16]. Emerging methods such as in-situ thermoplastic AFP leverage out-of-autoclave techniques to simplify processing and reduce costs, while maintaining the mechanical and thermal benefits of thermoplastics [4], [16].

Both ATL and AFP reduce material waste and production time compared to manual layup, ensuring consistent quality and structural integrity. These methods are integral to the production of aerospace structures such as wing skins, fuselage sections, and tailplanes, with ATL excelling in high-rate laminate stacking and AFP enabling precision in curved or intricate designs. Recent innovations include robotic systems, tailored fiber placement (TFP), and real-time monitoring, expanding the potential applications of these technologies into sectors like automotive and renewable energy [4], [7], [15].

In summary, ATL and AFP have transformed composite manufacturing, offering unmatched precision, scalability, and efficiency. By integrating advanced technologies and optimizing process parameters, these techniques continue to push the boundaries of composite production, ensuring their relevance across multiple industries [15].

Sacchetti et. al. [17] investigated the crystallinity development of PEKK and PEEK unidirectional thermoplastic composites during in-situ consolidation using 1/4-inch-wide tapes laminated via single-tow deposition with laser heating. The study analyzed crystallinity changes across layers, comparing unheated and self-heated tools. On unheated tools, cold crystallization was observed in the initial layers, occurring between the polymer's glass transition and melting temperatures. In contrast, self-heated tools ensured consistent crystallinity throughout the laminate. Additionally, increased layering reduced internal porosity for both tool types by enhancing intimate contact during consolidation.

Raps et. al. [18] investigated how tooling temperature, nip-point temperature, layup speed, and consolidation pressure affect the in-situ AFP process. The study utilized a novel CF/LM-PAEK composite with T700 fibers and applied a Face-Centered Cubic (FCC) Design of Experiments (DoE) method for process optimization. Findings indicated that increasing the nip-point temperature and consolidation pressure enhanced bonding strength, although pressure had a comparatively smaller effect. Composites formed on heated tools exhibited greater crystallinity and improved bonding strength than those produced on unheated tools. Interestingly, layup speed did not significantly influence bonding strength or crystallinity, which was linked to the polymer’s low melt viscosity.

Hoang et al. [19] studied composite fabrication using the AFP method with CF/PEEK material (60% fiber content), focusing on optimizing parameters like heater temperature (825 °C), roller pressure (100 lbf), and mandrel temperature (initially 200 °C, later reduced to 155 °C). Process speed increased incrementally from 0.5 in/s to 1 in/s across layers. The resulting laminates showed 22% higher tensile strength and 17% improved compressive strength compared to autoclave-fabricated parts, demonstrating AFP’s effectiveness for high-performance composites.

In a related study [20], investigated the quality of CF (AS4)/PEEK laminates fabricated using the AFP process was investigated. Unlike autoclave specimens, AFP laminates subjected to horizontal slip loads displayed distinct behavior, with cracks forming within plies rather than at interlayer interfaces. This indicated improved interlayer bond strength in AFP laminates. The research identified optimal process parameters, including a nozzle temperature of 925 °C, a processing

speed of 50.8 mm/s, a compaction force of 40 kgf, and a heater-to-compression point distance of 11.38 mm.

Kim et al. [21] analyzed the heat transfer and temperature distribution in an ATL system utilizing graphite/PEEK prepreg tapes. The research integrated a parameter estimation approach with a finite element-based thermal model. A small-scale tape lay-up setup was developed, and experimental trials were performed to monitor temperature variations within the composite during processing. To refine thermal analysis, the inverse method was applied, ensuring consistency between measured and simulated temperature values while determining unknown boundary conditions. The results confirmed the validity of the proposed methodology and demonstrated its effectiveness in accurately characterizing boundary conditions for tape lay-up operations.

Qureshi et al. [22] explored the in-situ consolidation of AS4-CF/PEEK using the Automated Tape Placement (ATP) process, examining compaction force, tape laying speed, and tool temperature. A wider nozzle improved heat distribution, enhancing lap-shear strength and fracture toughness, though increasing tape laying speed reduced interlaminar shear strength. ATP composites showed mechanical properties 45% lower than autoclaved samples, but post-consolidation could make them suitable for aerospace applications. Challenges such as inconsistent heat flux and poorly consolidated initial plies were identified, with recommendations for future research including improved heat flux control, assessment of thermal degradation, and the use of resin-rich tapes or secondary consolidation to enhance performance.

Sonmez and Akbulut [23] developed a process optimization scheme for tape placement using APC-2 (PEEK) prepregs. The objectives were to reduce residual stress and enhance productivity while maintaining bonding quality and minimizing thermal degradation. Residual stresses were reduced to 70 MPa, comparable to press molding, with full bonding achieved at slow lay-down speeds. By allowing partial bonding and relying on post-processing, roller velocities were increased to 8 cm/s, making non-in-situ thermoplastic tape laying a viable, faster alternative to thermoset tape placement.

Schledjewski and Latrille [24] studied ATL and filament winding processes using unidirectional (UD) fiber-reinforced thermoplastic tapes (APC-2). They identified heat transfer and consolidation as critical factors for high-quality bonding. Their process simulator, ProSimFRT, incorporated finite element modeling to support optimization.

Maurer and Mitschang [25] investigated the laser-assisted thermoplastic tape placement process for CF/PEEK tapes, focusing on optimizing laser settings to achieve autoclave-level quality with high efficiency. Using a verified FE simulation, key parameters such as laser beam height, angle, power distribution, and lay-up speed were analyzed. Optimum settings included a 3.8 mm laser height, 14.58° angle, and 528 W laser power, enabling a maximum placement speed of 12 m/min and a process efficiency of 15.8 m² per hour per kW. The Peel resistance of specimens matched autoclave standards. Economically, thermoplastic tape placement with multiple tapes simultaneously laid proved competitive with thermoset processes for complex parts like cylindrical shells.

Khan et al.[26] analyzed thermoplastic tape placement with in-situ consolidation to address challenges limiting its industrial adoption. The study explored how process parameters such as tool temperature, roller configuration, and tape characteristics impact bonding strength and void content. Results showed that higher tool temperatures (up to 300°C), lower placement velocities, and enhanced heating of tape and substrate improve bonding but can increase void content due to material relaxation. Tapes with low void content and smooth surfaces were found to enhance polymer healing and laminate quality. Roller configuration plays a critical role, with multiple rollers optimizing placement velocity and bonding, particularly for flat components. The study concludes that equipment and parameter optimization depend heavily on the geometry and requirements of the final component, emphasizing a tailored approach for achieving high-quality laminates.

Grouve et al. [27] investigated the processing of carbon fiber reinforced polyphenylene sulfide (CF/PPS) tapes using a laser-assisted tape-laying system. Rather than replacing the autoclave method, this technique was employed as a secondary process. CF/PPS tapes were welded onto pre-manufactured 5-Harness satin carbon–PPS laminates to enhance localized mechanical performance. A thermal camera, positioned on the tape placement head, captured the temperature

distribution of both the tape and laminate before reaching the nip-point during welding. The study examined the influence of laser power, incident laser angle, and placement speed on interfacial fracture toughness, assessed through mandrel peel tests. Comparison with press-consolidated samples indicated that achieving strong bonding was possible at high placement speeds with low energy input.

Comer et al. [28] conducted a comparative analysis of carbon fiber reinforced PEEK laminates manufactured by laser-assisted Automated Tape Placement (LATP) and autoclave processing. The study found that while LATP laminates exhibited enhanced interlaminar toughness, they demonstrated lower flexural strength, interlaminar shear strength, flexural stiffness, and open-hole compression strength compared to those produced using the autoclave method.

Rapid cooling rates and incomplete through-thickness melting during LATP led to suboptimal crystallinity and void formation, compromising mechanical properties. The study emphasizes the complexity of optimizing LATP, highlighting the need for tailored processing parameters and material modifications to achieve autoclave-level properties at economic lay-down speeds.

In summary, ATL and AFP represent the cutting-edge of automated composite manufacturing, offering unparalleled precision, scalability, and efficiency. As these technologies evolve, they are poised to address the increasing demand for lightweight, high-performance composite components across various industries.

1.2.9 Filament Winding (FW)

Filament winding is a precise manufacturing method used to produce high-performance composite structures, particularly axially symmetrical components like pipes, tanks, pressure vessels, and cylindrical parts. The process involves the controlled placement of continuous fibers onto a rotating mandrel, followed by resin impregnation and curing (thermosets) or consolidation (thermoplastics). Modern CNC-controlled systems enhance precision and productivity, making filament winding suitable for both thermoset and thermoplastic composites [10], [29].

Filament winding (illustrated in Figure 1.4) is an out-of-autoclave composite production method that follows similar principles to the laying process. The area where the mandrel and compaction roller interact is known as the nip point (see

“melt zone” in Figure 1.4), where heat application leads to polymer melting in and around this region. The roller applies pressure to both the incoming tape and the underlying substrate, promoting close contact. Once proper contact is established at the nip point, the tape naturally bonds to the substrate. To minimize void formation, pressure is maintained for a sufficient duration, allowing the temperature to drop below the polymer's melting point [30]. This method is suitable for both thermoset and thermoplastic composites; however, the majority of applications predominantly involve thermosets [3], [19], [31].

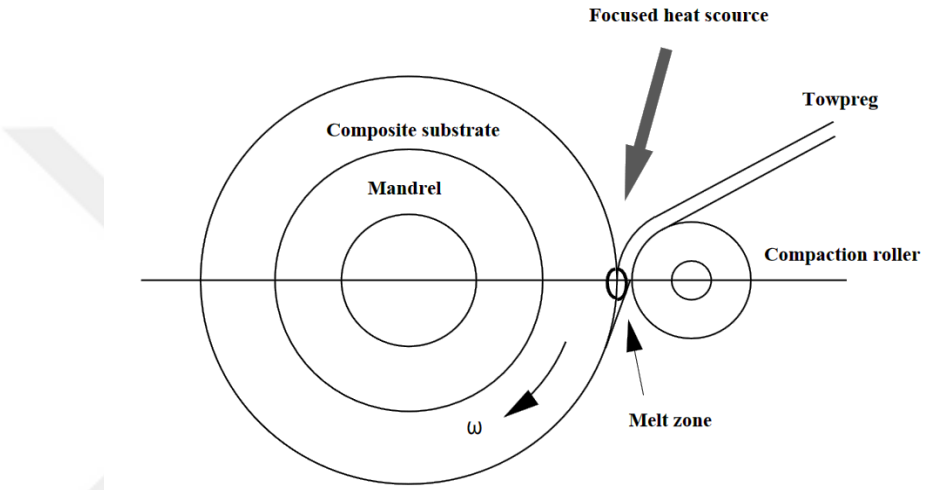


Figure 1.4 The thermoplastic filament winding process [32]

Thermosets require post-winding curing at room or elevated temperatures, while thermoplastics employ in-situ consolidation, eliminating the need for curing. This allows for advantages such as superior fracture toughness, unlimited shelf life, repairability, and weldability. However, the molten state of thermoplastics exhibits high viscosity, making fiber impregnation more challenging and necessitating precise control of parameters like temperature, winding speed, and consolidation pressure [29].

Filament winding is particularly effective for axially symmetrical geometries, such as cylinders for pressure vessels and spherical shapes for high-pressure storage. Recent advancements have enabled the creation of complex forms like cavities, sandwich structures, and freeform lattice geometries. Robotic filament winding systems further expand possibilities with fiber deposition tools mounted on robotic arms for precise placement and multi-stage processes [15]. As illustrated in Figure

1.5, various winding techniques are employed in FW, tailored to specific application requirements.

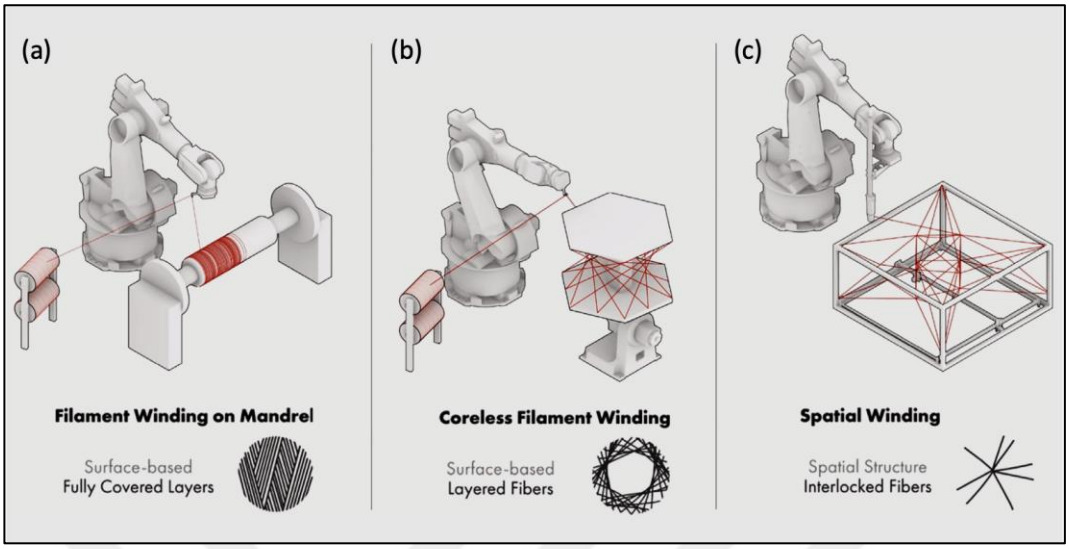


Figure 1.5 Various filament winding methos; (a) robotic, (b) coreless, and (c) spatial winding [15]

Filament winding integrates in-situ consolidation, where resin-impregnated fibers are oriented, laid, and compacted in a single step, eliminating additional consolidation cycles. Prepreg materials are typically prepared through film stacking, commingling, or powder impregnation, with compaction rollers facilitating bonding. Automated systems reduce costs, improve efficiency, and enable the production of complex, lightweight components with tailored structural properties [4], [15].

Thermoplastic filament winding (Figure 1.6) process involves the feeding of thermoplastic tape into a preheating unit, where it is softened before being wound onto a rotating mandrel. A focused heat source, such as hot gas, melts the resin, while a roller applies pressure to consolidate the layers and bond the tapes into laminates [17]. This on-site consolidation process eliminates the need for curing in autoclaves, reducing stress distortions commonly associated with such methods. The process is highly efficient, particularly for axially symmetrical components like cylinders and pressure vessels, with fiber orientations typically between 15° and 88° [49].

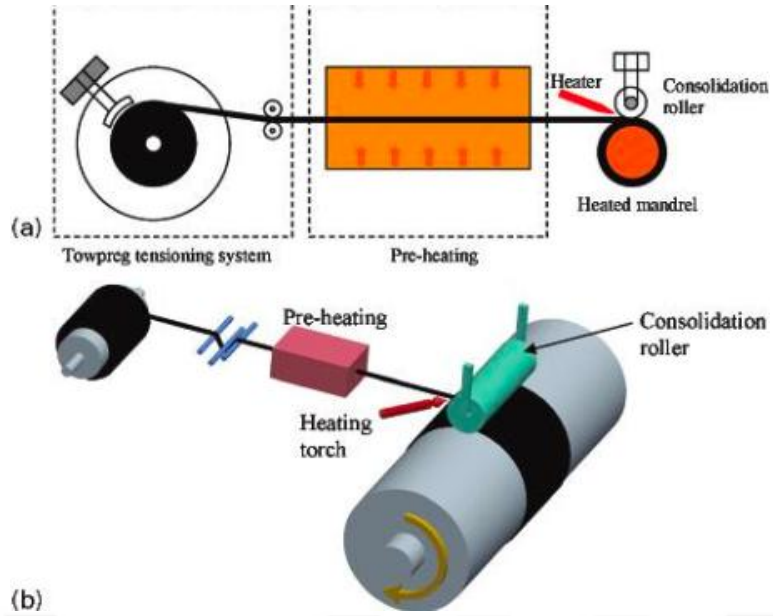


Figure 1.6 Thermoplastic filament winding system (a) scheme, (b) process [4]

The key parameters in thermoplastic filament winding include winding speed, fiber tension, temperature, and winding angle. The mandrel material and thermal control are critical to the process's success. Consolidation relies on intimate contact between layers, polymer chain interdiffusion, and proper heat and pressure management to eliminate voids and achieve strong interlayer bonds. Faster winding speeds reduce consolidation time, potentially impacting bond quality, while slow cooling enhances crystallinity and tensile strength [4].

Various heating methods, including laser heating, hot gas, hot roller heating, infrared radiation, and ultrasonic heating, are employed to achieve effective polymer melting and bonding.

- Laser Heating: Thermoplastic materials heat up as their molecules interact with high-frequency electromagnetic waves. This method is suitable for thermoplastics with polar molecules in their structure. While laser heating achieves high efficiency and enables rapid melting, making it ideal for precision processes, it is costly and requires strict safety measures. Consequently, it is not widely adopted on an industrial scale [33].
- Hot roller heating: This method employs a heated roller, making it one of the safest heating approaches. High energy is supplied via a system comprising an open flame and acetylene gas gun to warm the roller. However, uncontrolled heating can cause excessive temperature increases,

leading to polymer degradation. While less efficient than laser systems, hot roller heating is more efficient than hot air systems. Due to its affordability and flexibility in head design, it is the most commonly used method.

- Hot gas heating: This method involves heating nitrogen gas/air stored in pressure vessels with an electric system. The heated gas is passed through specially designed nozzles, transferring heat to the material via convection. It is widely used in thermoplastics due to its cost-effectiveness and familiarity. Nitrogen gas can be heated to temperatures as high as 1200°C. Despite its efficiency at high temperatures, this method consumes significant energy when applied to high-performance thermoplastics like PEEK [34].
- Infrared heating: Infrared heating transfers heat to composite parts through radiation. Its reproducibility, speed, and non-contact operation reduce contamination risks while requiring less labor. Thermoplastic prepregs contain varying pigments, additives, and fibers, which may affect IR absorption, potentially leading to inconsistencies and lower-quality results [34].
- Ultrasonic heating: Ultrasonic heating is being explored as an alternative to conventional methods. In this process, an ultrasonic horn contacts the prepreg layer, applying high-frequency vibrations under controlled pressure. This technique aims to increase welding speed while minimizing energy consumption [34].

The various heaters used in FW process and their heating zones are illustrated in Figure 1.7.

Filament winding systems typically include components such as material racks, tension controllers, preheating and main heating zones, consolidation rollers, and mandrels. These systems provide precise control over process parameters to ensure consistent quality [29].

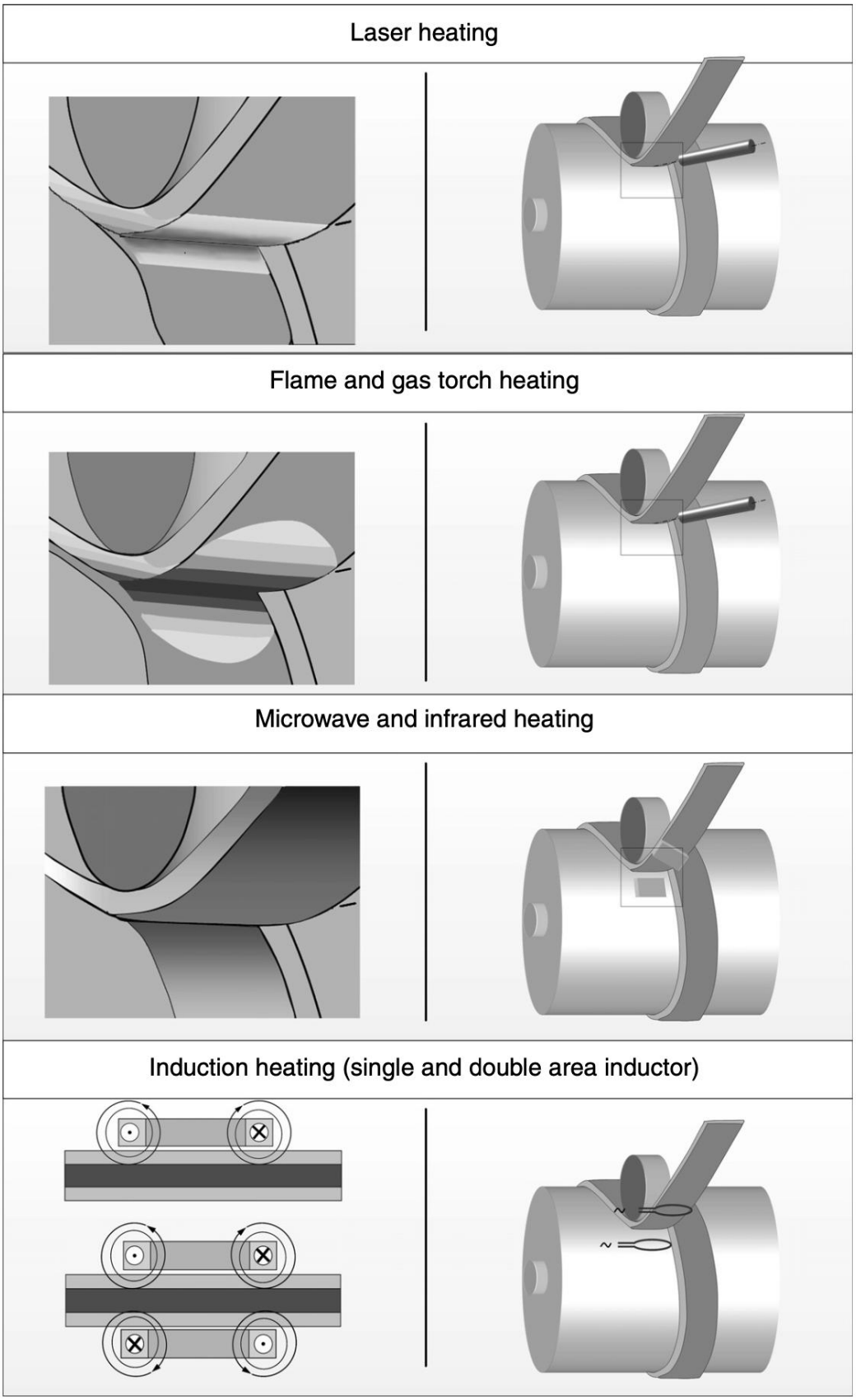


Figure 1.7 Different heating methods used in FW and their thermal expansions [29]

Table 1.4 outlines the six axes involved in the filament winding process for thermoplastics, which collectively ensure precise fiber placement and tension control during manufacturing. Together, these axes enable precise and consistent winding, accommodating a wide range of geometries and material requirements in composite manufacturing.

Table 1.4 Different axes in FW [29]

Axis	**Description**	**Function**
First Axis (X)	Mandrel Rotation	Controls the mandrel's rotation, determining the winding pattern and layer buildup.
Second Axis (Y)	Motion of the payout eye parallel to the mandrel	Ensures uniform fiber placement across the mandrel's surface.
Third Axis (Z)	Distance between the payout eye and mandrel rotation	Adjusts fiber tension and placement accuracy.
Fourth Axis (U)	Payout eye rotation around the horizontal axis	Enables precise angle adjustments for specific winding patterns.
Fifth Axis (V)	Payout eye rotation around the vertical axis	Allows accurate fiber placement on complex geometries.
Sixth Axis (W)	Changes the level of the payout eye	Ensures fiber alignment with the mandrel across different layers or shapes.

Two main techniques are used: direct impregnation, where fibers and polymers are combined during winding, and semi-finished material processing, involving pre-impregnated fibers or commingled yarns. Each approach offers specific advantages depending on the application and material requirements [12].

Thermoplastic winding processes use two types of semi-finished materials. The first includes pre-impregnated fibers, such as fully consolidated tapes. The second group

consists of materials that supply the fiber and matrix separately, without prior impregnation. Examples include commingled yarns, bicomponent fibers, and powder-impregnated fibers. All semi-finished materials are designed with precise fiber volume content, meaning adjustments to the fiber volume during the winding process are not possible without switching to a new semi-finished material [35].

The cooling rate significantly affects the crystallinity, strength, and fracture toughness of thermoplastic composites. Rapid cooling reduces crystallinity and increases interlaminar fracture toughness, while slower cooling enhances tensile strength but lowers fracture toughness [7].

Filament winding has evolved into a versatile and highly precise manufacturing process, benefiting from automation and advanced material technologies. Its adaptability to complex geometries and its ability to integrate consolidation and bonding in a single step makes it invaluable across industries like aerospace, automotive, and energy [15]. The transition to robotic systems and innovations in heating and compaction techniques continue to expand its capabilities, paving the way for even more sophisticated applications.

Studies by Funck and Neitzel [36] highlighted that lasers offer superior energy efficiency and fast response times, while direct flame heating delivers cost savings and higher production speeds. Recent advancements have also combined impregnation and winding into a single process step, with innovative developments led by researchers like Henninger and Friedrich [37].

Recent innovations in Filament Winding (FW) have significantly advanced composite manufacturing technology. The development of robotic filament winding has revolutionized the field by enabling the fabrication of highly complex, lightweight structures, even for architectural applications [15].

Mindermann et al. [38] developed a hybrid approach that integrates ultraviolet pultrusion with coreless filament winding. This method enables partial curing of the resin between pins, allowing for controlled fiber cross-sections and consistent fiber volume distribution. In a separate study [39], adjustments were made to the geometry of winding pins to improve multi-directional winding performance and reduce directional bias. By modifying pin orientation and spacing, the clustering of

tows near the pin base or head was minimized, leading to greater winding precision and improved overall functionality.

Radford et al. [5] explored the feasibility of integrating a fused deposition hot-end system with the filament winding technique. The wet-out of glass fibers with PET polymer was made by using the fused deposition hot-end, and the outcoming fiber was wound around a rotating mandrel to produce a composite cylinder. Two different filament winding temperatures (190 ℃ and 220 ℃) were examined and the results were compared with filament wound composites produced by commercially provided commingled glass fiber/PET. The results of metallographic evaluation and short beam tests (interlaminar bonding) proved that glass fibers were homogeneously distributed into PET matrix and fused deposition hot-end on a dry fiber filament winding system is feasible.

Duan et al. [40] investigated the filament winding modeling of a carbon fiber-reinforced pressure vessel with an HDPE liner. The finite element model was developed using the ANSYS ACP module. The study employed a combination of helical and toroidal winding techniques. To maintain consistency, the total fiber volume and cross-sectional area were kept constant while calculating the thickness distribution in the stratified winding. The results produced a validated finite element model, making it suitable for further simulations.

Wong et al. [41] analyzed the process parameters influencing the production of aramid-reinforced PA6 composites using the filament winding technique. The study focused on the impact of factors such as heat gun temperature, line speed, fiber tension, compaction force, and preheater temperature. Findings indicated that incorporating an inert gas in the gas torch, along with precise heating and cooling control in the compaction roller and mandrel, could significantly improve the overall quality of the final product.

Stefanovska et al. [2] studied the filament winding process for glass fiber-reinforced PP rovings. Their research examined the influence of various process parameters, including consolidation roller temperature, second roller temperature, air gun temperature, consolidation roller pressure, and winding speed. The study determined that an air gun temperature of 150–200 °C, a roller pressure of 5 bar, and a winding speed of 1.5 m/min were optimal for achieving high-quality

consolidation. Likewise, Deng et al. [42] explored the optimization of prepreg tape winding parameters and their impact on performance. By applying response surface methodology to carbon fiber-reinforced polyamide 66 (CF/PA66) tapes, they identified ideal settings for heating temperature, tape tension, and roller pressure. The findings emphasized the importance of these factors in maximizing tensile strength and enhancing mechanical properties.

In another innovative application, Mindermann et al. [43] investigated a multi-stage coreless filament winding technique for hybrid fiber composite/metal structures. Their approach notably improved tensile strength while achieving significant weight reduction compared to traditional metal components.

Gennaro et. al. [44] used fiberglass-reinforced PP hybrid yarns in filament winding using a two-component heating system consisting of an infrared heater and a hot air gun, as well as consolidation cylinders. In this work, it was found that the location of the infrared heater is not correct, the cooling rate of the polymer is too high and it starts to solidify before reaching the consolidation cylinder, so the impregnation cannot be achieved completely. The results of this study show how important the locations and activities of the heater components are in head design.

In a study conducted by Lionetto et al., ultrasonic welding was used as a heating medium in the consolidation of glass fiber-reinforced PP hybrid yarns by filament winding method. In an experimental system developed at the laboratory scale, an innovative method, ultrasonic welding, has been shown to provide sufficient temperature and pressure to melt and impregnate the polymer [45].

Dell'Anna et al. [46] examined the feasibility of using E-glass (GF) reinforced PET prepregs in composite pipe production, integrating an ultrasonic heater into the filament winding system. During the winding process, heat and compaction pressure were applied via the horn, and process parameters were analyzed through various characterization techniques. The study found that increasing horn force improved Lap Shear Strength (LSS), with optimal bonding strength achieved at 188 N compaction force and a 3-second welding time. The results confirmed that GF/PET prepreg tapes are suitable for composite pipe manufacturing using ultrasonic filament winding.

In the authors' previous work [47], the researchers focused on ultrasonic filament winding for commingled thermoplastic rovings, incorporating fiber impregnation and ply consolidation within a single setup. A finite element (FE) model was developed to simulate temperature distribution during consolidation, validated through experimental temperature measurements. Composite cylinders made from E-glass reinforced polypropylene (PP) were produced to verify micromechanical predictions, demonstrating that a 0.1-second contact time between the sonotrode and filament was sufficient for polymer melting without degradation. The study also showed that void content levels (4.6% for ultrasonic and 1.8% for compression molding) were consistent with literature values. However, further optimization of process parameters was recommended for improved results.

Karbuz et al. [48] investigated the fabrication of thermoplastic composite components with a hexagonal cross-section using glass fiber-reinforced polypropylene (GF/PP) prepreg tapes and an automated filament winding system. The study employed the Taguchi experimental design to optimize key parameters, including heater temperature, compression roller pressure, mandrel rotation speed, and corner radii, to enhance mechanical performance. Results indicated that corner radius plays a crucial role in the strength characteristics of non-cylindrical structures, providing valuable insights into the challenges and possibilities of applying filament winding to complex geometries.

Deng et al. [42] applied response surface methodology to optimize the winding parameters of CF/PA66 prepreg tapes. Their study determined the ideal heating temperature, tape tension, and roller pressure to enhance tensile strength. Likewise, Geng et al. [49] examined the impact of laser-assisted winding on CF/PPS composites, refining core mold temperature, winding speed, and laser power to improve mechanical performance.

Vedernikov et al. [50] found that composites produced from commingled yarns exhibited significantly greater flexural and interlaminar shear strength compared to those made with conventional prepreg tapes. Lin Ye et al. [51] investigated the consolidation of CF/PEEK hybrid yarns via filament winding, highlighting the need for higher pressure and temperature to achieve full impregnation compared to pressure molding techniques.

Xian et al. [52] enhanced the bending properties of GFRPP bars through fixture optimization, leading to a substantial increase in bending strength. Finally, Chen et al. [53] focused on optimizing the process parameters for continuous carbon fiber-reinforced polycarbonate (CCFRPC) prepreg filaments using a melt impregnation method. Their study identified ideal processing conditions that improved tensile strength and minimized diameter variation, confirming the approach's suitability for 3D printing applications.

Mo et al. [54] highlighted that refining winding sequences plays a crucial role in enhancing the compression strength of coreless filament-wound lattice structures. Lisbôa et al. [55] demonstrated that radial compression testing serves as a reliable approach for assessing delamination risks in filament-wound composite cylinders. Similarly, Mishra et al. [56] investigated the axial and radial compression behavior of hybrid tubular composites, which incorporate carbon and glass fibers embedded in an epoxy matrix and are fabricated using a robot-assisted filament winding technique.

1.3 Process Optimization by Response Surface Methodology (RSM)

Optimization involves identifying process conditions that yield the highest efficiency within a structured system operating under defined constraints [57]. Determining the optimal parameters of a physical system requires analyzing multiple independent variables over a broad spectrum [58].

The main objective of Design of Experiments (DOE) is to plan, design, and analyze experiments to derive valid, objective, and statistically sound conclusions, with statistical tools ensuring robust results and better decision-making. The success of industrial experiments relies on thorough planning, appropriate design selection, statistical analysis, and collaborative teamwork [59].

To optimize a process, it's crucial to understand the transformation of inputs, such as materials, equipment, and methods, into outputs like performance or quality characteristics. Designed experiments systematically vary these inputs to observe their impact on outputs, aiming to enhance robustness and minimize sensitivity to

external factors, improving overall quality and efficiency [59]. Figure 1.8 illustrates the general aspects of a system.

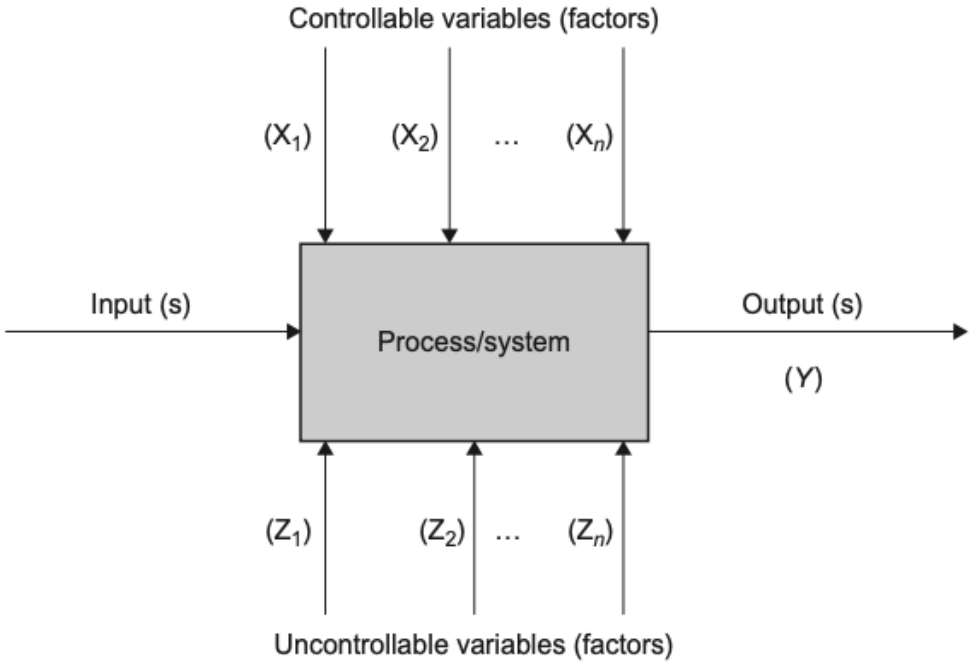


Figure 1.8 Fundamental structure of a process or system [59]

In many practical applications, the relationship between controllable variables and responses is either unknown or too complex for direct use. Response Surface Methodology (RSM), provides a structured approach for analyzing and optimizing such processes using mathematical and statistical tools. RSM focuses on developing empirical models to describe and optimize responses influenced by multiple factors. Its main objectives include generating insights within the experimental domain, estimating variability, predicting responses at untested points, minimizing cost and resource constraints, and reducing decision-making ambiguity under uncertain conditions [60], [61], [62].

RSM is a robust approach that integrates statistical and mathematical methods to model systems or processes based on experimental data [57], [62], [63]. By using empirical models, it establishes relationships between dependent and independent variables. Since these relationships are unknown at the outset, an initial approximation is developed and subsequently evaluated for accuracy using experimental results.

As represented in Equation (1.1), RSM represents the expected response (y) as a function of independent variables (x_1, x_2) with noise or error (ϵ):

$$y = f(x_1, x_2) + \varepsilon \tag{1.1}$$

The response surface, visualized graphically or as contour plots, aids in identifying trends and optimizing conditions. Most RSM problems use low-order polynomial models:

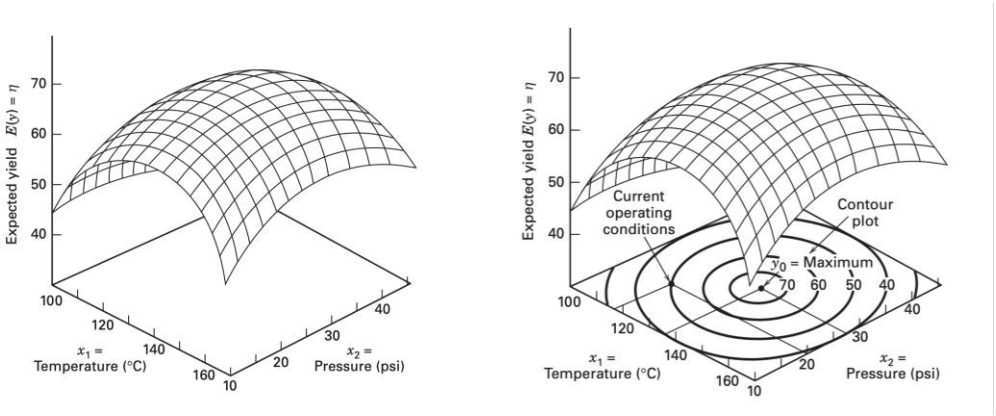
- First-order models: Effective for systems with minimal curvature, enabling rapid progression toward the optimum region. The first-order model is represented in Equation (1.2):

$$y = \beta_0 + \beta_1 x_1 + \beta_2 x_2 + \cdots + \beta_k x_k + \varepsilon \tag{1.2}$$

- Second-order models: Suitable for refining the response surface near the optimum and locating the exact optimum. The second-order model is represented in Equation (1.3):

$$y = \beta_0 + \sum_{i=1}^{k} \beta_i x_i + \sum_{i=1}^{k} \beta_{ii} x_i^2 + \cdots + \sum\sum_{i<j} \beta_{ij} x_i x_j + \varepsilon \tag{1.3}$$

These models, fitted using the method of least squares, rely on proper experimental designs to estimate parameters and ensure accuracy. Figure 1.9 presents a three-dimensional response surface graph alongside a corresponding contour plot, illustrating the variation of responses across the experimental domain [60].



(a) (b)

Figure 1.9 (a) A three-dimensional response surface graph, (b) contour plot [60]

The second-order model is particularly effective in capturing curvature, allowing for precise optimization near the optimum. Proper experimental designs are critical for ensuring model adequacy, checking for lack of fit, and facilitating practical implementation. RSM is widely applied in chemical engineering, manufacturing, and quality improvement to optimize process parameters, enhance performance, and reduce costs [60], [61].

The Box–Behnken is a three-level experimental design that combines features of factorial and incomplete block designs. It is particularly efficient, requiring fewer experimental runs compared to other designs. Table 1.5 illustrates a three-variable (factor) Box–Behnken design.

Table 1.5 A three-variable Box-Behnken design [60], [64], [65]

Run	X_1	X_2	X_3
1	−1	−1	0
2	1	−1	0
3	−1	1	0
4	1	1	0
5	−1	0	−1
6	1	0	−1
7	−1	0	1
8	1	0	1
9	0	−1	−1
10	0	1	−1
11	0	−1	1
12	0	1	1
13	0	0	0
14	0	0	0
15	0	0	0

The Box–Behnken design is also depicted geometrically in Figure 1.10. It is a spherical design, where all experimental points lie on a sphere with a radius of 2. Notably, this design excludes points at the vertices of the cubic region defined by the upper and lower limits of each variable. This feature is particularly beneficial in cases where vertex points correspond to factor-level combinations that are either excessively costly or impractical to evaluate due to physical constraints [60].

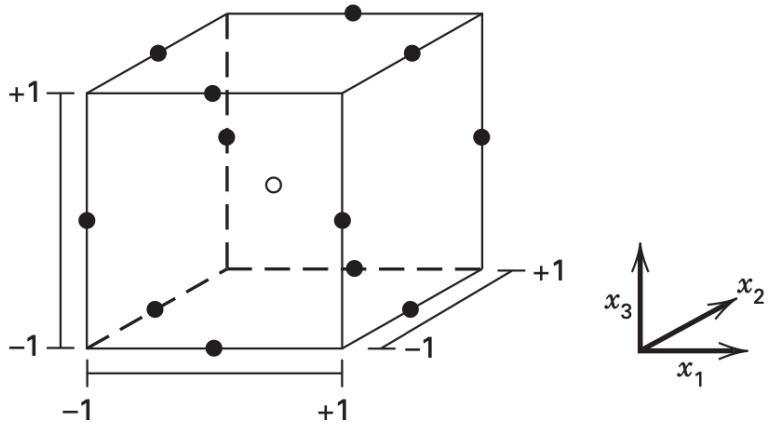


Figure 1.10 A Box-Behnken design for three factors [60]

1.4 Finite Element Analysis

Finite Element Analysis (FEA) is a numerical simulation method used to predict the behavior of materials and structures under various physical conditions. By dividing a system into small, finite elements, FEA allows for detailed calculations of stress, strain, and deformation at localized regions within a complex geometry. This approach is especially valuable in the study of composite materials, where the interplay between fibers and the matrix introduces unique mechanical responses that are difficult to analyze experimentally.

1.4.1 Fundamental Principles of FEA

The core concept of FEA involves discretizing a continuous domain into smaller elements, forming a mesh that represents the geometry of the structure. Numerical methods are then applied to solve governing equations, such as those derived from elasticity or thermo-mechanics, across these elements. For composite materials, the analysis must account for the anisotropic nature of fibers and the heterogeneous properties of the matrix, making the selection of material models and boundary

conditions critical to obtaining accurate results. Key input parameters include elastic constants, fiber orientations, and material interactions [66], [67].

1.4.2 Applications of FEA in Composite Manufacturing

FEA has become an indispensable tool in composite research due to its ability to simulate and predict complex behaviors. Common applications in composite manufacturing include:

- Structural Performance Analysis**:** Simulating the behavior of composites under tensile, compressive, or shear loads to evaluate their suitability for specific applications [67], [68].
- Failure Prediction**:** Identifying potential failure modes, such as matrix cracking, fiber buckling, or delamination, and predicting their onset under given loading conditions [67], [69].
- Process Optimization**:** Assisting in the design of manufacturing parameters, such as fiber orientation, layer stacking, and compaction pressure, to improve product quality [70], [71].
- Validation of Experimental Results**:** Ensuring consistency between theoretical predictions and experimental outcomes, reducing reliance on costly physical testing [71].

1.5 Motivation of the Thesis

This research aimed to optimize the thermoplastic hot-air filament winding process by analyzing the effects of key process parameters. Although some studies have explored thermoplastic filament winding, particularly for GF/PP, GF/PPS, and GF/PA66 composites, systematic optimization and detailed investigations into the influence of process parameters on mechanical properties remain limited.

To address this gap, Response Surface Methodology (RSM) and the Box–Behnken design were employed to evaluate the impact of critical factors—including heater temperature, roller pressure, and winding speed—on the mechanical properties of GF/PP, GF/PPS, and GF/PA66 composites. These statistical techniques helped reduce the number of required experiments while ensuring accuracy, offering

valuable insights into the interplay between process parameters and material performance.

An air-blowing heater was selected for the filament winding system due to its cost-effectiveness, availability, and ease of integration, making it a practical choice for industrial applications. The study materials—GF/PP, GF/PPS, and GF/PA66—each exhibit distinct melting points (173 °C for PP, 282 °C for PPS, and 260 °C for PA66), enabling a comprehensive assessment of processing conditions. GF/PP is widely used in industrial, automotive, and sports applications due to its balance of strength, toughness, and chemical resistance, combined with affordability and ease of processing. PPS, despite its higher processing complexity and cost, provides superior flame resistance and exceptional mechanical and chemical stability, making it ideal for aerospace and industrial applications. PA66 is recognized for its high strength, rigidity, and thermal stability, with widespread use in the automotive, electrical, and industrial sectors due to its excellent wear and fatigue resistance.

By examining these materials within a unified study framework, this research highlights the adaptability of the filament winding process across multiple industries. It provides a significant contribution to both academic knowledge and the industrial application of thermoplastic filament winding, addressing an important research gap.

Ultimately, this study establishes a structured methodology for optimizing thermoplastic filament winding, contributing to the increasing demand for lightweight, high-strength composite materials. By overcoming key processing challenges and applying advanced experimental design techniques, this research paves the way for further innovations in composite manufacturing.

2
MATERIALS AND METHODS

2.1 Materials

Glass fiber-reinforced polyamide 66 (nylon 66), polypropylene (GF/PP) and polyphenylene sulfide (GF/PPS) composite tapes, provided by Celanese (Irving, Texas, USA), were used in this study. The properties of the GF/PP, GF/PPS, and GF/PA66 tapes are presented Table 2.1, as outlined in their commercial technical datasheets (TDS).

Table 2.1 The properties of GF/PP, GF/PPS, and GF/PA66 composite tapes

Properties	**GF/PP**	**GF/PPS**	**GF/PA66**
Density (g/cm^3)	1.656	1.885	1.730
Fiber Content (% by wt.)	70	60	60
Fiber Volume (%)	45	44	40
Tape Thickness (mm)	0.25	0.25	0.30
Tape Areal Weight (g/m^2)	435	620	485
Fiber Areal Weight (g/m^2)	305	372	291
Melt Temperature (°C)	173	282	260
Glass Transition Temperature (°C)	−10	90	50

Celstran® CFR-TP PA66 GF60-02 is a 60% E-glass fiber-reinforced polyamide 66 (nylon 66) composite tape with a high strength-to-weight ratio, excellent toughness, and impact resistance. Its superior thermal stability makes it ideal for industrial, automotive, and sporting goods applications where strength and durability are essential.

Celstran® CFR-TP PP GF70-13 is a 70% E-glass fiber-reinforced polypropylene (PP) composite tape, offering a balance of strength, toughness, and chemical resistance. It is well-suited for cost-sensitive industrial and automotive applications due to its ease of processing.

Celstran® CFR-TP PPS CF60-01 is a 60% carbon fiber-reinforced polyphenylene sulfide (PPS) composite tape with high mechanical strength, chemical resistance, and excellent flame, smoke, and toxicity (FST) performance. It is widely used in aerospace, oil and gas, and industrial sectors, where lightweight and high-performance materials are required.

Before composite production, the tapes were slit into 5 mm wide strips (slit tapes).

2.2 Method

The methodology of the study is given in Figure 2.1. The flowchart illustrates the sequential steps undertaken in this research to optimize the filament winding process for continuous fiber reinforced thermoplastic composites.

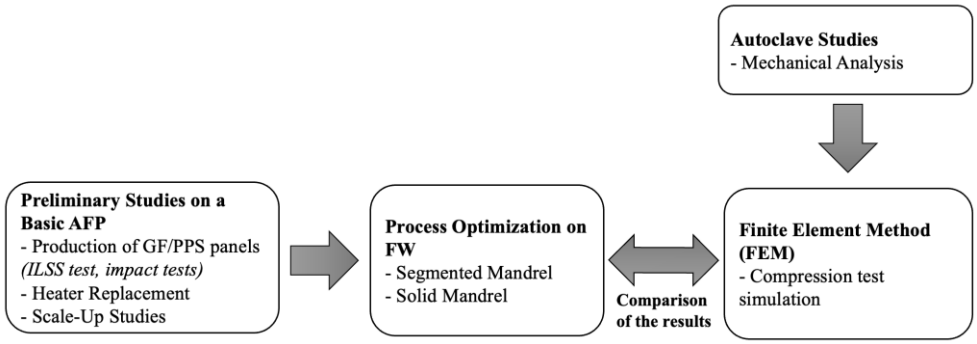


Figure 2.1 Methodology of the thesis

2.3 Preliminary Studies on a Basic AFP

The preliminary studies were conducted using a lab-scale Automated Fiber Placement (AFP) system (Figure 2.2). The system was equipped with a towpreg unloading, tensioning, and tractor/feeder mechanism, supported by a carousel placed in front of the setup for efficient material handling. For heating, a Steinel HL2020E gas blower heater capable of delivering air at temperatures up to 630 °C was employed. Compaction of the materials was achieved using a pressure-

controlled roller connected to a pneumatic regulator for precise pressure application.



Figure 2.2 Lab-scale AFP system

The primary objective was to optimize the processing conditions of GF/PPS composites. The process parameters of heater temperature, roller pressure, and winding speed were systematically studied to understand their influence on the quality and consistency of the fiber placement process. These trials provided crucial insights into the behavior of the GF/PPS under varying processing conditions, laying the groundwork for subsequent optimization and scale-up efforts. The process factors and their corresponding levels, which were used in the Box-Behnken experimental design are listed in Table 2.2.

Table 2.2 The coded process parameters

Parameters	**Code**	**Levels**		
		-1	**0**	**1**
Temperature (°C)	A	450	500	550
Pressure (bar)	B	3	4	5
Speed (mm/min)	C	50	75	100

Table 2.3 Box–Behnken experimental design used in the production of GF/PPS composite panels

No	Levels of the Parameters			Process Parameters		
	A	**B**	**C**	**Temperature (°C)**	**Pressure (MPa)**	**Speed (mm/min)**
1	-1	-1	0	450	0.3	75
2	1	-1	0	550	0.3	75
3	-1	1	0	450	0.5	75
4	1	1	0	550	0.5	75
5	-1	0	-1	450	0.4	50
6	1	0	-1	550	0.4	50
7	-1	0	1	450	0.4	100
8	1	0	1	550	0.4	100
9	0	-1	-1	500	0.3	50
10	0	1	-1	500	0.5	50
11	0	-1	1	500	0.3	100
12	0	1	1	500	0.5	100
13	0	0	0	500	0.4	75
14	0	0	0	500	0.4	75
15	0	0	0	500	0.4	75

The process window was established based on insight from the DSC analysis of the GF/PPS, GF/PP, and GF/PA66 tapes, where the melting and degradation temperatures were determined (see Section 2.6).

A 3-factor, 3-level, 15-experiment Box-Behnken experimental design, as illustrated in Table 2.3, was implemented to systematically evaluate the effects of key process parameters of GF/PPS composites. Interlaminar shear strength (ILSS) and impact tests were conducted to assess the degree of adhesion between the composite layers.

2.3.1 Heater Replacement

An air-blowing heater, featuring a 5 mm pipe-type nozzle, was integrated into the AFP system to improve thermal efficiency (Figure 2.3). The main difference compared to the previous heater (Steinel HL2020E) is the adjustable airflow, which allows for precise temperature control. It was insulated with refractory material to prevent heat loss around the heater and the nozzle. The nozzle's design enabled a focused and precise application of heat to the processing area, addressing the limitations of the previous heater and enhancing the overall thermal performance of the system. Additionally, the new heater allowed for adjustments in both air flow rate and temperature, providing greater control over the heating process.



Figure 2.3 The heater used in FW and AFP systems

The properties of the new heater are detailed in Table 2.4. These properties were carefully selected to ensure compatibility with the required processing conditions and to facilitate consistent heating across the system.

Table 2.4 Properties of the heater used in Filament Winding (FW) and Automated Fiber Placement (AFP) systems

Brand / Model	Leister / Diode PID
Voltage	~230 V
Power	1600 W
Frequency	50 / 60 Hz
Temperature Range	20 – 600 ˚C
Dimensions	265 x 57 mm
Weight	1.15 kg
Heating Mechanism	Adjustable-flow pressurized air

To study the effects of airflow, two experiments were conducted under different air pressure conditions. To observe the temperature changes during the laying process in the AFP system (Figure 2.4), K-type thermocouples were integrated into the system, and connected to a data logger capable of continuous temperature measurement. This setup enabled precise monitoring of temperature variations in real-time, providing critical data to evaluate the heater's performance. Continuous temperature measurements were made from various regions of the laying system while GF/PPS slit tapes were consolidated as three-layer laminates.

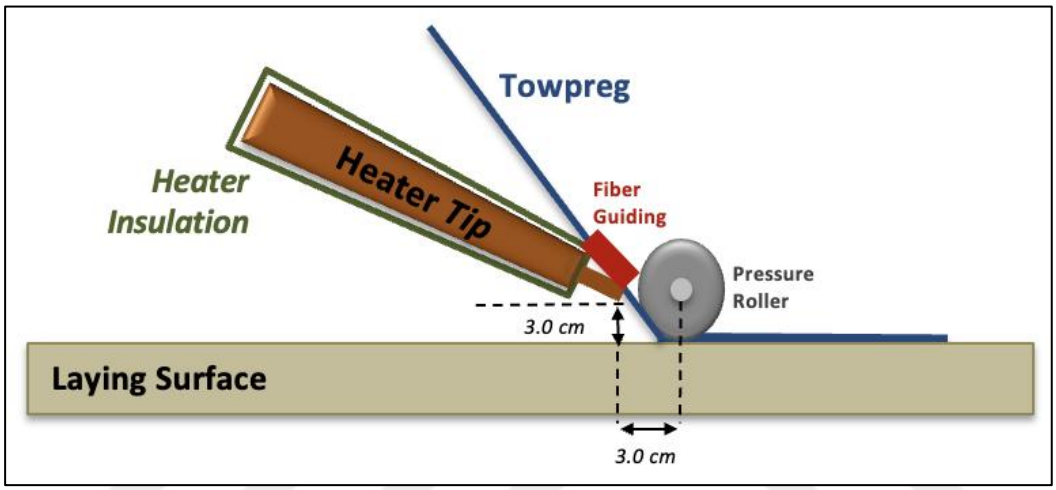


Figure 2.4 Schematic of the AFP system used in this study

Table 2.5 defines the abbreviations and parameters used throughout the study. Key abbreviations are as follows:

- T_{S0} represents the adjusted surface temperature, which is the set temperature of the laying surface.
- T_{S1} denotes the measured surface temperature, the actual temperature recorded at the surface during the laying process.
- v indicates the laying speed, which represents the speed of the laying head and so the slit tape feed in mm/min.
- P_R refers to the roller pressure, indicating the applied pressure on the slit tape during the laying process.
- P_H shows the heater's air pressure, which represents the air pressure output of the heater.

- T_{H0} refers to the adjusted heater temperature, the target temperature set for the heater.
- T_1, T_2, and T_3 represent the measured temperatures recorded during the laying process, corresponding to different layers of the slit tape. These measurements were taken at the same location but on separate layers. The compaction roller traversed all three thermocouples simultaneously, allowing for precise and synchronized temperature recordings across the different layers at the same point. This approach ensures an accurate representation of the thermal behavior within each layer during the process.

Table 2.5 Abbreviations used in the temperature investigation study

Adjusted Surface Temperature (°C)	T_{S0}
Measured Surface Temperature (°C)	T_{S1}
Laying Speed (mm/min)	v
Roller Pressure (bar)	P_R
Heater Air Pressure (bar)	P_H
Adjusted Heater Temperature (°C)	TH_0
Measured Temperature During the Laying of First Layer (°C)	T_1
Measured Temperature During the Laying of Second Layer (°C)	T_2
Measured Temperature During the Laying of Third Layer (°C)	T_3

The parameters of the experiments are outlined in Table 2.6. The primary objective was to analyze the system's thermal behavior under different pressure conditions and minimize the discrepancy between the heater's set temperature and the actual temperature applied to the process.

The introduction of the new heater, combined with the advanced temperature monitoring system, enabled a comprehensive analysis of the temperature profile within the AFP system. This ensured that stable and uniform heating conditions were achieved, which are essential for the successful processing of thermoplastic composites.

Table 2.6 Temperature change investigation studies

Experiment No	T_{S0}	T_{S1}	v	P_R	P_H	T_{H0}
1	90	70	400	5	0.50	595
2	90	70	400	5	0.25	550

2.3.2 Scale-Up Studies

The schematic of the thermoplastic filament winding system is illustrated in Figure 2.5.

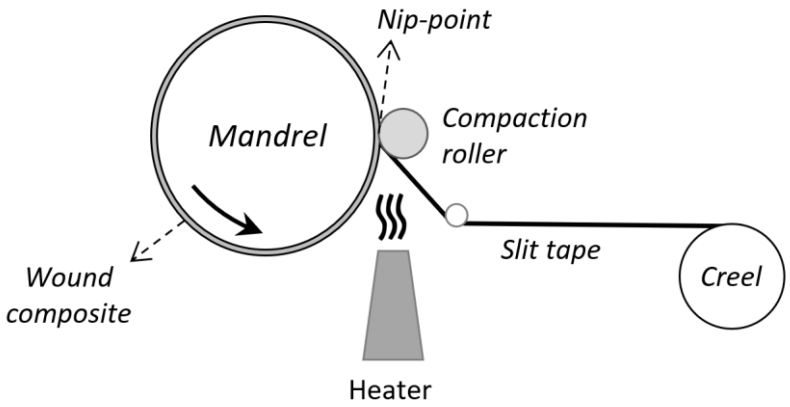
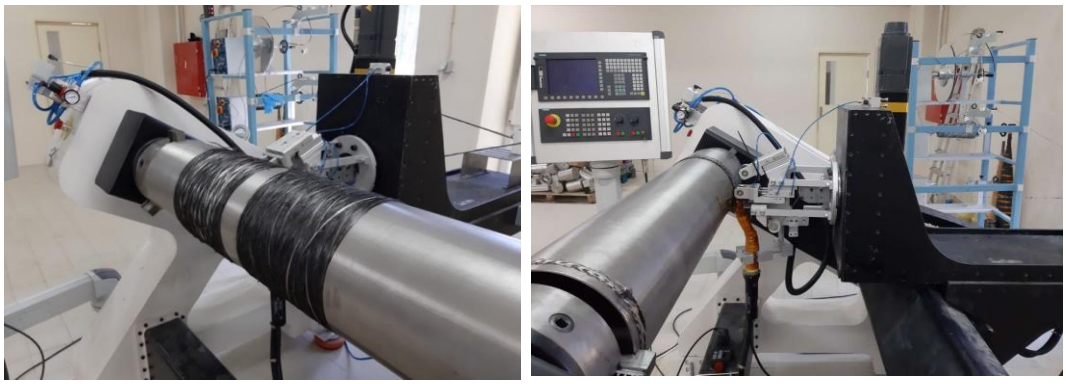


Figure 2.5 Schematic of filament winding system

The results from the preliminary studies were applied to the filament winding system, a tailor-made laboratory-scale machine developed by Mir Araştırma ve Geliştirme Inc. (Figure 2.6). The same heater, heater position, roller, and roller compaction force that were determined with AFP studies were integrated into the system to ensure consistency.



(a) **(b)**

Figure 2.6 Filament winding system (a) front view, (b) side view

The compaction force of the roller (32 mm diameter, 28 mm length), was regulated using a pneumatic valve, and the corresponding linear compaction forces are presented in Table 2.7. The heater temperature was adjustable and varied for different experiments. The heater's nozzle position was fixed within the tape feeding system to maintain consistent heating at the nip point. Tension in the slit tapes was kept constant by the electronic creel, ensuring uniform application during all trials.

Table 2.7 Roller pressure and compaction force

Compaction Pressure (bar)	Compaction Force (N)
4	321.70
5	402.12
6	482.55

For the scale-up experiments, GF/PPS composites were produced using a 200 mm diameter cylindrical mandrel made of stainless steel. The slit tapes utilized in the process were cut GF/PPS prepregs into 5 mm wide. These tapes were carefully prepared to maintain uniformity and compatibility with the winding process.

Specific process conditions were applied, including a heater temperature of 595°C, roller pressure of 5 bar, and a winding speed of 130 mm/min. These conditions were selected based on insights from previous GF/PPS studies to evaluate the feasibility of producing high-temperature composite parts using the filament winding system. The winding process followed a predefined hoop winding pattern (0°) generated in CADWIND® software as illustrated in Figure 2.7.

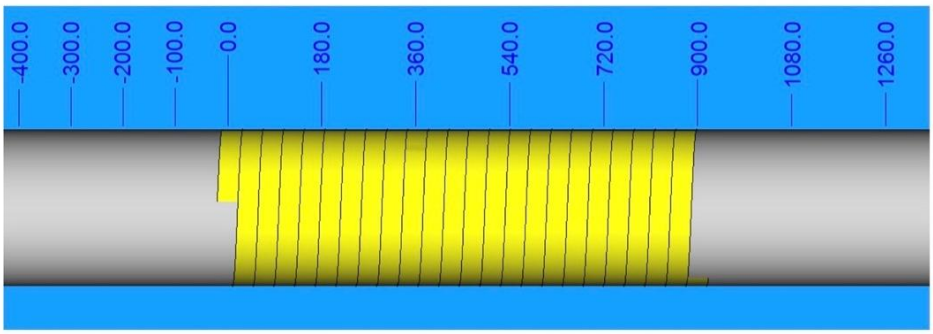


Figure 2.7 The winding pattern created in CADWIND® software

The primary objective was to establish a foundation for assessing the system's performance and identifying opportunities for optimization in future studies. To evaluate the mechanical performance of the manufactured GF/PPS composites, Interlaminar Shear Strength (ILSS) tests were conducted, providing valuable insights into the quality and adhesion between the composite layers.

2.4 Process Optimization on Filament Winding (FW)

This section focuses on the systematic optimization of the filament winding process to improve efficiency, enhance material properties, and minimize defects. Through a combination of experimental analysis and data-driven adjustments, the study aims to establish a robust process framework for the production of advanced composite materials.

Figure 2.8 outlines the systematic methodology that was used in this study, emphasizing the steps required to identify and achieve optimal conditions for composite manufacturing through filament winding.

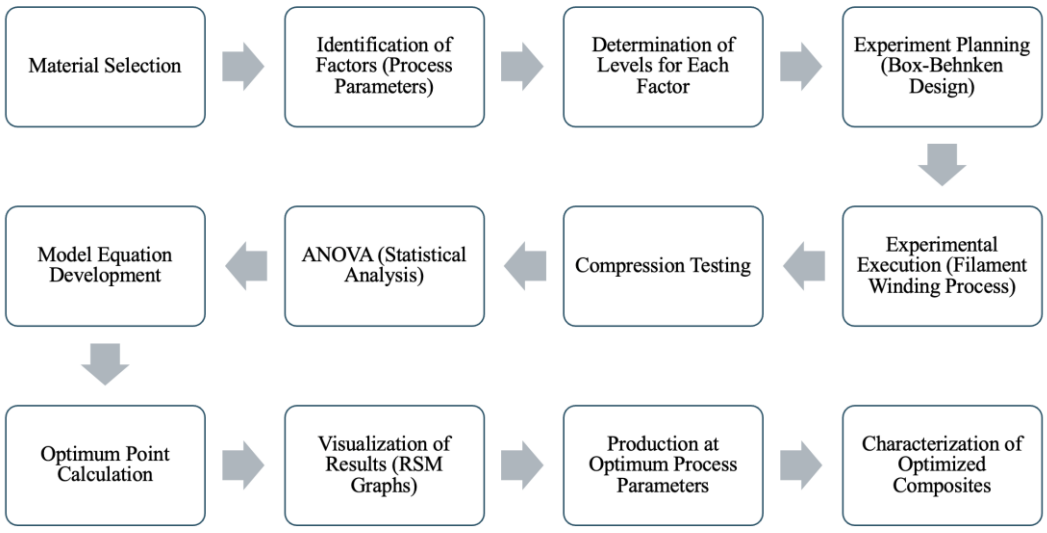


Figure 2.8 Flowchart of the process optimization methodology

A detailed explanation of each step in the flowchart is given as follows:

1. Material Selection: The process begins with selecting the appropriate materials for the study.
2. Identification of Factors (Process Parameters): The critical process parameters, such as heater temperature, roller pressure, and winding speed,

are identified as the key factors that significantly impact the performance of the composites.

3. Determination of Levels for Each Factor: The levels of the identified factors define the boundaries of the process window and represent the range of experimental conditions to be explored. The goal is to establish a feasible range that ensures successful composite production without compromising material quality or process stability. The defined levels serve as the foundation for the experimental design, allowing for systematic exploration and optimization of the process parameters. This approach ensures that the process remains within practical and achievable limits while targeting improved performance.
4. Experiment Planning (Box–Behnken Design): Box–Behnken experimental design minimizes the number of trials while allowing exploration of variable interactions and optimization.
5. Experimental Execution (FW Process): The process involves fabricating composite samples based on the experimental matrix defined in the previous step.
6. Test Results: The quality of the fabricated composite samples is evaluated, particularly bond strength and structural integrity.
7. ANOVA (Statistical Analysis): Analysis of variance (ANOVA) is applied to the test results to determine the statistical significance of the factors and their interactions. This analysis helps to identify the most influential parameters.
8. Model Equation Development: A mathematical model is developed to describe the relationship between the process parameters and the performance of the composites. This model serves as a predictive tool for optimization.
9. Optimum Point Calculation: The optimum combination of process parameters is calculated based on the developed model equation, targeting the highest possible performance.

10. Visualization of Results (RSM Graphs): The results of the analysis are visualized using Response Surface Methodology (RSM) graphs. These graphs provide insights into the effects of the process parameters and their interactions.
11. Production at the Optimum Process Parameters: Composite samples are produced under the calculated optimum process conditions to validate the results and confirm the improvements.
12. Characterization of the Optimized Composites: The optimized composite samples are characterized through additional tests to assess their properties and confirm the success of the optimization process.

Consequently, the defined methodology represents a comprehensive and systematic approach to process optimization, integrating experimental design, statistical analysis, and validation steps to ensure reliable and reproducible results.

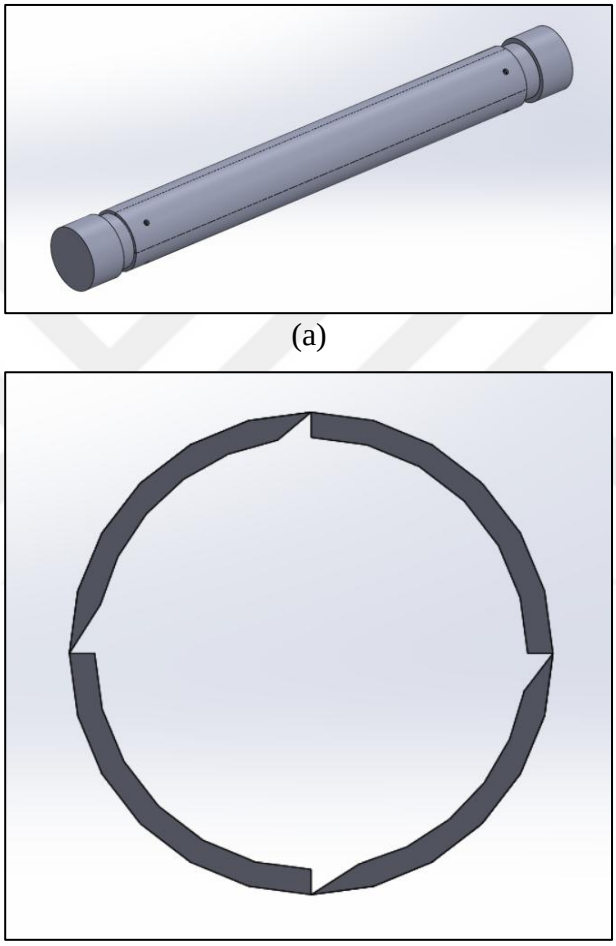
Preliminary studies were carried out to identify the process windows of GF/PP, GF/PPS, and GF/PA66 composites by evaluating adhesion quality and preventing issues such as polymer degradation. Slit tapes obtained from GF/PP, GF/PPS, and GF/PA66 prepregs were used in the experiments. Various combinations of heater temperature (T), roller pressure (P), and winding speed (v) were systematically tested based on the insights gained from AFP studies.

The resulting composite samples were assessed through visual inspections to evaluate adhesion quality and identify potential polymer degradation. These evaluations provided critical insights into the boundaries of each process parameter, so the levels of process parameters were clearly defined. These data served as the foundation for developing a systematic Box-Behnken experimental design plan enabling further optimization and validation of the filament winding process.

In the subsequent step, the Box-Behnken experimental design was implemented, and 70 mm diameter, 2 mm wall thickness (7 layers) and 55 mm length cylindrical GF/PP, GF/PPS, and GF/PA66 composites were fabricated following the defined experimental plan. The winding process followed a predefined hoop winding pattern (0°) generated in CADWIND® software (Figure 2.7).

Two different mandrels were used for the optimization of the FW system: segmented mandrel and solid mandrel.

Firstly, a segmented mandrel (four pieces) was designed, as shown in Figure 2.9, to overcome challenges associated with removing samples from the mandrel. The mandrel had dimensions of 67 mm in diameter, 2 mm wall thickness, and 500 mm in length.

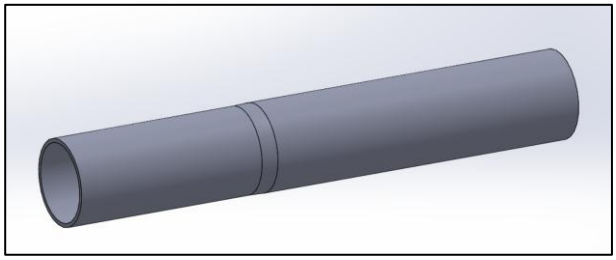


(a)

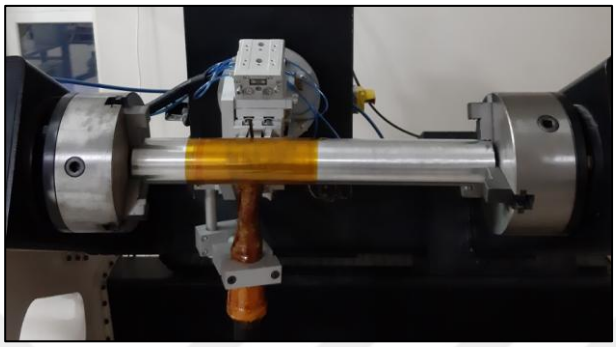
(b)

Figure 2.9 Segmented mandrel; (a) overview, (b) sectional view

Secondly, a solid mandrel (one-piece) was designed, as shown in Figure 2.11, and utilized for the experiments. The mandrel was at the same dimensions as the segmented mandrel (67 mm diameter, 2 mm wall thickness, and 500 mm length), only half of it had a diameter of 66 mm with a smooth transition to facilitate composite movement during removal. Polyimide film and a mold release agent were used to easily remove the composite cylinder after winding.



(a)



(b)

Figure 2.10 Solid mandrel (a) design, (b) mounted on FW system

The manufactured cylindrical composites were subjected to compression testing (Figure 2.11) to assess their rigidity and measure the performance of the processing conditions. Each composite was produced in 3 replicates and the tests were carried out at a speed of 2.5 mm/min.

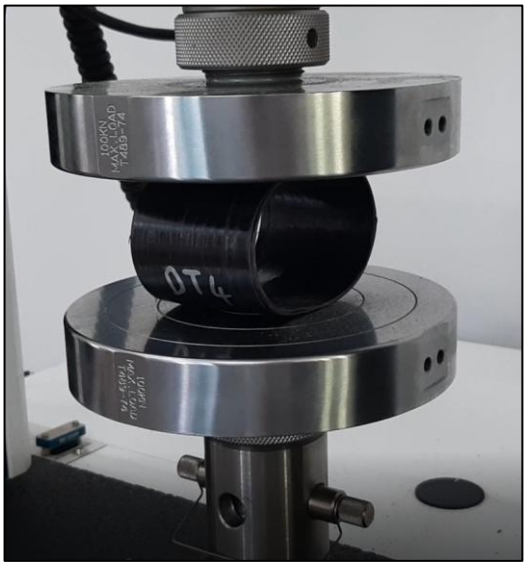


Figure 2.11 Compression test

Once the optimum point of the filament winding process was determined, the cylindrical composites were manufactured at the optimal process conditions and characterized by measurements of density, void content, and crystallinity.

2.5 Autoclave Processing

This section discusses the methodology and outcomes of manufacturing composites through autoclave processing. GF/PP, GF/PPS, and GF/PA66 composite panels were fabricated using the autoclave process.

The autoclave cycle defines the process of material processing under specific temperature and pressure conditions. Initially, the process is carried out under a vacuum. The consolidation process followed specific autoclave cycles tailored for each composite material, as illustrated in Figure 2.12, Figure 2.13, and Figure 2.14 for GF/PPS, GF/PA66, and GF/PP composites, respectively.

In Figure 2.12, the first holding temperature is set to 280°C, which is increased at a rate of 5°C/min and held for 15 minutes under 2 bar pressure. After that, the temperature is increased to a second holding temperature of 320°C at a rate of 5°C/min, holding for 30 minutes under 8 bar pressure.

After the heating process, the cooling is carried out at a rate of 3°C/min. This controlled cooling ensures that the material is gradually brought to a safe processing temperature, preserving its properties. This cycle lasts for 220 min and ensures that the necessary chemical reactions and polymerization processes take place correctly in composite material production.

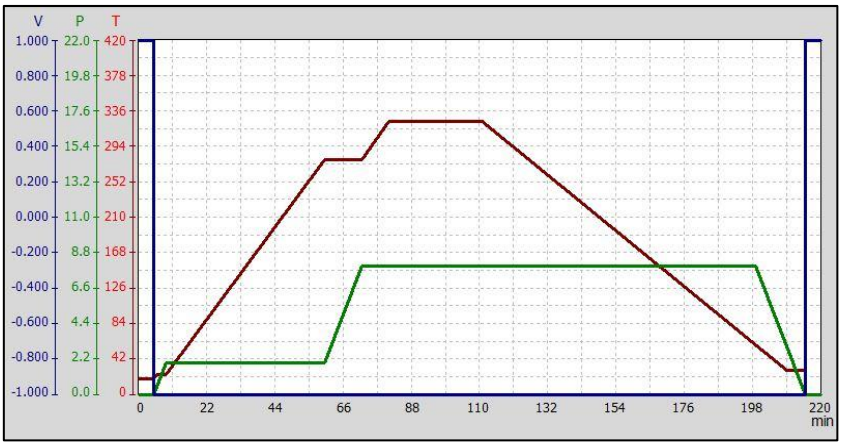


Figure 2.12. Autoclave cycle of GF/PPS (V for vacuum in bar, P for pressure in bar, T for temperature in °C)

In Figure 2.13, the first holding temperature is set to 260°C, which is increased at a rate of 5°C/min and held for 15 minutes under 2 bar pressure. Following this, the temperature is raised to the second holding temperature of 280°C at a rate of 5°C/min, and the material is held for 30 minutes under 8 bar pressure, during which

consolidation takes place. After the heating process, the cooling is carried out at a rate of 3°C/min. The cycle duration was 190 min.



Figure 2.13. Autoclave cycle parameters of GF/PA66 (V for vacuum in bar, P for pressure in bar, T for temperature in °C)

In Figure 2.14, the first holding temperature is set to 180°C, which is increased at a rate of 5°C/min and held for 5 minutes under 2 bar pressure. After that, the temperature is increased to the second holding temperature of 200°C at a rate of 5°C/min, holding for 30 minutes under 5 bar pressure. During this phase, consolidation takes place. After the heating process, the cooling is carried out at a rate of 3°C/min. The cycle duration was 140 min.

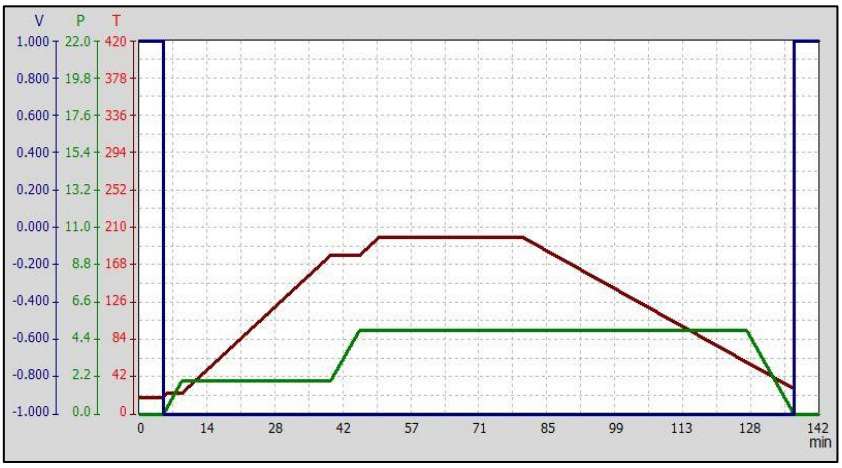


Figure 2.14. Autoclave cycle parameters of GF/PP (V for vacuum in bar, P for pressure in bar, T for temperature in °C)

The autoclave cycles involve the coordinated control of vacuum (V, bar), pressure (P, bar), and temperature (T,°C) to consolidate thermoplastic composite materials. Initially, a vacuum is applied to remove trapped air and volatiles, while temperature

and pressure remain low. As the temperature begins to rise steadily during the heating phase, pressure gradually increases, transitioning from a vacuum-dominated state to pressurization.

During the high-temperature hold phase, both temperature and pressure stabilize, ensuring proper material consolidation. In the cooling phase, temperature and pressure steadily decrease, allowing the material to solidify and stabilize. By the end of the cycle, all parameters return to ambient conditions, completing the process. This cycle ensures proper degassing, curing, and stabilization of the material to achieve optimal properties. Tensile, 3-point bending, impact and ILSS (interlaminar shear strength) tests were applied to all composite laminates.

2.6 Characterization Studies

The test samples were collected from three distinct zones (labelled as zones a, b, and c) of the composites for density measurements and DSC tests, as depicted in Figure 2.15. This sampling approach enabled a comprehensive assessment of the material properties across various regions of the composite structure.

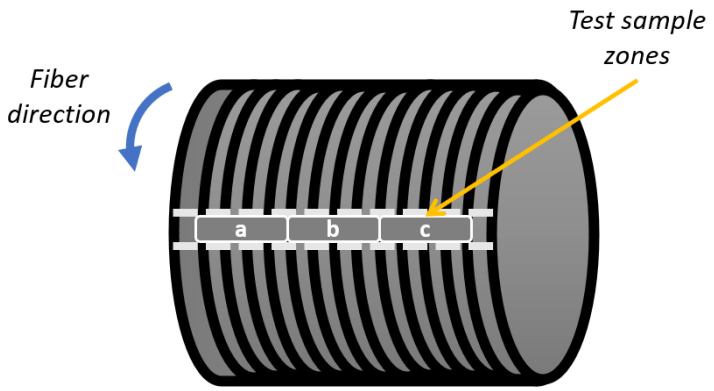


Figure 2.15 Composite structure and test sampling

Archimedes' principle, as outlined in ASTM D792, was utilized to determine the density of the composites [72]. Given that commercial prepreg tapes were utilized in the composite manufacturing process, the theoretical tape density (ρ_t) provided in the commercial TDS, and presented in Table 2.1, was accepted as the reference density for the analysis of composite void content.

DSC tests were conducted by performing a heating run between 30 °C and 290 °C at a heating ramp rate of 10 °C /min. The crystallinity degree (X_C) was calculated by using the following data and Equation (2.1) [73]; heat of fusion (ΔH_f) of PPS is

76.5 J/g [73], heat of fusion of PP is 165 J/g [74], the resin content of GF/PPS composites is 40%, while GF/PP composites have a resin content of 30%, as indicated in Table 2.1.

$$\%X_c = \left(\frac{\Delta H_f}{\Delta H_f^0}\right) x100 \tag{2.1}$$

The void content (V_v), which represents the air trapped within the composite structure, can be determined by calculating the difference between the theoretical and measured composite density using the Equation (2.2) [75].

$$V_v = 100 - \rho_{c,m}\,(^{W_r}/_{\rho_r} + {}^{W_f}/_{\rho_f}) \tag{2.2}$$

W: weight percentage, ρ:density, c: composite, r: resin, f: fiber, m: measured, t: theoretical. So, the Equation (2.2) becomes:

$$V_v = 100\,(1 - {}^{\rho_c}/_{\rho_t}) \tag{2.3}$$

Thus, the void content of filament wound composites was calculated according to Equation (2.3).

DSC tests were conducted using the Perkin Elmer DSC 4000 (Perkin Elmer, Massachusetts, USA) to evaluate the thermal transitions of the materials.

TGA tests were performed with the TA Instruments TGA Q50 (TA Instruments, New Castle, USA) to analyze the thermal stability and decomposition characteristics of the composites.

Tensile (DIN EN ISO 527-5) [76], 3-point bending (DIN EN ISO 14125) [77], and ILSS (DIN EN 2377:1989-10) [78] tests were carried out using the Zwick Universal Testing Machine (Zwick Z250 Allround) (ZwickRoell GmbH & Co. KG, Ulm, Germany) to determine the mechanical performance of the composite materials.

Impact tests were performed following the EN ISO 179-1 standard for unnotched Type 2 [79] using the Instron CEAST 9050 Pendulum Impact Tester (Instron, Norwood, Massachusetts, ABD), with a Devotrans CD-A Notch Cutter (Devotrans, Istanbul, Türkiye) employed for sample preparation to ensure precision.

Unitron Z10 (UNITRON, Commack, New York, USA) microscope was used for morphological analysis of the composites after ILSS test.

The Angelantoni DY1200 Conditioning Chamber (Angelantoni Test Technologies Srl, Perugia, Italy) was utilized to precondition all samples before mechanical testing, ensuring consistent environmental conditions for reliable results.

Italmatic (Via Tazio Nuvolari, Italy) autoclave with air/nitrogen circulation for composite materials & thermoplastics was used in composite panel production.

2.7 Finite Element Method (FEM)

In this study, FEM was utilized to simulate the compressive behavior of GF/PPS, GF/PP, and GF/PA66 composites. The analysis aimed to replicate experimental conditions, using a 3% diameter deflection as the critical deformation criterion, consistent with the compression test (Figure 2.16). This allowed for a direct comparison with physical tests performed on filament-wound (FW) and autoclave-manufactured composites. The simulations provided detailed insights into stress distribution and deformation patterns, helping to identify the strengths and limitations of each manufacturing method [71].

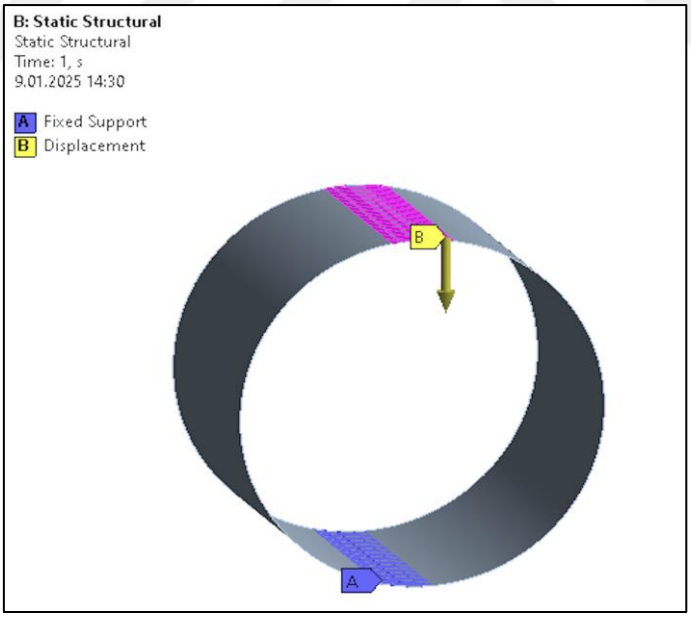


Figure 2.16 The direction of the force in FEA for GF/PPS, GF/PP, and GF/PA66 composites by ANSYS ®

The analysis was conducted using ANSYS 2022, utilizing its comprehensive suite of tools for advanced simulation. The geometry was created using the SpaceClaim module, ensuring efficient and precise modeling. For composite material simulation, the Advanced Composite Preprocessor (ACP) module was employed,

which allowed for the integration of multi-layered composite laminates into the model. A linear static analysis was selected to evaluate the structural response under applied loads, which is suitable for determining stress, strain, and displacement in the composite material.

The meshing process was carried out using the quadrilateral method, providing high-quality elements for accurate stress distribution analysis. The mesh size was set at 2.0 mm, balancing the need for precision with computational efficiency (Figure 2.17). The model utilized a total of 3,190 nodes and 3,080 elements, ensuring a balanced and smooth mesh that captures critical regions while avoiding errors. The system used for solving the analysis was equipped with high-performance hardware: an Intel Core i9-14900HX processor, featuring 8 performance cores and 12 efficiency cores, which ensures smooth parallel processing for complex simulations; a NVidia RTX 4000 Ada graphics card, providing powerful GPU acceleration for visualization and solving large-scale models; and 32GB of DDR5 5600MHz RAM, offering ample memory capacity to handle the intensive demands of the simulation software. This configuration, coupled with ANSYS' advanced features, enabled the accurate modeling and analysis of composite materials, contributing to a deeper understanding of their behavior under different loading conditions.

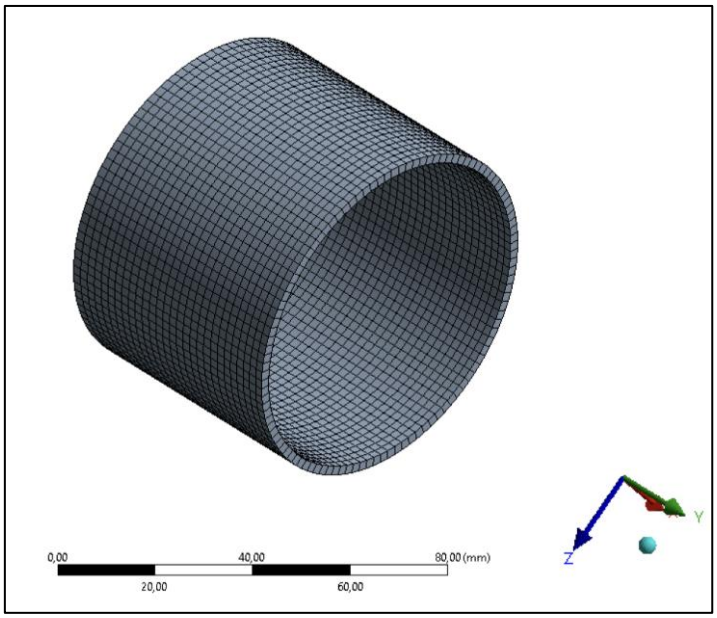


Figure 2.17 Finite element mesh of filament-wound composites (ANSYS ®)

The Young's Modulus values used in the analysis were derived from the tensile test results conducted on panels obtained through the autoclave process (Table 3.2, see section 3.1). By applying these values, the analysis reflects the actual material properties of the composite panels, ensuring the accuracy and relevance of the simulation results in predicting the structural performance under similar conditions. This method of incorporating experimentally obtained material properties enhances the reliability of the simulation and provides a more realistic representation of the composite's behavior in real-world applications.

The material density values used in the analysis were adopted from the TDS (Technical Data Sheets) for the respective composites (Table 2.1, see Section 2.1). Since these values were also applied as the theoretical density in the void content calculations, they have been consistently used throughout the study to maintain alignment and coherence across all components of the analysis.

3
RESULTS AND DISCUSSIONS

3.1 Materials

The thermal properties of the raw materials were analyzed using DSC and TGA tests, while the mechanical properties were evaluated through tensile, 3-point bending, impact, and ILSS tests. The results of the TGA and DSC analysis are shown in Table 3.1. GF/PA66 has a melting temperature of 262°C and a degradation temperature of 362°C, while GF/PPS exhibits a higher melting temperature of 284°C and a degradation temperature of 418°C, indicating better high-temperature resistance. In contrast, GF/PP has the lowest melting temperature of 164°C and a degradation temperature of 299°C, making it less suitable for high-temperature applications. These data are crucial for optimizing manufacturing processes, as they help to select the appropriate process temperatures, ensuring the stability and longevity of composite products during production.

Table 3.1 Thermal properties of GF/PP, GF/PPS, and GF/PA66 tapes

	GF/PA66	**GF/PPS**	**GF/PP**
Melting Temperature	262	284	164
Degradation Temperature	362	418	299

Table 3.2 presents the tensile test results together with relative standard deviations (RSD) for GF/PA66, GF/PP, and GF/PPS composites produced via the autoclave process. GF/PA66 shows a tensile strength of 601 MPa and a modulus of 28.9 GPa with minimal variation (1.11%). GF/PP has a tensile strength of 758 MPa and a

modulus of 32.4 GPa, with a slightly higher variation (1.63%). GF/PPS exhibits a tensile strength of 651 MPa and a modulus of 35.7 GPa, with the greatest variation (3.53%). GF/PP and GF/PPS have higher strength and modulus values compared to GF/PA66, with GF/PPS showing the highest modulus but also the greatest variability.

Table 3.2 Tensile test results of the composites produced by the autoclave process

Sample No	GF/PA66		GF/PP		GF/PPS	
	Tensile Strength (MPa)	**Tensile Modulus (GPa)**	**Tensile Strength (MPa)**	**Tensile Modulus (GPa)**	**Tensile Strength (MPa)**	**Tensile Modulus (GPa)**
1	605	29.3	761	32.0	660	35.5
2	593	29.1	756	33.0	619	34.5
3	604	28.2	756	32.2	673	37.0
Mean	601	28.9	758	32.4	651	35.7
RSD	1.11	2.03	0.38	1.63	4.33	3.53

Figure 3.1 shows tensile test samples before and after testing, as indicated by the captions (a) and (b).



(a) **(b)**

Figure 3.1 Tensile test samples (a) before and (b) after the test

Table 3.3 presents the ILSS test results for GF/PA66, GF/PP, and GF/PPS composites produced via the autoclave process. GF/PA66 shows the highest shear strength consistency, with a mean value of 68.63 MPa and a low standard deviation of 0.34%. GF/PP has a mean shear strength of 33.13 MPa, with a slightly higher standard deviation of 0.86%, indicating some variability. GF/PPS, while having the

highest shear strength of 55.16 MPa, also shows the most variation, with a standard deviation of 1.12%.

Table 3.3 ILSS test results of the composites produced by the autoclave process

Sample No	GF/PA66	GF/PP	GF/PPS
	Shear Strength (MPa)	**Shear Strength (MPa)**	**Shear Strength (MPa)**
1	68.90	33.42	54.63
2	68.51	32.85	55.84
3	68.49	33.11	55.02
Mean	68.63	33.13	55.16
RSD	0.34	0.86	1.12

Table 3.4 presents the impact test results for GF/PA66, GF/PP, and GF/PPS composites. GF/PPS shows the highest impact strength (280.08 kj/m²) and energy (8.82 J), with low variability (1.11% and 0.57%, respectively). GF/PP follows with consistent performance, exhibiting a mean impact strength of 249.24 kj/m² and impact energy of 7.82 J, with very low standard deviations. GF/PA66, while having the lowest impact strength (165.34 kj/m²) and energy (5.16 J), shows higher variability, especially in impact strength (1.70%) and energy (2.64%). These results highlight GF/PPS's superior impact resistance and GF/PP's consistent performance.

Table 3.4 Impact test results of the composites produced by the autoclave process

Sample No	GF/PA66		GF/PP		GF/PPS	
	Impact Strength (kj/m^2)	**Impact Energy (J)**	**Impact Strength (kj/m^2)**	**Impact Energy (J)**	**Impact Strength (kj/m^2)**	**Impact Energy (J)**
1	166.12	5.11	249.74	7.78	280.3	8.87
2	167.69	5.31	249.07	7.74	276.86	8.77
3	162.22	5.05	248.92	7.95	283.08	8.82
Mean	165.34	5.16	249.24	7.82	280.08	8.82
RSD	1.70	2.64	0.18	1.43	1.11	0.57

Table 3.5 presents the three-point bending test results for GF/PA66, GF/PP, and GF/PPS composites. GF/PPS shows the highest flexural strength (804 MPa) and modulus (27.8 GPa), followed by GF/PP, which has a moderate strength (641 MPa) and modulus (26.3 GPa). GF/PA66 displays the lowest flexural modulus (24.0 GPa) but similar strength (740 MPa). The standard deviation for modulus is higher in GF/PA66 and GF/PPS, indicating more variability in stiffness, while GF/PP demonstrates more consistency in flexural strength. These results guide the selection of materials based on the desired balance of strength and stiffness.

Table 3.5 Three-point bending test results of the composites produced by the autoclave process

Sample No	GF/PA66		GF/PP		GF/PPS	
	Flexural Strength (MPa)	**Flexural Modulus (GPa)**	**Flexural Strength (MPa)**	**Flexural Modulus (GPa)**	**Flexural Strength (MPa)**	**Flexural Modulus (GPa)**
1	727	20.1	630	27.5	822	26.5
2	744	25.5	664	27.4	787	32.5
3	749	26.3	629	23.9	802	24.5
Mean	740	24.0	641	26.3	804	27.8
RSD	1.56	14.07	3.11	7.81	2.18	14.96

3.2 Preliminary Studies on a Basic AFP

In the filament winding process, the optimization of the laying process is critical for achieving high-quality material properties. To achieve this, a Box-Behnken experimental design was employed for GF/PPS composite production. This design involves the investigation of three process parameters, each tested at three distinct levels, resulting in a total of 15 experiments.

The composite panels produced through this approach were subjected to two important mechanical tests: the Interlaminar Shear Strength (ILSS) test and the impact test. The ILSS test, denoted as R_1, provides insight into the shear strength between layers of the composite, a key indicator of the material's durability under stress. The impact test, referred to as R_2, evaluates the composite's ability to withstand sudden forces or shocks. The results of these tests, alongside the

corresponding process conditions for each experiment, are summarized in Table 3.6. This table provides a comprehensive overview of how different parameters affect the composite's mechanical performance, offering valuable insights into the optimization of the filament winding process for improved material properties.

Table 3.6 Experimental design of GF/PPS composites for process optimization in the AFP system

Exp. No	Process Parameters			ILSS	Impact
	Temp. (°C)	Pressure (MPa)	Speed (mm/min)	R_1 (MPa)	R_2 (kj/m^2)
1	450	0.3	75	27.07	153.49
2	550	0.3	75	31.47	243.31
3	450	0.5	75	28.71	147.15
4	550	0.5	75	32.07	266.57
5	450	0.4	50	23.37	240.92
6	550	0.4	50	33.05	304.19
7	450	0.4	100	20.40	191.73
8	550	0.4	100	34.84	183.32
9	500	0.3	50	30.42	178.38
10	500	0.5	50	29.37	258.85
11	500	0.3	100	24.74	204.66
12	500	0.5	100	25.97	200.33
13	500	0.4	75	24.79	206.87
14	500	0.4	75	25.40	189.77
15	500	0.4	75	25.10	191.60

Second-degree polynomial regression was applied to the ILSS (Table 3.7 and Table 3.8. In Table 3.7, the regression statistics for the GF/PPS composites based on the ILSS results show a moderate correlation, with a Multiple R-value of 0.8452. The

R Square value of 0.7144 suggests that approximately 71.44% of the variance in the ILSS results can be explained by the model. However, the Adjusted R Square of 0.2002 is relatively low, indicating that the model's predictive power diminishes when accounting for the number of predictors used. The Standard Error of 3.6154 is relatively low, suggesting that the model's predictions are reasonably close to the actual values.

Table 3.7 Regression statistics of GF/PPS composites according to ILSS results

Multiple R	0.8452
R Square	0.7144
Adjusted R Square	0.2002
Standard Error	3.6154
Observations	15

Despite the findings in Table 3.7, the ANOVA results in Table 3.8 indicate that the model may not be statistically significant. The F-value of 1.3893, coupled with a high Significance F value of 0.3751, suggests that the model is not a significantly better fit than a model with no predictors. Therefore, while the model explains a good portion of the variance in ILSS results, its overall reliability and statistical significance need further improvement.

Table 3.8 ANOVA results of GF/PPS composites according to ILSS results

	df	**SS**	**MS**	**F**	**Significance F**
Regression	9	163.4410	18.1601	1.3893	0.3751
Residual	5	65.3552	13.0710		
Total	14	228.7962			

In Table 3.9, the regression statistics for the GF/PPS composites based on the impact test results indicate a moderate correlation, with a Multiple R of 0.8010. The R Square value of 0.6416 suggests that the model explains about 64.16% of the variance in the impact test results. However, the Adjusted R Square value of -0.0035 is negative, indicating that the model is overfitted and does not improve prediction when accounting for the number of predictors. The Standard Error of

47.6883 is relatively high, suggesting that the model's predictions may have substantial errors.

Table 3.9 Regression statistics of GF/PPS composites according to impact test results

Multiple R	0.8010
R Square	0.6416
Adjusted R Square	-0.0035
Standard Error	47.6883
Observations	15

The ANOVA results in Table 3.10 further highlight the model's limitations, with a low F-value of 0.9946 and a high Significance F-value of 0.5331, indicating that the model is not statistically significant. In conclusion, although the model explains some of the variation in the impact test results, it lacks the statistical significance needed to be considered reliable. Further optimization and model refinement are necessary to improve its predictive accuracy and statistical power.

Table 3.10 ANOVA results of GF/PPS composites according to impact test results

	df	**SS**	**MS**	**F**	**Significance F**
Regression	9	20356.8493	2261.8721	0.9946	0.5331
Residual	5	11370.8668	2274.1734		
Total	14	31727.7160			

Although the PPS polymer melted during the experiments, the established models did not fit well with the second-degree polynomial approach. As a result, it was decided to replace the heating system with a more efficient alternative to enhance the system's performance and achieve more reliable results in future experiments.

3.2.1 Heater Replacement

In the AFP process, temperature control is crucial for ensuring the proper bonding and quality of the composite layers. The temperature profiles for each layer during the process are shown in Tables 3.11 and 3.12, which illustrate the temperature variations across the layers in different experiments.

In the first experiment (Table 3.11), it can be observed how the temperature decreases progressively from the first to the third layer. The maximum temperature in the first layer reaches 149°C, which is the highest in this sequence. As the layers are laid down, the temperature begins to drop, reaching 134°C in the second layer and 118°C in the third layer. This gradual decrease indicates that heat is being dissipated across the layers during the process, potentially impacting the consolidation and the overall integrity of the composite.

Table 3.11 Maximum temperature in AFP laying during Experiment-1

Laying Number	max. T_1	max. T_2	max. T_3
1st Layer	149	24	25
2nd Layer	134	151	25
3rd Layer	118	124	146

Figure 3.2 illustrates the temperature profile during the laying of the first layer in the AFP process during Experimen-1.

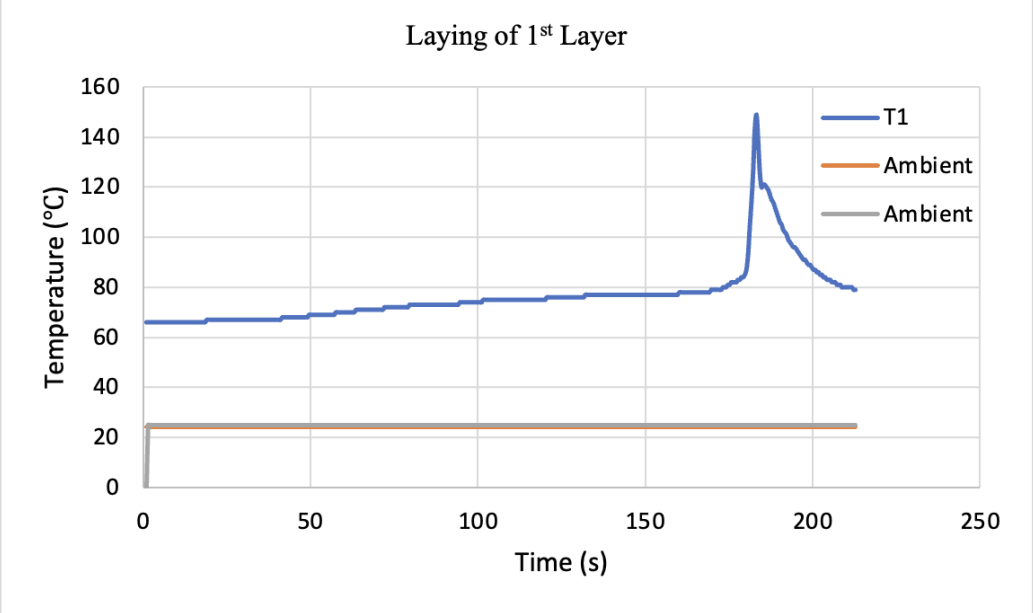


Figure 3.2 Temperature profile of the 1st layer laying during Experiment-1

Figure 3.3 illustrates the temperature profile during the laying of the second layer in the AFP process during Experimen-1.

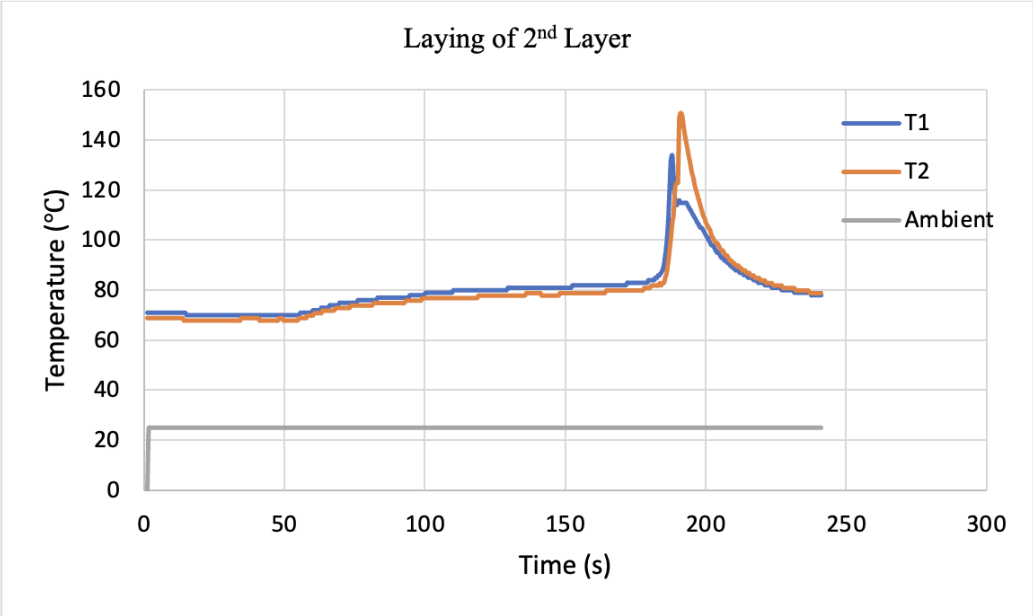


Figure 3.3 Temperature profile of the 2nd layer laying during Experiment-1

Figure 3.4 illustrates the temperature profile during the laying of the third layer in the AFP process during Experimen-1.

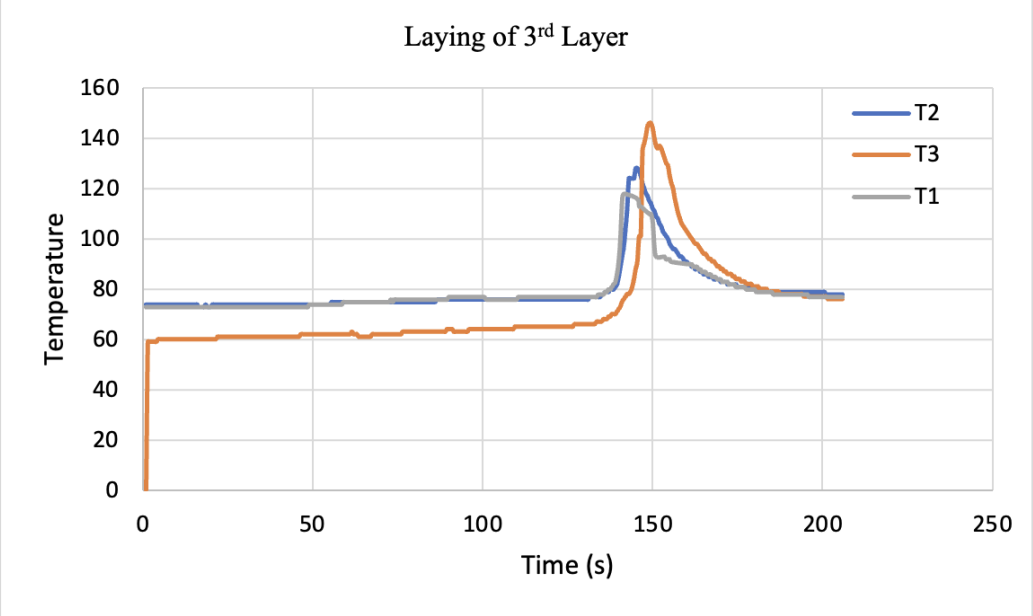


Figure 3.4 Temperature profile of the 3rd layer laying during Experiment-1

The second experiment in Table 3.12 shows similar trends, with temperatures dropping from 125°C in the first layer to 122°C in the subsequent layers, reaching a significant peak of 203°C and 209°C in the third layer, likely due to the specific conditions of the heating system.

Table 3.12 Maximum temperature in AFP laying during Experiment-2

Laying Number	max. T_1	max. T_2	max. T_3
1st Layer	125	27	28
2nd Layer	122	157	28
3rd Layer	122	203	209

Figure 3.5 illustrates the temperature profile during the laying of the first layer in the AFP process during Experimen-2. In the first layer, the temperature reached a maximum of 125°C for T_1, with temperatures for T_2 and T_3 remaining quite low at the ambient temperature of 27°C and 28°C, respectively

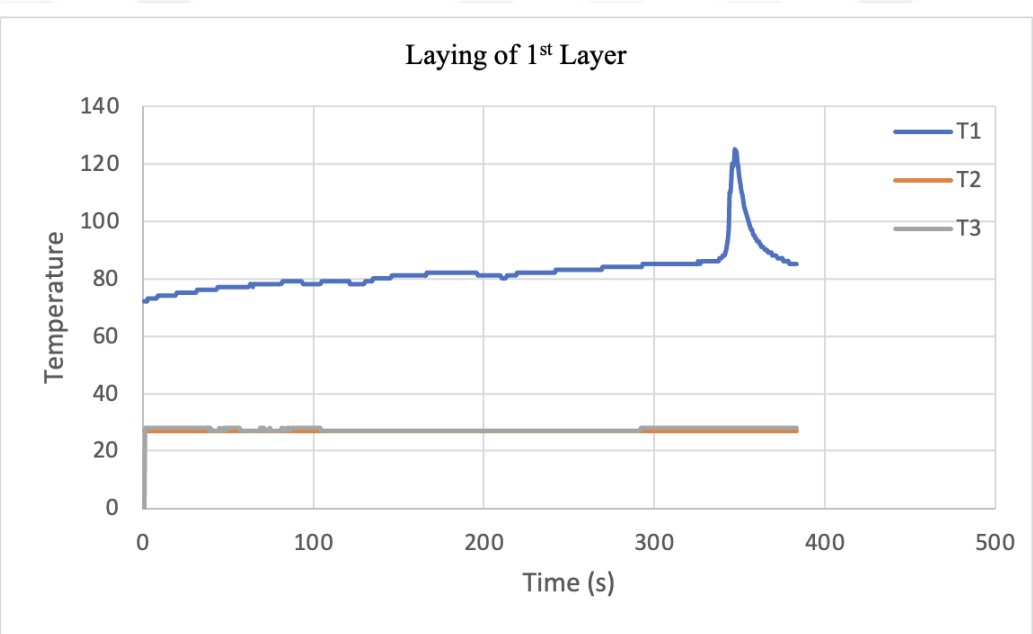


Figure 3.5 Temperature profile of the 1st layer laying during Experiment-2

Figure 3.6 illustrates the temperature profile during the laying of the second layer in the AFP process during Experimen-2. The temperature of T_1 drops slightly to 122°C, but T_2 increases to 157°C as expected.

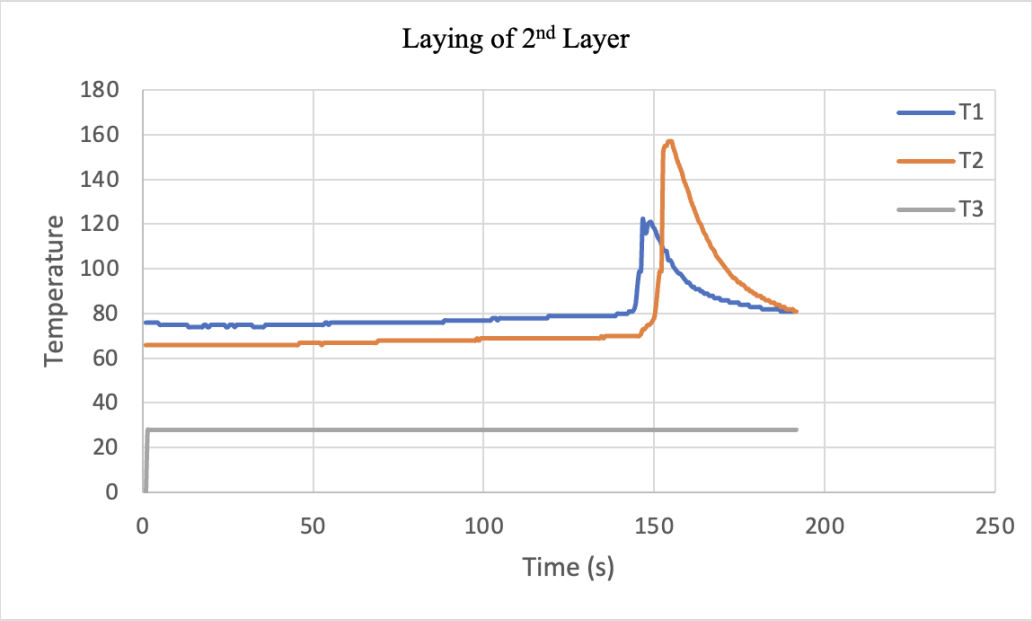


Figure 3.6 Temperature profile of the 2nd layer laying during Experiment-2

Figure 3.7 illustrates the temperature profile during the laying of the third layer in the AFP process during Experimen-2. T_1 remains at 122°C, but T_2 and T_3 increase significantly to 203°C and 209°C, respectively.

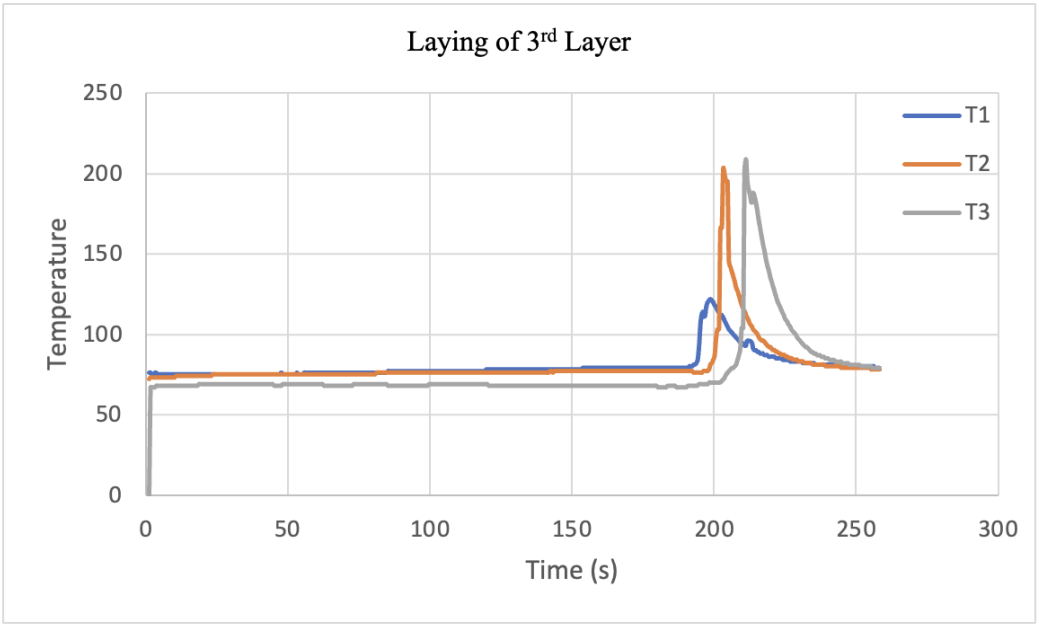


Figure 3.7 Temperature profile of the 3rd layer laying during Experiment-2

The temperature reductions between layers (approximately 10–15°C) suggest that the system experiences significant heat loss, which could be due to the open system's vulnerability to external airflow fluctuations. The observed lower temperatures compared to the melting point of the PPS polymer and the heater

temperature could be further influenced by challenges in accurately measuring the temperature at the nip point. Despite these discrepancies, the visual confirmation of PPS polymer melting indicates that the process temperature remains within the expected range.

The results indicate that higher temperature values can be achieved when a lower airflow is set on the heater. In Experiment-1, the heater air pressure was set to 0.5 bar, while in Experiment-2, it was reduced to 0.25 bar. As a result, the maximum recorded temperatures in Experiment-2 were consistently higher than those in Experiment-1. This suggests that reducing air flow minimizes heat loss, leading to improved thermal efficiency during the AFP process. Therefore, 0.25 air pressure was used during the rest of the study.

3.2.2 Scale-Up Studies

After completing the AFP trials, the process was scaled up to filament winding. This transition allowed the findings from the AFP studies to be applied and validated in a larger, more advanced filament winding system, demonstrating the feasibility of scaling up the composite production process while maintaining consistency and performance.

The preliminary studies conducted on the AFP system yielded the following results, which were subsequently implemented in the filament winding system:

- Heater Nozzle Position: The nozzle position was optimized to maintain a maximum horizontal and vertical distance of 3-3 cm from the roller nip point for effective heating.
- Heat Loss: Insulation of the heater minimized air output at the nozzle connection point and reduced heat loss significantly.
- Fiber Angle: The optimal angle between the fiber and the roller was determined to be 45°, ensuring proper alignment and tension during winding.
- Mandrel Size: To simulate the laying process, a large diameter (200 mm) mandrel was used for initial/scale-up trials to produce GF/PPS composites.

GF/PPS slit tapes were successfully consolidated in the filament winding system. A high-quality, rigid GF/PPS composite cylinder was produced as illustrated in Figure 3.8, and ILSS tests were conducted to assess its performance.



Figure 3.8 GF/PPS composite produced by filament winding process

The test results of filament wound GF/PPS composite demonstrate consistent interlaminar shear strength (ILSS) under identical process conditions (heater temperature of 595°C, pressure of 5 bar, and speed of 130 mm/min). In Table 3.13, ILSS test results of the three samples are presented. The average ILSS is 158 ± 8 MPa and the results indicate a stable and reliable production process, with strong interlaminar bonding achieved across the samples. The close range of ILSS values reflects the repeatability of the AFP system and confirms its effectiveness in producing high-quality composites under these specific conditions.

Table 3.13 Filament winding process conditions and ILSS test results of GF/PPS composites

Material	**T_{S0} (°C)**	**P_R (bar)**	**v (mm/min)**	**ILSS (MPa)**
1	595	5	130	156
2	595	5	130	167
3	595	5	130	151
			Mean	158 ± 8

It can be concluded that the successful application of findings from the AFP studies to the filament winding system enabled an effective scale-up of the production process while ensuring consistency and reliability. In the subsequent phase of the

study, the process optimization for GF/PP, GF/PPS, and GF/PA66 composites was carried out using the filament winding system.

3.3 Process Optimization of Filament Winding (FW)

3.3.1 Segmented Mandrel

Preliminary studies were conducted to identify the process windows for GF/PP, GF/PPS, and GF/PA66 composites by evaluating adhesion quality and preventing polymer degradation. Various combinations of heater temperature (T), roller pressure (P), and winding speed (v) were tested, with the results visually assessed for adhesion quality and potential polymer degradation.

For GF/PPS composites, Table 3.14 shows that lower temperatures (450°C, 500°C) and high winding speeds (1600 mm/min) led to poor adhesion, while excessive thermal exposure at 550°C with lower pressures (3-4 bar) caused polymer degradation. In contrast, good adhesion was achieved at higher temperatures (600°C), moderate pressures (4-6 bar), and winding speeds between 400–1200 mm/min. These findings suggest that optimal adhesion requires high temperature, moderate pressure, and controlled winding speed.

Table 3.14 Preliminary studies of GF/PPS composites

Exp. No	T(˚C)	P (bar)	v (mm/min)	Results of Visual Test
1	450	5	400	Poor adhesion
2	550	3	240	Degradation of polymer
3	450	6	800	Poor adhesion
4	550	4	320	Degradation of polymer
5	500	6	1600	Poor adhesion
6	600	4	800	Good adhesion
7	550	6	1200	Good adhesion
8	600	4	400	Good adhesion

For GF/PA66 composites, the findings in Table 3.15 indicate that at 600°C, high winding speeds (1600–2000 mm/min) resulted in poor adhesion, while extremely low speeds (400–800 mm/min) led to polymer degradation and very poor adhesion.

Moderate winding speeds (1200 mm/min) at 600°C and 5–6 bar pressure produced good adhesion, suggesting this as an optimal range. Additionally, at a lower temperature of 550°C and 6 bar pressure, good adhesion was also observed, indicating that reducing the temperature slightly may still yield effective bonding. However, at 500°C, poor adhesion was noted, highlighting that an inadequate temperature compromises bonding. Overall, 600°C with moderate pressure (5–6 bar) and a winding speed of 1200 mm/min appears to be the most effective combination, while excessively high or low speeds negatively impact adhesion quality.

Table 3.15 Preliminary studies of GF/PA66 composites

Exp. No	T(C)	P (bar)	v (mm/min)	Results of Visual Test
1	600	5	2000	Poor adhesion
2	600	5	1600	Poor adhesion
3	600	6	1600	Poor adhesion
4	600	6	1200	Good adhesion
5	600	5	1200	Good adhesion
6	600	6	800	Very Poor adhesion/ Degradation of polymer
7	600	6	400	Very Poor adhesion/ Degradation of polymer
8	500	6	1200	Poor adhesion
9	550	6	1200	Good adhesion

For GF/PP composites, the results in Table 3.16 indicate that higher temperatures (450°C and 350°C) led to polymer degradation, particularly at moderate pressures (5–6 bar) and high winding speeds (1200–2000 mm/min). In contrast, good adhesion was achieved at lower temperatures (300°C and 250°C) with 4 bar pressure and controlled winding speeds (1200–2000 mm/min), suggesting these as optimal conditions. However, at 250°C with 5 bar pressure and 2000 mm/min winding speed, poor adhesion was observed.

Table 3.16 Preliminary studies of GF/PP composites

Exp. No	T(C)	P (bar)	v (mm/min)	Results of Visual Test
1	450	5	1200	Degradation of polymer
2	450	5	1600	Degradation of polymer
3	450	5	2000	Degradation of polymer
4	350	6	2000	Degradation of polymer
5	300	4	1600	Good Adhesion
6	300	4	2000	Good Adhesion
7	250	4	1200	Good Adhesion
8	250	5	2000	Poor Adhesion

Process window for each composite type was determined according to the results of the preliminary studies. The experimental design factors and their respective codes were defined.

Table 3.17 presents the experimental design factors and their respective levels for the GF/PPS composites. Temperature (A) is measured in °C, with three levels specified: 550°C, 575°C, and 600°C, corresponding to factor codes of -1, 0, and 1. Pressure (B), measured in bars, varies between 4, 5, and 6 bars, also represented by the codes -1, 0, and 1. Speed (C), defined as the feed rate in mm/min, is adjusted at three levels: 800, 1200, and 1600 mm/min, with factor codes -1, 0, and 1.

Table 3.17 Experimental design factors and levels of GF/PPS composites

Factors Name	Factor Unit	Factor Codes	Factor Levels		
			-1	0	1
Temperature	^{0}C	A	550	575	600
Pressure	bar	B	4	5	6
Speed	mm/min	C	800	1200	1600

Table 3.18 presents the results of the Box-Behnken experimental design along with the compression tests on GF/PPS composites, including the compressive load values for 15 different experiments across three runs. Each experiment varies the

temperature (T in °C), pressure (P in bar), and speed (v in mm/min), with the compressive load measured for the 1st, 2nd, and 3rd runs. The mean values and relative standard deviation (RSD) for each experiment are also provided. The high RSD values indicate substantial inconsistency in the compressive load measurements, implying that the experimental conditions for this run were not stable or reproducible.

Table 3.18 Box Behnken experimental design and compression test results of GF/PPS composites

Exp. No	T (˚C)	P (bar)	v (mm/min)	Compressive Load (N)				
				1st Run	2nd Run	3rd Run	Mean	RSD
1	550	4	1200	401.32	211.69	159.33	257.45	49.45
2	600	4	1200	483.22	363.03	321.68	389.31	21.55
3	550	6	1200	363.14	329.54	302.28	331.65	9.19
4	600	6	1200	502.99	372.89	383.48	419.78	17.21
5	550	5	800	482.73	409.69	405.27	432.56	10.06
6	600	5	800	455.50	399.04	387.76	414.10	8.76
7	550	5	1600	472.93	345.49	193.81	337.41	41.41
8	600	5	1600	527.91	335.69	383.88	415.83	24.05
9	575	4	800	429.39	409.48	412.39	417.09	2.58
10	575	6	800	391.00	367.45	386.26	381.57	3.27
11	575	4	1600	322.37	382.20	361.26	355.28	8.54
12	575	6	1600	257.60	369.68	305.72	311.00	18.08
13	575	5	1200	536.29	361.56	387.10	428.32	22.03
14	575	5	1200	474.45	366.86	311.46	384.26	21.57
15	575	5	1200	461.13	404.76	401.81	422.57	7.91

Table 3.19 presents the experimental design factors and their respective levels for the GF/PP composites, which are used to optimize the filament winding process. The factors considered are Temperature (A), Pressure (B), and Speed (C), each with

three levels to assess their impact on the composite's performance. Temperature (A) is measured in °C, with three levels: 250°C, 275°C, and 300°C, represented by factor codes -1, 0, and 1, respectively. Pressure (B) is controlled in bars, with levels set at 4, 5, and 6 bars, also represented by factor codes -1, 0, and 1. Pressure plays a critical role in the consolidation of the composite layers during the filament winding process. Speed (C) is expressed in millimeters per minute (mm/min), with levels of 400, 800, and 1200 mm/min, represented by factor codes -1, 0, and 1. This factor controls the rate at which the filament is wound, affecting both the efficiency of the process and the quality of the composite.

Table 3.19 Experimental design factors and levels of GF/PP composites

Factors Name	**Factor Unit**	**Factor Codes**	**Factor Levels**		
			-1	**0**	**1**
Temperature	^{0}C	A	250	275	300
Pressure	bar	B	4	5	6
Speed	mm/min	C	400	800	1200

Table 3.20 presents the Box-Behnken experimental design and the compression test results for the GF/PP composites. The table provides data for 15 different experiments, each varying the three process factors—Temperature (T in °C), Pressure (P in bar), and Speed (v in mm/min)—across different levels. For each experiment, the compressive load is measured for three runs (1st, 2nd, and 3rd), and the mean value for each experiment is calculated. The relative standard deviation (RSD) is also provided to indicate the variability of the compressive load values across the runs for each experiment.

The RSD values are notably high, indicating a significant variability in the compressive load results for the GF/PP composites. For instance, Experiment-1 shows an RSD of 30.93%, which is relatively high, suggesting that the measurements are inconsistent, and the reproducibility of the results might be compromised. Similarly, other experiments such as Experiment-2 (14.20%), Experiment-8 (16.80%), and Experiment-13 (19.46%) also show elevated RSD values, which imply that the compressive load results are fluctuating considerably across different runs.

Table 3.20 Box Behnken experimental design and compression test results of GF/PP composites

Exp. No	T (˚C)	P (bar)	v (mm/min)	Compressive Load (N)				
				1st Run	2nd Run	3rd Run	Mean	RSD
1	550	4	800	401.32	211.69	306.50	306.50	30.93
2	600	4	800	483.22	363.03	423.13	423.13	14.20
3	550	6	800	363.14	458.84	364.14	395.37	13.90
4	600	6	800	502.99	372.89	437.94	437.94	14.85
5	550	5	400	482.73	409.69	446.21	446.21	8.18
6	600	5	400	455.50	399.04	427.27	427.27	6.61
7	550	5	1200	434.93	345.49	390.21	390.21	11.46
8	600	5	1200	527.91	376.71	446.52	450.38	16.80
9	575	4	400	429.39	409.48	419.44	419.44	2.37
10	575	6	400	391.00	367.45	379.23	379.23	3.11
11	575	4	1200	322.37	365.13	343.75	343.75	6.22
12	575	6	1200	257.60	369.68	313.64	313.64	17.87
13	575	5	800	536.29	361.56	448.93	448.93	19.46
14	575	5	800	474.45	366.86	420.65	420.65	12.79
15	575	5	800	461.13	404.76	432.94	432.94	6.51

Table 3.21 provides the experimental design factors and their respective levels for the GF/PA66 composites. Similar to the previous composites, three key process parameters—Temperature (A), Pressure (B), and Speed (C)—are considered in the study. Temperature (A) is measured in °C, with three levels: 550°C, 575°C, and 600°C, corresponding to factor codes of -1, 0, and 1. Pressure (B) is measured in bars, with levels of 4, 5, and 6 bars, represented by the factor codes -1, 0, and 1. Speed (C) is the feed rate in mm/min, with three levels: 400, 800, and 1200 mm/min, again corresponding to factor codes of -1, 0, and 1.

Table 3.21 Experimental design factors and levels of GF/PA66 composites

Factors Name	Factor Unit	Factor Codes	Factor Levels		
			-1	**0**	**1**
Temperature	^{0}C	A	550	575	600
Pressure	bar	B	4	5	6
Speed	mm/min	C	400	800	1200

Table 3.22 presents the Box-Behnken experimental design and the compression test results for GF/PA66 composites. Similar to previous tables, the data includes the three process factors—Temperature (T in °C), Pressure (P in bar), and Speed (v in mm/min)—varied across different levels for 15 experiments. The compressive load (in N) is recorded for three runs (1st, 2nd, and 3rd) in each experiment, with the mean value and the relative standard deviation (RSD) also provided.

Notably, the RSD values indicate the variability of the compressive load results across the three runs for each experiment. For example, Experiment-1 shows an RSD of 22.79%, highlighting a considerable variability in the results, while Experiment 10 exhibits a lower RSD of 8.04%, suggesting more consistency in the compression test results. The mean compressive load values range from around 328.38 N in Experiment-7 (with 550°C, 5 bar, and 1200 mm/min) to 428.27 N in Experiment-6 (with 600°C, 5 bar, and 400 mm/min).

The high RSD values observed in some experiments, such as Experiment-3 (35.85%) and Experiment-1 (22.79%), indicate that the compressive load results fluctuate significantly between runs, which could be due to several factors like inconsistency in the experimental setup or material variability. These variations in the compressive load suggest a need for better control over the process conditions to ensure reproducibility and reliability of the results.

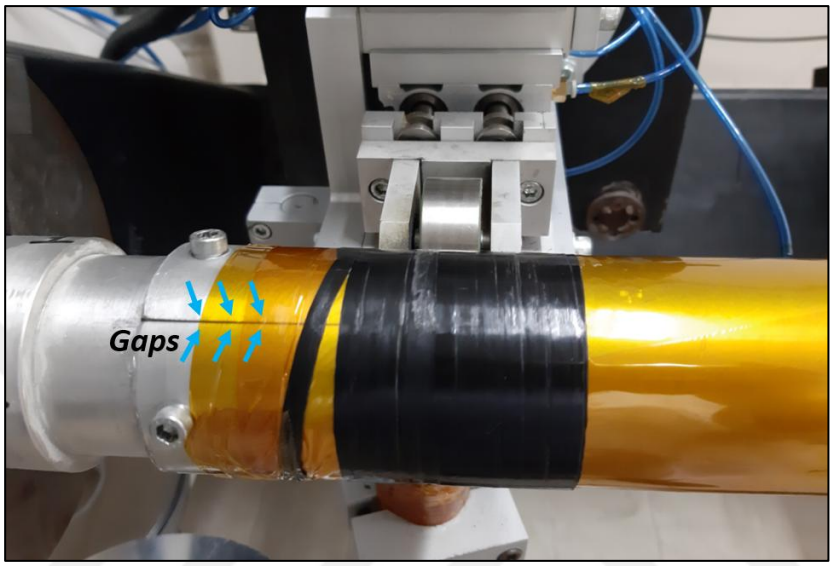
Reducing the RSD and improving the consistency of the compression test results is crucial for ensuring the quality and reliability of the GF/PA66 composites produced under these process conditions. Achieving lower variability will enhance the predictability of the composite's performance, leading to more controlled manufacturing processes and more reliable final products.

Table 3.22 Box Behnken experimental design and compression test results of GF/PA66 composites

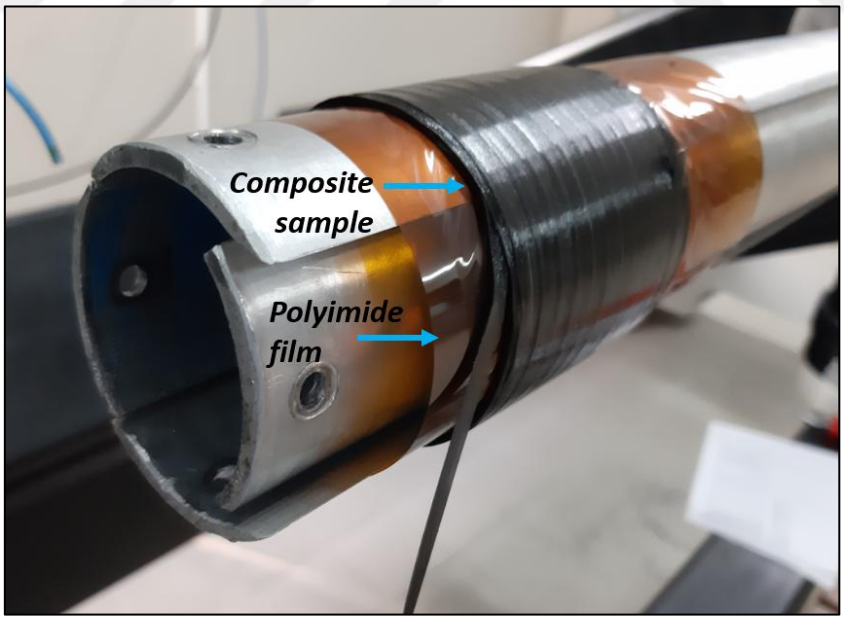
Exp. No	T (°C)	P (bar)	v (mm/min)	Compressive Load (N)				
				1st Run	2nd Run	3rd Run	Mean	RSD
1	550	4	800	533.42	375.43	358.95	422.60	22.79
2	600	4	800	514.95	361.36	321.68	399.33	25.56
3	550	6	800	561.81	329.54	302.28	397.88	35.85
4	600	6	800	502.88	334.13	392.64	409.89	20.91
5	550	5	400	492.46	365.07	402.88	420.14	15.57
6	600	5	400	504.44	377.26	403.11	428.27	15.70
7	550	5	1200	413.73	346.87	224.56	328.38	29.21
8	600	5	1200	429.38	335.69	367.83	377.63	12.61
9	575	4	400	480.13	430.91	365.44	425.49	13.52
10	575	6	400	434.65	370.48	397.45	400.86	8.04
11	575	4	1200	415.03	382.20	374.66	390.63	5.50
12	575	6	1200	478.21	330.14	364.11	390.82	19.85
13	575	5	800	470.09	354.54	379.10	401.24	15.17
14	575	5	800	387.32	345.59	311.46	348.12	10.91
15	575	5	800	410.41	364.73	401.81	392.32	6.19

The compression test results reveal that the high standard deviations indicate poor repeatability in the results for the GF/PPS, GF/PA66, and GF/PP composites. This variability can be attributed to the unwanted gaps between the pieces of the mandrel, as shown in Figure 3.9. These gaps likely caused a notch effect during the compression tests, leading to inconsistent and unstable test outcomes. The notch effect occurs when the test specimens experience concentrated stresses at the gaps, which can affect the uniformity of the compressive force applied and cause fluctuations in the results.

To address this issue and improve the reliability of the process, it was decided to use a solid mandrel in the subsequent experiments. By eliminating the gaps and potential variability caused by the segmented mandrel, the process is expected to become more stable, leading to more consistent and reproducible test results. This adjustment is a critical step in optimizing the manufacturing process and ensuring the quality of the composites produced.



(a)



(b)

Figure 3.9 Segmented mandrel; (a) gaps between pieces, (b) triangle edges

3.3.2 Solid Mandrel

GF/PA66, GF/PPS and GF/PP composites were produced at various process conditions according to a 3-factor, 3-level Box-Behnken experimental design, and a parallel plate compression test was applied. Each sample was manufactured in 3 replicates. The examples of the filament-wound composite cylinders produced in the experiments can be seen in Figure 3.10.



Figure 3.10 Filament-wound composites

The goal of the experiments was to relate the process parameters—temperature, pressure, and speed—to the compressive loads of the composite samples. To analyze the data, ANOVA (Analysis of Variance) was used, and the compliance of a second-order polynomial equation was examined for both GF/PPS and GF/PP composites. The calculations for the analysis were performed using the Stat-Ease 360® software.

Table 3.23 shows the Box-Behnken experimental design and the compression test results for the GF/PPS composites. The table includes data for 15 experiments, with temperature (T in °C), pressure (P in bar), and speed (v in mm/min) as the varying process factors. For each experiment, the compressive load (in N) is measured for three runs (1st, 2nd, and 3rd), and the mean value along with the relative standard deviation (RSD) is provided. For example, Experiment-1, with 550°C, 4 bar, and 1200 mm/min, has a very low RSD of 0.1%, indicating excellent consistency between the runs.

Table 3.23 Box-Behnken experimental design for GF/PPS composites

Exp. No	T (˚C)	P (bar)	v (mm/min)	Compressive Load (N)				
				1st Run	2nd Run	3rd Run	Mean	RSD
1	550	4	1200	3026.3	3024.2	3022.1	3024.2	0.1
2	600	4	1200	3138.8	3002.2	3034.8	3058.6	2.3
3	550	6	1200	2571.6	2704.7	2640.8	2639.0	2.5
4	600	6	1200	3062.9	3118.1	3132.1	3104.4	1.2
5	550	5	800	2866.6	2826.6	3041.4	2911.5	3.9
6	600	5	800	3149.4	3160.2	3170.9	3160.2	0.3
7	550	5	1600	2885.2	2807.5	2851.2	2848.0	1.4
8	600	5	1600	3304.4	3207.6	3241.2	3251.1	1.5
9	575	4	800	3228.0	3272.5	3348.0	3282.8	1.8
10	575	6	800	3133.8	3229.9	3217.1	3193.6	1.6
11	575	4	1600	3497.0	3386.6	3178.7	3354.1	4.8
12	575	6	1600	3039.7	3165.0	3146.2	3117.0	2.2
13	575	5	1200	2976.0	3109.5	3114.7	3066.8	2.6
14	575	5	1200	3028.8	2969.4	3156.6	3051.6	3.1
15	575	5	1200	3062.0	3066.3	3070.2	3066.2	0.1

Each GF/PP sample was manufactured in 3 replicates and the results of compression tests are given Table 3.24. Similar to the previous composites, temperature (T in °C), pressure (P in bar), and speed (v in mm/min) are the factors varied across three levels for 15 experiments. For each experiment, the compressive load (in N) is measured for three runs, with the mean value and relative standard

deviation (RSD) also provided. It can be seen that RSD values are relatively small, indicating that the compression test results for the GF/PP composites are quite consistent and reproducible. For instance, Experiment-2 has an RSD of just 0.7%, suggesting that the measurements are highly stable across the three runs.

Table 3.24 Box-Behnken experimental design for GF/PP composites

Exp. No	T (˚C)	P (bar)	v (mm/min)	Compressive Load (N)				
				1st Run	2nd Run	3rd Run	Mean	RSD
1	250	4	800	2980.6	2699.7	2881.6	2854.0	5.0
2	300	4	800	2791.3	2812.5	2775.5	2793.1	0.7
3	250	6	800	2721.6	2808.2	2756.0	2761.9	1.6
4	300	6	800	2651.3	2506.7	2510.7	2556.3	3.2
5	250	5	400	2650.5	2703.8	2515.7	2623.3	3.7
6	300	5	400	2591.3	2627.5	2725.7	2648.2	2.6
7	250	5	1200	2781.9	2769.0	2764.7	2771.8	0.3
8	300	5	1200	2448.3	2637.9	2494.2	2526.8	3.9
9	275	4	400	2524.5	2597.5	2876.4	2666.2	7.0
10	275	6	400	2649.4	2880.7	2777.0	2769.0	4.2
11	275	4	1200	2906.8	2949.2	3000.1	2952.0	1.6
12	275	6	1200	2423.0	2502.3	2556.3	2493.9	2.7
13	275	5	800	2529.2	2413.8	2644.6	2529.2	4.6
14	275	5	800	2435.9	2440.3	2734.5	2536.9	6.7
15	275	5	800	2502.3	2450.0	2692.3	2548.2	5.0

Table 3.25 presents the results of the compression tests for the GF/PA66 composites. Each sample was manufactured in three replicates. The RSD values in the table indicate the level of variability in the compressive load measurements across the three runs.

Table 3.25 Box-Behnken experimental design for GF/PA66 composites

Exp. No	T (˚C)	P (bar)	v (mm/min)	Compressive Load (N)				
				1st Run	2nd Run	3rd Run	Mean	RSD
1	550	4	800	3401.9	3496.5	3432.2	3443.5	1.4
2	600	4	800	3385.2	3446.1	3507.6	3446.3	1.8
3	550	6	800	3618.9	2915.0	3116.9	3216.9	11.3
4	600	6	800	3091.7	3008.7	2938.9	3013.1	2.5
5	550	5	400	3276.7	3585.6	3689.3	3517.2	6.1
6	600	5	400	3717.5	3570.0	3412.9	3566.8	4.3
7	550	5	1200	3612.2	3570.2	3644.5	3609.0	1.0
8	600	5	1200	3562.8	3809.3	3489.6	3620.6	4.6
9	575	4	400	3517.9	3564.5	3747.4	3609.9	3.4
10	575	6	400	3713.7	3631.1	3457.3	3600.7	3.6
11	575	4	1200	3373.9	3304.6	3290.5	3323.0	1.3
12	575	6	1200	3037.0	3086.5	3201.9	3108.5	2.7
13	575	5	800	3061.4	3053.5	3177.1	3097.3	2.2
14	575	5	800	3333.4	3028.6	3064.6	3142.2	5.3
15	575	5	800	2824.0	2606.4	2648.2	2692.9	4.3

Table 3.26 demonstrates the ANOVA results of the GF/PPS experimental design. The Model F-value of 77.91 indicates the mathematical model's significance, with P-values below 0.0500 for terms A, B, AB, AC, BC, A^2, B^2, and C^2, making them significant. The Lack of Fit F-value of 13.64 suggests that the Lack of Fit is not significant, as there is only a 6.91% chance it could occur due to noise. The Predicted R^2 of 0.8913 and Adjusted R^2 of 0.9802 confirm the model's accuracy, with the difference being less than 0.2. Adeq Precision, with a ratio of 35.8940, indicates an adequate signal (a ratio greater than 4 is desirable). Thus, the model can effectively define the design space for the GF/PPS composite production process.

Table 3.26 ANOVA results of GF/PPS experimental design

Source	**Sum of Squares**	**df**	**Mean Square**	**F-value**	**p-value**
Model	$4.45x10^5$	9	49416.04	77.91	< 0.0001
A	$1.66\ x10^5$	1	$1.66x10^5$	261.54	< 0.0001
B	55342.91	1	55342.91	87.26	0,0002
C	60.62	1	60.62	0.0956	0.7697
AB	46494.91	1	46494.91	73.31	0.0004
AC	5963.36	1	5963.36	9.40	0.0279
BC	5467.76	1	5467.76	8.62	0.0324
A^2	82546.63	1	82546.63	130.15	< 0.0001
B^2	7365.61	1	7365.61	11.61	0.0191
C^2	63055.05	1	63055.05	99.42	0.0002
Residual	3171.23	5	634.25		
Lack of Fit	3023.45	3	1007.82	13.64	0.0691
Pure Error	147.77	2	73.89		
Cor Total	$4.48x10^5$	14			
Fit Statistics					
RSD	25.18	R^2		0.9929	
Mean	3075.29	Adjusted R^2		0.9802	
C.V. %	0.8189	Predicted R^2		0.8913	
		Adeq Precision		35.8940	

ANOVA results of GF/PP composites are shown in Table 3.27, indicate that the model is significant with a Model F-value of 267.68 and a very low probability (0.01%) that such an F-value could occur due to noise. Significant model terms include A, B, AB, AC, BC, A^2, B^2, and C^2, with P-values under 0.0500. The Lack of Fit F-value of 1.43 shows the model fits the experimental data well. The

Predicted R^2 (0.9759) and Adjusted R^2 (0.9942) are in good agreement, with a difference of less than 0.2. Adeq Precision of 51.665 indicates an adequate signal, confirming the model's ability to relate process parameters to the compressive load of the GF/PP composites.

Table 3.27 ANOVA results of GF/PP experimental design

Source	**Sum of Squares**	**df**	**Mean Square**	**F-value**	**p-value**
Model	$2.76x10^5$	9	30670.51	267.68	< 0.0001
A-A	29579.80	1	29579.80	258.16	< 0.0001
B-B	58510.55	1	58510.55	510.66	< 0.0001
C-C	176.51	1	176.51	1.54	0.2696
AB	5245.40	1	5245.40	45.78	0.0011
AC	18175.35	1	18175.35	158.63	< 0.0001
BC	78682.04	1	78682.04	686.71	< 0.0001
A^2	14516.54	1	14516.54	126.69	< 0.0001
B^2	72912.72	1	72912.72	636.35	< 0.0001
C^2	6407.61	1	6407.61	55.92	0.0007
Residual	572.89	5	114.58		
Lack of Fit	390.56	3	130.19	1.43	0.4371
Pure Error	182.33	2	91.17		
Cor Total	$2.77x10^5$	14			
Fit Statistics					
RSD	10.70	R^2		0.9979	
Mean	2668.70	Adjusted R^2		0.9942	
C.V. %	0.4011	Predicted R^2		0.9759	
		Adeq Precision		51.6648	

ANOVA results of GF/PA66 composites are presented in Table 3.28. The findings reveal that the regression coefficients are relatively low. Specifically, the Multiple R-value is 0.8716, which indicates a moderate linear correlation between the predictors and the response variable. However, the R-squared value of 0.7596 shows that only about 75.96% of the variance in the response can be explained by the model. The Adjusted R-squared value of 0.3270 is quite low, which suggests that the model may not be a reliable fit for the data, as it indicates that when adjusting for the number of predictors, the model's explanatory power is significantly reduced. The Standard Error of 228.7972 further confirms the variability in the predictions, meaning the model may have significant errors when predicting future observations. Given the low values of the regression coefficients and the adjusted R-squared, it can be concluded that no robust mathematical model for GF/PA66 composites can be reliably generated from this data. The process likely needs further optimization and refinement to improve the predictive power and ensure the accuracy of the model.

Table 3.28 ANOVA results of GF/PA66 experimental design

Multiple R	0.8716
R Square	0.7596
Adjusted R Square	0.3270
Standard Error	228.7972
Observations	15

ANOVA results prove that a second-order polynomial model equation is applicable for both GF/PPS and GF/PP composites. The coefficient estimations of each term in the second-order polynomial equations are presented in Table 3.29 and Table 3.30 for GF/PPS and GF/PP composites, respectively. The intercept in an orthogonal design is the overall average response of all the runs. The coefficients are adjustments around that average based on the factor settings. When the factors are orthogonal the VIFs are 1; VIFs greater than 1 indicate multicollinearity, and the higher the VIF the more severe the correlation of factors (VIFs less than 10 are tolerable).

Table 3.29 Coefficient estimation of the quadratic model of GF/PPS experimental design

Factor	Coefficient Estimate	df	Standard Error	95% CI Low	95% CI High	VIF
Intercept	3061.51	1	14.54	3024.14	3098.89	
A	144.00	1	8.90	121.11	166.88	1.0000
B	-83.17	1	8.90	-106.06	-60.29	1.0000
C	2.75	1	8.90	-20.14	25.64	1.0000
AB	107.81	1	12.59	75.44	140.18	1.0000
AC	38.61	1	12.59	6.24	70.98	1.0000
BC	-36.97	1	12.59	-69.34	-4.60	1.0000
A^2	-149.52	1	13.11	-183.21	-115.83	1.01
B^2	44.66	1	13.11	10.97	78.35	1.01
C^2	130.68	1	13.11	96.99	164.37	1.01

Table 3.30 Coefficient estimation of the quadratic model of GF/PP experimental design

Factor	Coefficient Estimate	df	Standard Error	95% CI Low	95% CI High	VIF
Intercept	2538.09	1	6.18	2522.21	2553.98	
A-A	-60.81	1	3.78	-70.54	-51.08	1.0000
B-B	-85.52	1	3.78	-95.25	-75.79	1.0000
C-C	4.70	1	3.78	-5.03	14.43	1.0000
AB	-36.21	1	5.35	-49.97	-22.45	1.0000
AC	-67.41	1	5.35	-81.17	-53.65	1.0000
BC	-140.25	1	5.35	-154.01	-126.49	1.0000
A^2	62.70	1	5.57	48.38	77.02	1.01
B^2	140.52	1	5.57	126.20	154.84	1.01
C^2	41.66	1	5.57	27.34	55.98	1.01

The model equations, which relate the process factors to the compressive load of the GF/PPS and GF/PP composites are shown in Equation (3.1) and Equation (3.2) respectively. Only the significant factors ($p<0.0500$) in Table 3.29 and Table 3.30 are included in the model equations. The equations are given as coded factors and can be used to find the compressive load of each composite under an unknown process condition (only the coded process conditions can be used in the equation).

$$R_1 = 3061.51 + 144.00(A) - 83.17(B) + 107.81(AB) + 38.61(AC) - 36.97(BC) - 149.52(A^2) + 44.66(B^2) + 130.68(C^2) \quad (3.1)$$

$$R_2 = 2538.09 - 60.81(A) - 85.52(B) - 36.21(AB) - 67.41(AC) - 140.25(BC) + 62.70(A^2) + 140.52(B^2) + 41.66(C^2) \quad (3.2)$$

The optimum process conditions of GF/PPS and GF/PP composites were calculated from the corresponding model equations by aiming for the maximum compressive load that can be reached within the process limits.

For the GF/PPS production process, the optimum point in terms of coded values is A=0.09 (≈0), B=-0.99(≈1), C = 1.00. The actual values are 575 °C heater temperature, 4 bar roller pressure, and 1600 mm/min winding speed, and the corresponding compressive load calculated from the model equation is 3357.0 N. These process conditions are the same as the 11th experiment of the Box-Behnken design (see

Table **3.23**), so the actual compressive load is 3354.1 ± 4.8 (%). The difference between the calculated and actual value is 2.99 N, which is negligible.

For GF/PP composite production, the optimum process conditions are calculated as A=-0.04 (≈0), B=-0.99 (≈-1), and C=0.99 (≈1). The optimum process conditions in terms of actual values are 275 °C heater temperature, 4 bar roller pressure (321.70 N compaction force), and 1200 mm/min winding speed, and the corresponding calculated compressive load of the composite is 2946.0 N. These process conditions are the same as the 11th experiment of the Box-Behnken design, so the actual compressive load is 2952.0 ± 1.6 (%). The difference between the calculated and actual value is 6.0 N, which is negligible.

The sum of differences between theoretical (predicted) and actual data is another indicator that needs to be checked to prove the validity of a model equation. The predicted compressive load values of GF/PPS and GF/PP composites were

calculated according to their model equations, and the results were compared with the actual experimental findings.

Table 3.31 presents the sum of differences was calculated as -0.1 for GF/PPS, and -0.1 for GF/PP composites. The closer the sum of the differences to zero, the more likely the model equation fits well with the experimental data. It can be concluded that the derived model equations can successfully be used to define GF/PPS and GF/PP production processes.

Table 3.31 Sum of differences between predicted and actual compressive loads of GF/PPS composites

No	GF/PPS Calculated Compressive Load (N)	GF/PPS Actual Compressive Load, R1 (N)	Difference	GF/PP Calculated Compressive Load (N)	GF/PP Actual Compressive Load, R2 (N)	Difference
1	3003.6	3024.2	-20.5	2851.4	2854.0	-2.5
2	3076.0	3058.7	17.4	2802.2	2793.1	9.1
3	2621.7	2639.0	-17.4	2752.8	2761.9	-9.1
4	3125.3	3104.8	20.5	2558.8	2556.3	2.5
5	2937.3	2911.5	25.8	2635.9	2623.3	12.5
6	3148.1	3160.2	-12.1	2649.1	2648.2	0.9
7	2860.1	2848.0	12.1	2770.7	2771.6	-0.9
8	3225.3	3251.1	-25.8	2514.2	2526.8	-12.5
9	3283.1	3282.8	0.2	2665.5	2666.2	-0.6
10	3190.7	3193.6	-2.9	2775.0	2769.0	6.0
11	3357.0	3354.1	2.9	2946.0	2952.0	-6.0
12	3116.7	3117.0	-0.3	2494.5	2493.9	0.6
13	3061.5	3066.8	-5.2	2538.1	2529.2	8.9
14	3061.5	3051.6	9.9	2538.1	2536.9	1.2
15	3061.5	3066.2	-4.7	2538.1	2548.2	-10.1
Sum of Differences:			$-0.1 \approx 0$	**Sum of Differences:**		$-0.1 \approx 0$

The regression coefficients of predicted vs. actual values are found as 0.9928 and 0.9973 for GF/PPS and GF/PP, respectively. The results are illustrated in Figure 3.11.

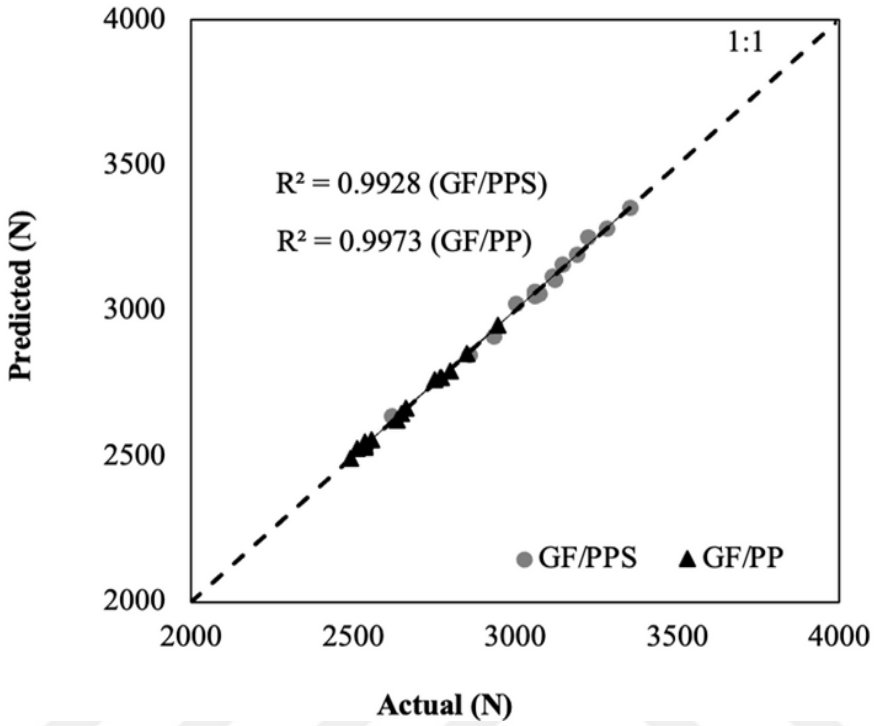


Figure 3.11 Predicted vs. actual compressive loads of the composites

3.3.2.1 Response Surface Methodology (RSM)

The response surface is a three-dimensional graphical representation of the data that facilitates the interpretation and understanding of the relationships between independent and dependent variables.

The effects of process parameters on the compressive load of GF/PPS and GF/PP composites are visually represented through response surface graphs. These graphs were generated based on the model Equations (3.1) and (3.2), clearly illustrating how variations in process parameters influence the compressive load.

In each graph, the third parameter is constant at the center point, which corresponds to zero. Keeping one parameter constant enables a more focused analysis of the interactions between the other two parameters and their influence on the response. The central value, representing the midpoint of the experimental range, serves as a balanced reference point, ensuring consistent comparisons across parameter combinations. This systematic approach, combined with the mathematical model

equations, comprehensively accounts for the effects of all three parameters, providing detailed insights into their individual and combined impacts on the system response.

The optimal process conditions were determined based on the model Equations (3.1) and (3.1). Figure 3.12-Figure 3.17 are designed solely to visualize the effects of the process parameters on the system's response. Such visualizations provide valuable insights into the relationships between process variables and the response. The effects of process factors on the compressive load of GF/PPS and GF/PP composites are illustrated by response surface graphics, which are constructed according to the model equations.

Figure 3.12 illustrates the effects of roller pressure (B) and heater temperature (A) on the compressive load (R1) of the GF/PPS composites, with the winding speed (C) held constant at the center point. The 3D surface plot indicates that higher temperatures and reduced roller pressure contribute to higher compressive loads, suggesting that these conditions are ideal for achieving strong GF/PPS composites. The temperature (A) appears to have a more significant impact on the compressive load compared to the roller pressure (B).

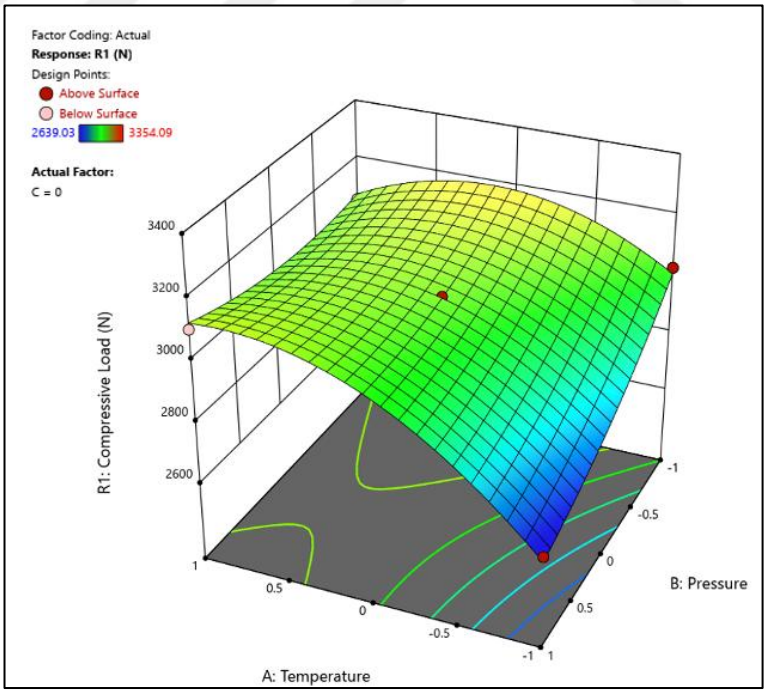


Figure 3.12 The effects of pressure and temperature on the compressive load of GF/PPS composites produced by FW

Figure 3.13 examines the combined effects of winding speed (C) and heater temperature (A) on the compressive load (R1) of GF/PPS composites, with roller pressure kept constant at the center point. The 3D surface plot reveals that the winding speed (C) has a relatively minimal effect on the compressive load, as the surface remains relatively flat in the direction of speed. In contrast, the heater temperature (A) shows a much more pronounced effect on the compressive load, with the compressive strength of the GF/PPS composites improving as the temperature increases.

This suggests that temperature plays a key role in enhancing the compressive strength of the composites, likely by improving the polymer flow and bonding during the filament winding process. Higher temperatures may lead to better impregnation, resulting in stronger and more durable composites. On the other hand, the limited impact of winding speed on the compressive load implies that, within the tested range, changes in speed do not significantly alter the material's performance.

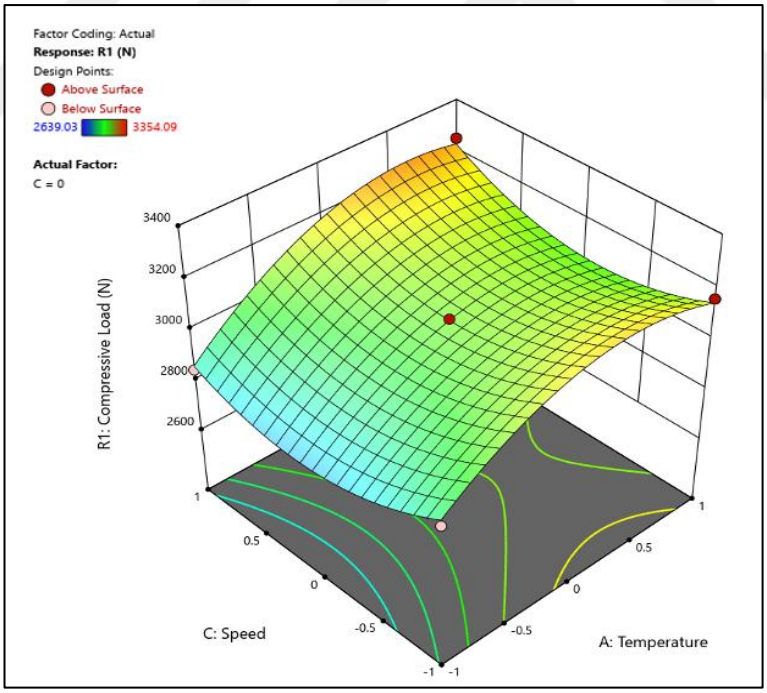


Figure 3.13 The effects of winding speed and temperature on the compressive load of GF/PPS composites produced by FW

Furthermore, Figure 3.14 emphasizes that lower roller pressure values are more favorable for achieving higher compressive loads for GF/PPS, with the influence of

winding speed (C) being negligible compared to roller pressure (B). The heater temperature remains constant at the center point in Figure 3.14.

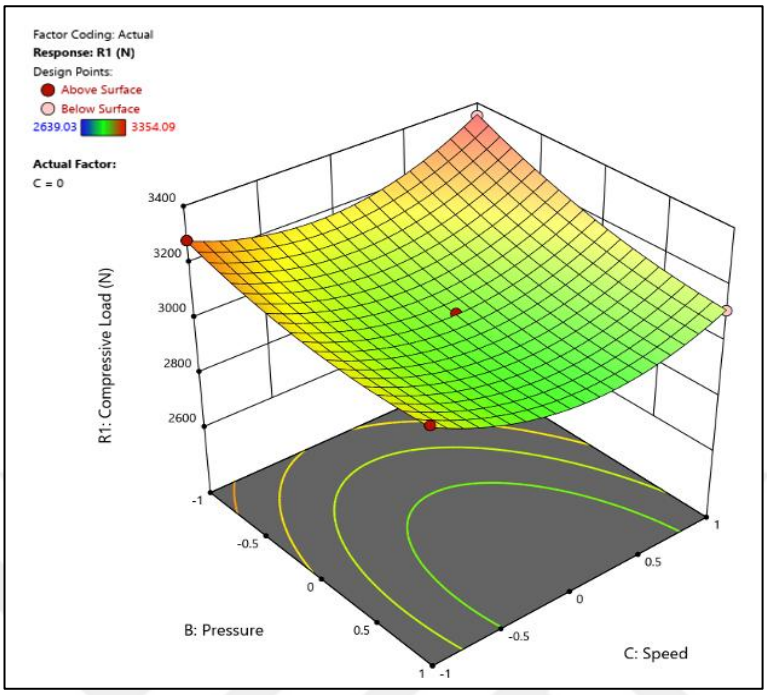


Figure 3.14 The effects of pressure and winding speed on the compressive load of GF/PPS composites produced by FW

These observations underscore that temperature is the most critical factor, positively influencing product quality. As the temperature nears the upper boundary of the defined process window, composite strength significantly improves. In contrast, roller pressure, while the second most influential parameter, has a negative effect on quality. Reduced roller pressure leads to better composite strength, as excessive pressure can cause fiber deformation, misalignment, and potential breakage. Thus, operating near the lower pressure limits of the process window is advantageous. Lastly, winding speed has a relatively minor role in influencing product quality when compared to temperature and roller pressure.

Figure 3.15 indicates that for the production of high-quality GF/PP composites, lower temperature (A) and lower roller pressure (B) are preferred. The graph demonstrates that roller pressure has a stronger effect on the compressive load compared to temperature, as indicated by the steepness of the surface in relation to pressure changes. This suggests that optimizing roller pressure is more critical than adjusting temperature in enhancing the compressive load for GF/PP composites.

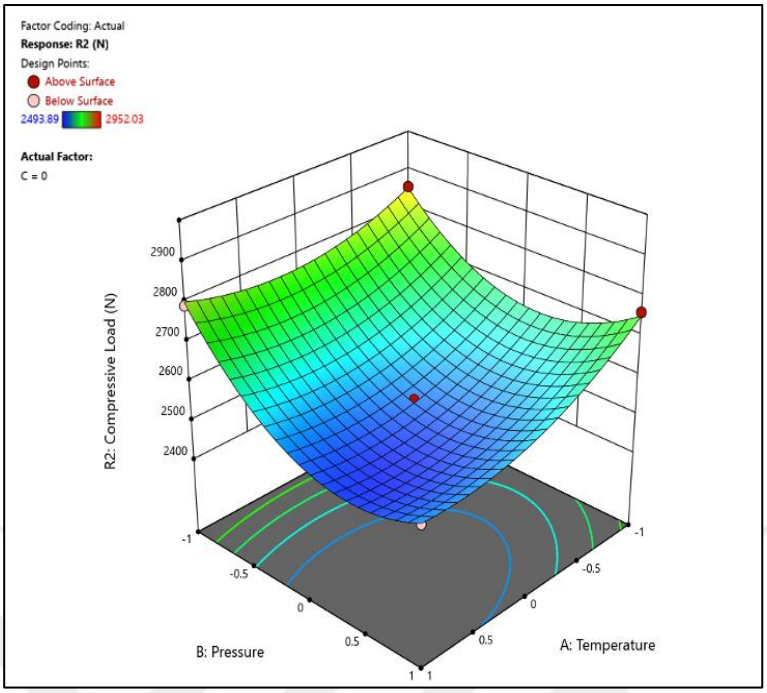


Figure 3.15 The effects of pressure and temperature, on the compressive load of GF/PP composites produced by FW

Figure 3.16 shows that the effect of winding speed (C) is insignificant compared to temperature (A), and the compressive load of GF/PP increases with the decreasing temperature.

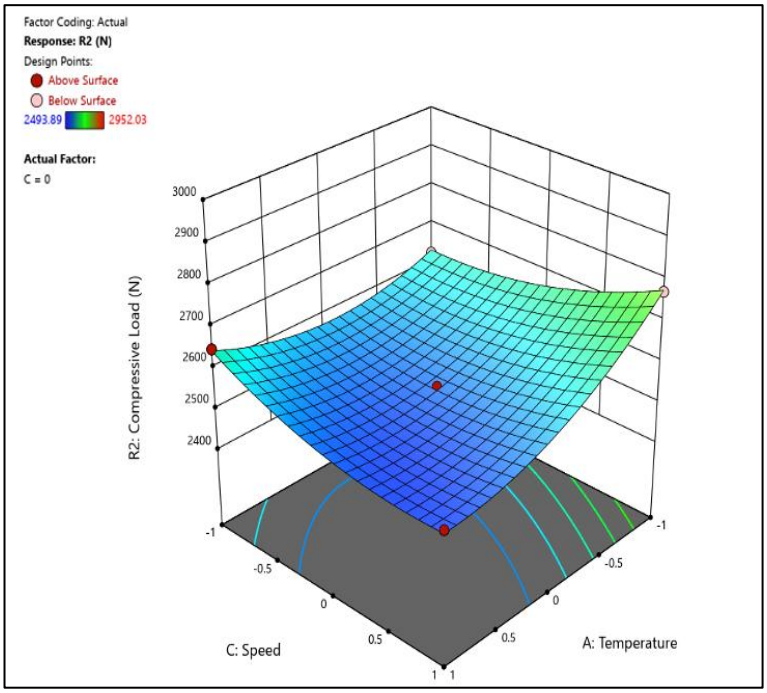


Figure 3.16 The effects of winding speed and temperature on the compressive load of GF/PP composites produced by FW

Figure 3.17 indicates that lower pressure is desired for high compressive loads and the effect of winding speed (C) is very low compared to pressure (B).

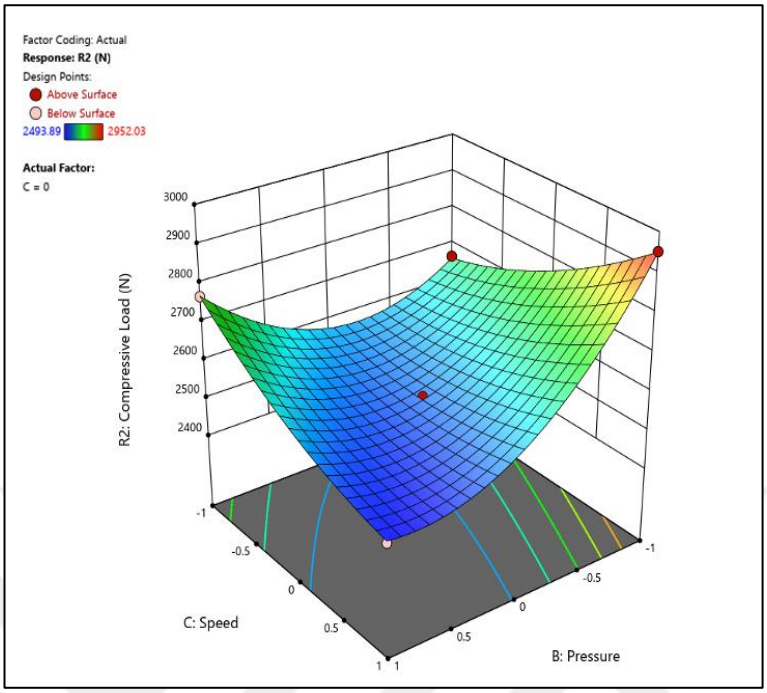


Figure 3.17 The effects pressure and winding speed on the compressive load of GF/PP composites produced by FW

As the processing temperature nears the upper boundary of the defined operating range, the risk of polymer degradation increases, potentially diminishing the quality and strength of the composite material. To mitigate this, maintaining operations at the lower end of the temperature range is generally deemed safer. Interestingly, despite expectations that temperature would have the most significant effect on product quality, roller pressure emerges as the dominant factor. This could be due to the limited temperature variation within the operating range. Given that roller pressure directly impacts the alignment of fibers within the molten polymer, it plays a critical role in determining the composite's strength. Thus, utilizing the lower roller pressure limits is recommended for GF/PP composites. Additionally, winding speed appears to have a relatively minor effect on quality compared to temperature and pressure.

In conclusion, achieving superior quality in GF/PPS composites benefits from higher temperatures and lower pressure settings within the defined process range. On the other hand, lower temperature and pressure conditions are more suitable for producing high-strength GF/PP composites.

3.3.3 Production at the Optimum Point of FW Process

The performance of the filament-wound composites produced under optimized conditions is assessed through mechanical, thermal, and physicochemical tests, including compression testing, DSC crystallinity analysis, and density and void content measurements. These tests help verify the effectiveness of the optimized process parameters and provide insight into the composite's quality.

It is important to note that compression tests were not repeated, as the optimal process parameters corresponded to the 11^{th} trial in the experimental design. This trial yielded compressive load values of 3354.1 N for GF/PPS and 2952.0 N for GF/PP, as detailed in Table 3.23 and Table 3.24.

3.3.3.1 Thermal Analysis

Crystallinity (X_C) measures the molecular arrangement within the polymer matrix, influencing stiffness, thermal stability, and chemical resistance. While higher crystallinity increases rigidity, it can also make composites more brittle, reducing their impact resistance. Factors such as processing temperature and cooling rate significantly affect crystallinity. By carefully controlling these variables during filament winding, the crystallization process can be optimized without compromising toughness or flexibility. For GF/PPS, higher temperatures near the process window's upper boundary improve crystallinity, but controlled cooling is required to prevent brittleness. Conversely, lower temperatures in GF/PP prevent polymer degradation, preserving both strength and flexibility.

According to Table 3.32, GF/PP composites exhibit crystallinity ranging from 58.94% to 64.47%, while GF/PPS composites display a range of 48.39% to 61.80%. The higher crystallinity of GF/PP enhances rigidity and thermal stability but may increase brittleness. In contrast, GF/PPS composites show lower crystallinity due to the cross-linking reaction of PPS at elevated temperatures. Crosslinking above PPS’s melting point in an air environment reduces crystallizability and crystallinity, as time, temperature, and atmosphere play significant roles in these changes. Studies also indicate that PPS curing diminishes both crystallinity and crystallizability [80].

Table 3.32 DSC test results of the composites produced by FW

Sample No	Peak (°C)	Area (mJ)	ΔH (J/g)	% X_C	Mean %X_C
GFPPS-a	283.88	342.279	18.9105	61.80	50.73 ± 19.92(%)
GFPPS-b	284.26	251.914	12.8527	42.00	
GFPPS-c	283.39	293.175	14.8068	48.39	
GFPP-a	165.42	641.463	31.9136	64.47	58.96 ± 9.32(%)
GFPP-b	166.18	502.992	26.4733	53.48	
GFPP-c	164.89	571.873	29.1772	58.94	

For GF/PP composites, the FW process achieved an average crystallinity of 58.96% with a coefficient of standard deviation of ±9.32%. For GF/PPS composites, FW composites had an average crystallinity of 50.73% with a variability of ±19.92%.

3.3.3.2 Density and Void Content

Density, defined as the mass per unit volume, indicates how fibers and matrix material are distributed within a composite. In thermoplastic composites, it serves as a key measure of consolidation quality. A higher density often reflects improved fiber impregnation and minimal void content, which are essential for achieving strong mechanical properties and long-term durability in structural applications. Achieving consistent and near-theoretical density requires precise control over roller pressure, temperature, and winding speed during filament winding. While adequate compaction reduces voids and improves impregnation, excessive pressure may damage fibers or alter their alignment. To enhance the quality of the composite, maintaining optimal pressure, ensuring temperature stability, and keeping the winding speed constant are critical. Although roller pressure and winding speed were precisely controlled during processing, convective heat transfer between the heater tip and the nip point created slight temperature variations, making it the only parameter with uncertainty during production.

The density and void content of the GF/PPS and GF/PP composites, along with their respective standard deviations, are presented in Table 3.33. Theoretical density values listed in Table 3.33 indicate densities of 1.656 g/cm³ for GF/PP slit tape and 1.885 g/cm³ for GF/PPS slit tape. In comparison, filament-wound composites

demonstrate density ranges of 1.558 to 1.575 g/cm³ for GF/PP and 1.819 to 1.834 g/cm³ for GF/PPS. The difference from theoretical densities suggests voids or incomplete impregnation during the winding process. Notably, GF/PPS composites exhibit densities closer to theoretical values, indicating more effective consolidation and improved fiber-matrix bonding.

Void content, caused by trapped air within the composite, negatively impacts mechanical properties by introducing weak spots that may lead to crack formation under stress. Voids reduce composite strength, stiffness, and fatigue resistance, making their reduction essential for high-performance applications. Table 3.33 reveals void content between 5.5% and 5.9% for GF/PP composites, whereas GF/PPS composites exhibit significantly lower void content, ranging from 2.3% to 3.5%. This demonstrates that GF/PPS composites achieve better consolidation, resulting in reduced void formation and enhanced mechanical performance for demanding applications. These results are consistent with literature findings, which report that automated fiber placement (AFP) composites typically demonstrate porosity levels between 3% and 4%, slightly higher than those achieved through autoclave processes. Despite this, AFP and, similarly, FW remain competitive manufacturing methods due to their efficiency in producing complex geometries and significantly reducing production times [81].

Table 3.33 Density and void content of the composites produced by FW at the optimum process conditions

Specimen	**ρ_t (g/cm^3)**	**ρ_c (g/cm^3)**	**Mean ρ_c (g/cm^3)**	**V_C %**	**Mean V_C (%)**
GFPPS-a	1.885	1.819	1.832 ± 0.012	3.5	2.8 ± 0.5
GFPPS-b	1.885	1.834		2.7	
GFPPS-c	1.885	1.842		2.3	
GFPP-a	1.656	1.565	1.566 ± 0.009	5.5	5.4 ± 0.4
GFPP-b	1.656	1.575		4.9	
GFPP-c	1.656	1.558		5.9	

Minimizing void content necessitates optimizing heating temperature, roller pressure, and winding speed. Higher temperatures improve matrix flow and fiber

wetting, facilitating the removal of air pockets. However, excessive heat can degrade the polymer matrix, particularly in GF/PP composites operating near the upper limits of the process window. To avoid fiber damage, balancing temperature and pressure is critical. Additionally, slower winding speeds provide more time for the matrix to fill gaps between fibers, further enhancing consolidation.

3.3.3.3 Morphological Analysis

In the microscopic examination of the GF/PP composite material, the side view of the sample after the ILSS test is shown in Figure 3.18 Although delamination areas have formed after the test, the image demonstrates strong consolidation within the composite structure. The material layers are arranged in parallel, and the filaments are well-aligned, indicating good interlaminar bonding and a high degree of material integrity. The presence of delamination suggests localized weakness, yet the overall structure remains robust, demonstrating the composite's resilience under shear stress.

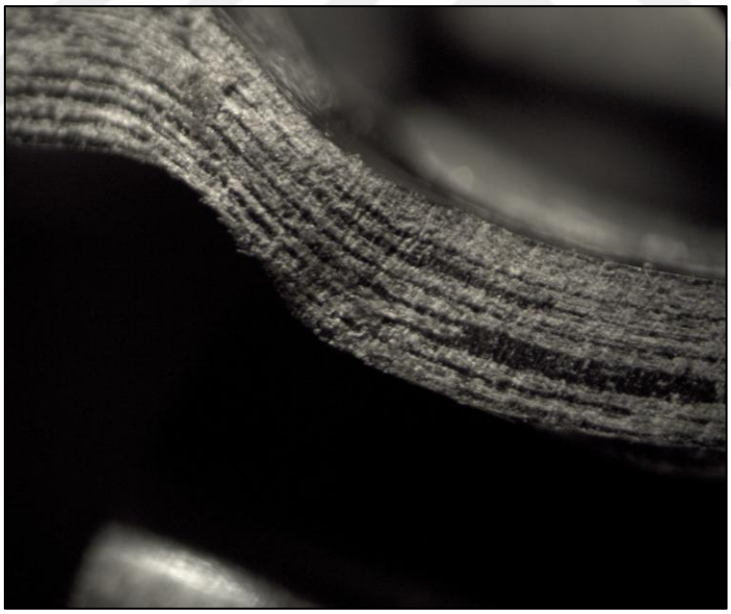


Figure 3.18 Side view of GF/PP composite

Figure 3.19 illustrates the microscopic analysis of GF/PPS composites. Similar results with the GF/PP composite are also observed in here. Despite the presence of delamination areas following the ILSS test, the composite structure still exhibits strong consolidation, with the material layers aligned in parallel and the filaments properly oriented. This suggests that the GF/PPS material maintains a high degree of interlaminar bonding and material integrity like GF/PP composite. These

observations provide valuable insight into the composites' mechanical performance and the effectiveness of their consolidation during the FW process.

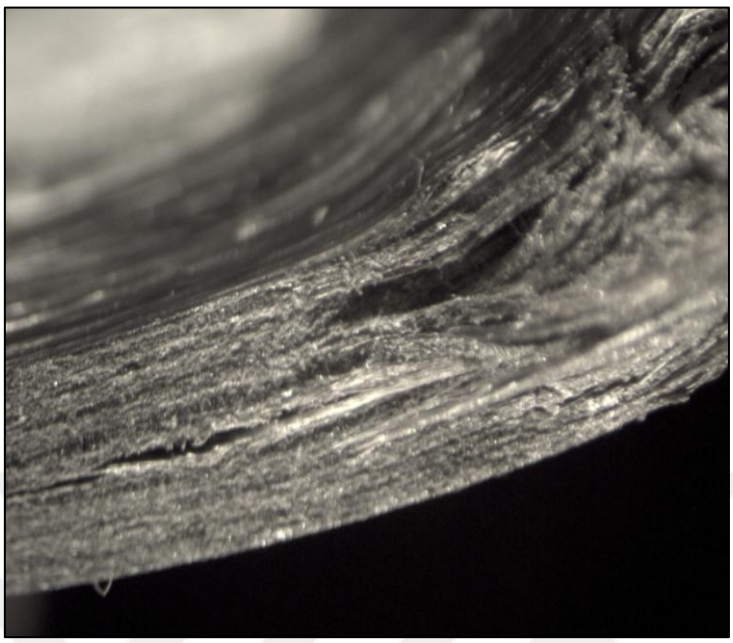


Figure 3.19 Side view of GF/PPS composite

3.4 Finite Element Method (FEM)

The compressive performance of GF/PPS, GF/PP, and GF/PA66 composites was simulated via finite element method (FEM).

For GF/PP composites, the material properties of 1,656 g/cm³ density and 32,400 MPa Young's Modulus were used to model the material behavior under the given conditions.

For GF/PPS composites, the material properties of 1,885 g/cm³ density and 35,700 MPa Young's Modulus were used, and for GF/PA66 composites, the material properties of 1.730 g/cm³ density and 28,900 MPa Young's Modulus were used to model the material behavior under the given conditions.

The results of the finite element analysis (FEA) for GF/PP composites are illustrated in Figure 3.20. The maximum compression load was found as 3096.1 N.

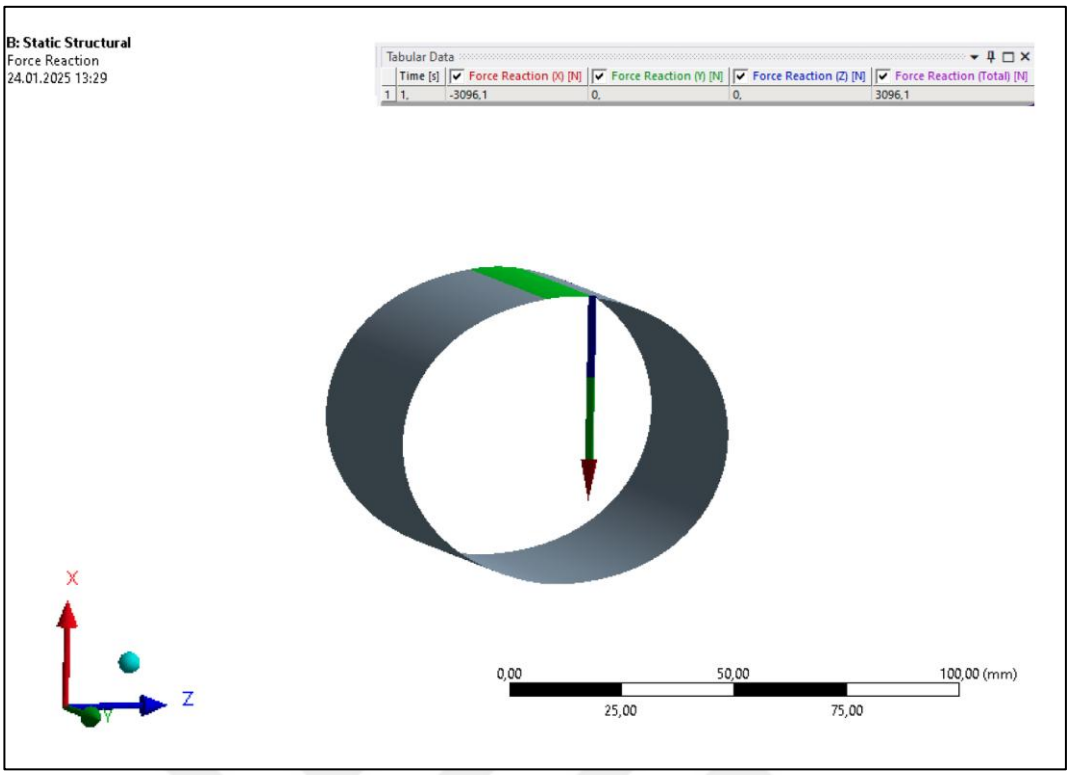


Figure 3.20 Reaction force of PP composites

The results of the finite element analysis (FEA) for GF/PPS composites are illustrated in Figure 3.21. The maximum compression load was found as 3454.1 N.

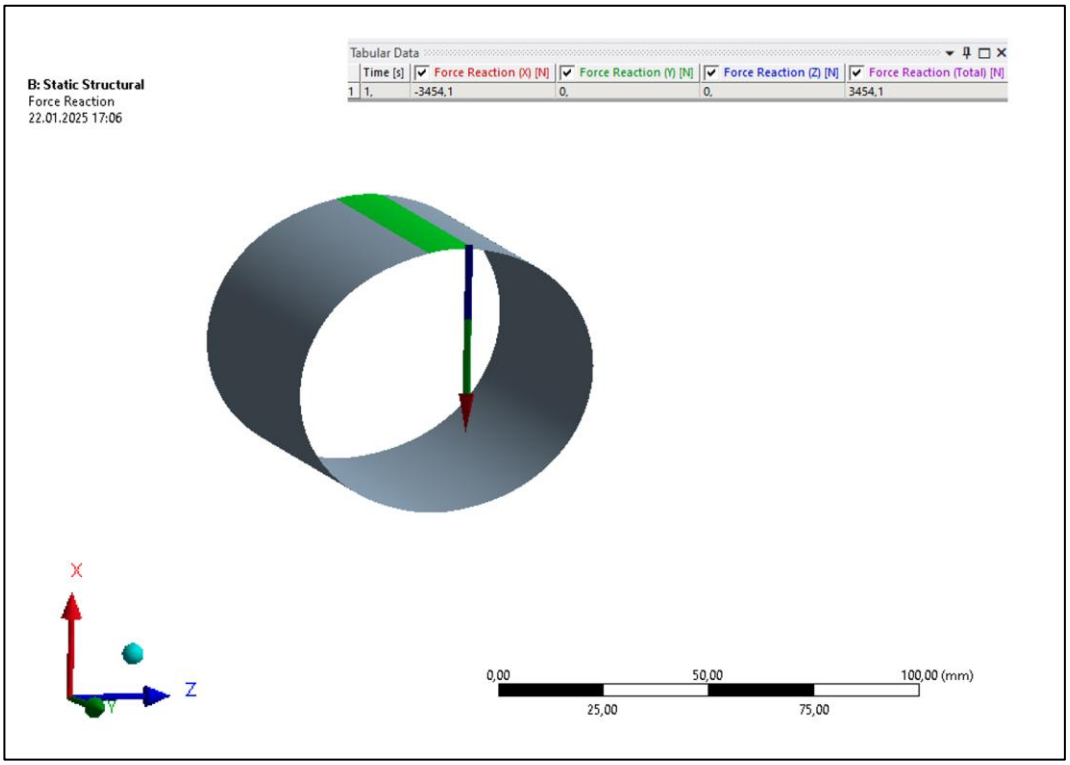


Figure 3.21 Reaction force of PPS composites

The results of the finite element analysis (FEA) for GF/PA66 composites are illustrated in Figure 3.22. The maximum compression load was found as 2796.2 N.

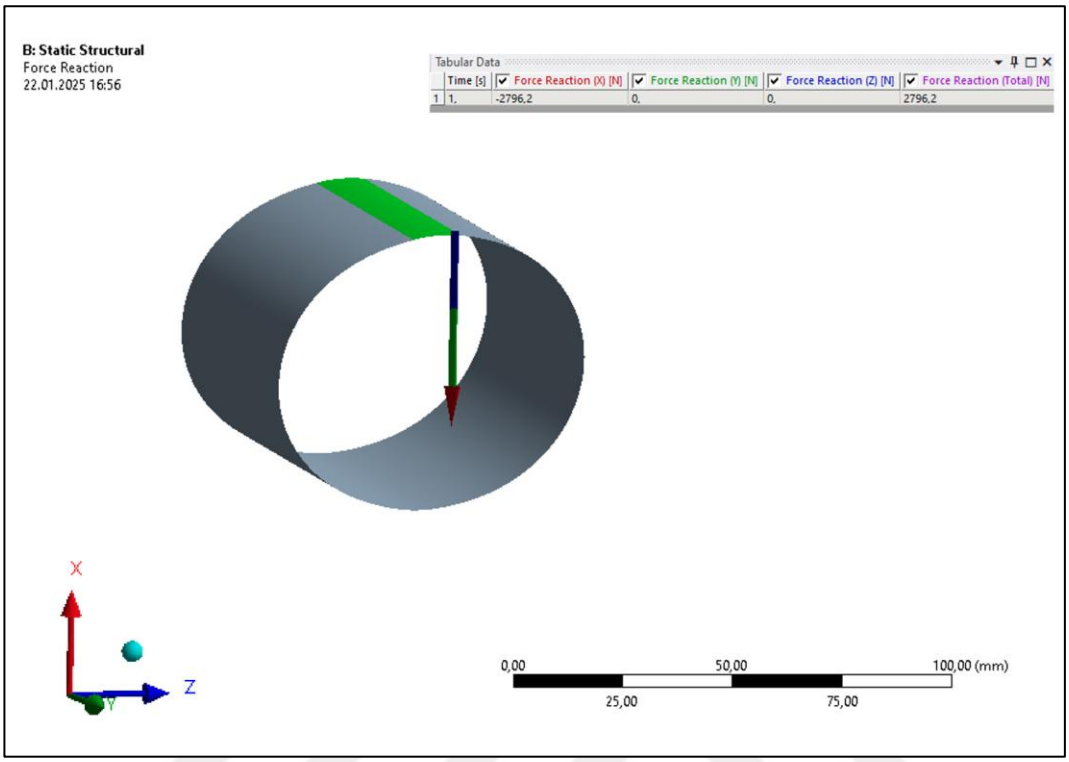


Figure 3.22 Reaction force of PA66 composites

The comparison of the FEA and FW results are presented Table 3.34. The compressive load for GF/PPS in FW was measured at 3357.0 N, while the FEA predicted a slightly higher value of 3454.1 N, resulting in a 2.8% difference. Similarly, the GF/PP specimen exhibited a compressive load of 2946.0 N experimentally, compared to 3096.1 N in FEA, with a 4.8% difference. The GF/PA66 specimen lacked FW data, but the FEA predicted a compressive load of 2796.2 N.

Table 3.34 Comparison of compressive load results between Filament Winding (FW) experiments and Finite Element Analysis (FEA)

Specimen	FW[1]	FEA	Difference
GF/PPS	3357.0 N	3454.1 N	2.8 %
GF/PP	2946.0 N	3096.1 N	4.8 %
GF/PA66	-	2796.2 N	-

[1] Under the optimum FW processing conditions for GF/PP and GF/PPS, the GF/PA66 results are not available due to unsuccessful FW process optimization for GF/PA66.

The integration of finite element analysis (FEA) in this research serves a dual purpose. First, it validates the experimental results obtained from compression tests, demonstrating the reliability of FW as a composite manufacturing technique. Second, it highlights the role of computational modeling in understanding how process-induced variations influence mechanical performance. By bridging experimental and theoretical approaches, this study leverages FEA to gain a deeper understanding of composite behavior under compressive loads and to explore opportunities for optimizing manufacturing processes.

These results validate FW as a reliable manufacturing method, capable of producing high-performance composite structures with consistent mechanical properties. The strong correlation between FW and FEA findings reinforces the applicability of FW, paving the way for broader industrial applications of advanced composites.

4
CONCLUSION

This study successfully demonstrated the production of E-glass fiber-reinforced polypropylene (GF/PP), polyphenylene sulfide (GF/PPS), and polyamide 6,6 (GF/PA66) cylindrical composites using the filament winding (FW) technique. The research aimed to optimize key process parameters, including heater temperature, roller pressure, and winding speed, to assess their influence on compressive load performance. The key conclusions are as follows:

- Optimization of Process Parameters: The Box-Behnken experimental design combined with Response Surface Methodology (RSM) was used to develop predictive models for process optimization. The optimal conditions for GF/PPS and GF/PP composites were identified as a heater temperature of 575 °C and 275 °C, roller pressure of 4 bar (321.70 N compaction force), and winding speeds of 1600 mm/min and 1200 mm/min, respectively. These conditions resulted in compressive loads of 3357 N and 2946 N. However, the optimization process for GF/PA66 composites did not yield satisfactory outcomes, necessitating further investigation.
- Efficiency in Time and Cost: Compared to autoclave processing, the FW method demonstrated notable advantages in terms of efficiency. While autoclave cycles required 140-220 minutes, FW reduced production time to 30-45 minutes per cylinder, with pre-processing durations shortened from 2 hours to 30 minutes. These findings confirm that FW offers a faster and more cost-effective approach for producing thermoplastic composites.
- Material-Specific Considerations: The findings are specific to glass fiber reinforcement, as different fiber-polymer interactions can impact process outcomes. The research identified a suitable temperature range for PP and

PPS, yet materials with higher melting points require additional study to determine their suitability for FW. Future investigations could explore alternative fiber types, optimized heating/cooling rates, and further process variables to improve mechanical performance.

- Industrial Feasibility: Assessing scalability and reproducibility on an industrial level is crucial for real-world applications. Additionally, heat source selection significantly influences process parameters, meaning different heating systems may require parameter adjustments to maintain optimal composite quality.

While autoclave processing remains the conventional choice for high-performance composite manufacturing, this study highlights FW as a viable alternative, offering cost efficiency, scalability, and design flexibility. By establishing a structured framework for process optimization, this research contributes to the advancement of thermoplastic FW techniques, paving the way for their integration into various industrial applications requiring lightweight, high-strength composites.

Building upon the findings of this study, several areas require further investigation to enhance the effectiveness and industrial viability of filament winding for thermoplastic composites. Future studies should explore the feasibility of processing materials with higher melting points, such as PEEK and PEKK, by adjusting heating profiles and process parameters. Additionally, investigating the compatibility of different fiber reinforcements, such as carbon or aramid fibers, with the filament winding process could expand material options and improve mechanical properties.

Implementing in-situ process monitoring techniques, such as infrared thermography or fiber optic sensing, could further enhance quality control and reproducibility. By addressing these aspects, future research can facilitate the broader adoption of thermoplastic filament winding in advanced composite applications, ensuring its competitiveness with traditional processing techniques.

REFERENCES

[1] T. P. Sathishkumar, S. Satheeshkumar, and J. Naveen, “Glass fiber-reinforced polymer composites - A review,” SAGE Publications Ltd., 2014, doi: 10.1177/0731684414530790.

[2] M. Stefanovska, B. Samakoski, S. Risteska, and G. Maneski, “Influence of some technological parameters on the content of voids in composite during on-line consolidation with filament winding technology,” Int. J. Chem. Nucl. Mater. Metall. Eng, vol. 8, no.5, 2014.

[3] F. Henninger and K. Friedrich, “Thermoplastic filament winding with online-impregnation. Part A: Process technology and operating efficiency,” Compos Part A Appl Sci Manuf, vol. 33, no. 11, pp. 1479–1486, 2002, doi: 10.1016/S1359-835X(02)00135-5.

[4] U. K. Vaidya and K. K. Chawla, “Processing of fibre reinforced thermoplastic composites,” International Materials Reviews, vol.53 no.4, 2008, doi: 10.1179/174328008X325223.

[5] D. W. Radford and K. M. Hedin, “Fused deposition technology applied to thermoplastic matrix placement and wetout in filament winding,” ICCM International Conferences on Composite Materials, vol. 2015, no.7, pp. 19–24, 2015.

[6] P. Peltonen and P. Törmälä, “Melt impregnation parameters,” Compos Struct, vol. 27, no. 1–2, pp. 149–155, 1994, doi: 10.1016/0263-8223(94)90076-0.

[7] R. Krueger and A. Bergan, “Advances in Thermoplastic Composites Over Three Decades-A Literature Review,” http://www.sti.nasa.gov, 01.01.2025.

[8] R. Patole, N. Ambhore and D. Agrawal, “Carbon Composites in Aerospace Application - A Comprehensive Review,” Materials International, vol. 5, no.4, 2023, doi: 10.33263/Materials54.002.

[9] S. mahboubizadeh, A. Sadeq, Z. Arzaqi, O. Ashkani, and M. Samadoghli, “Advancements in fiber-reinforced polymer (FRP) composites: an extensive review,” Discover Materials, vol.4, no.22, 2024, doi: 10.1007/s43939-024-00091-9.

[10] F. Khan, N. Hossain, J. J. Mim, S. M. Rahman, M. J. Iqbal, M. Billah, and M. A. Chowdhury, "Advances of composite materials in automobile applications – A review," *Journal of Engineering Research*, in press. doi: 10.1016/j.jer.2024.02.017.

[11] H. Mohammadi, Z. Ahmad, S. A. Mazlan, M. A. F. Johari, G. Siebert, M. Petrů, and S. S. R. Koloor, “Lightweight Glass Fiber-Reinforced Polymer Composite

for Automotive Bumper Applications: A Review," Polymers, vol.15, no.1, doi: 10.3390/polym15010193.

[12] F. C. Campbell, "Fibers and Reinforcements: The String That Provides the Strength," in Manufacturing Processes for Advanced Composites, Elsevier Science, 2004, pp. 39–62, doi: 10.1016/B978-185617415-2/50003-4.

[13] P. Robinson, E. Greenhalgh, and S. Pinho, "Autoclave processing for composites," in Manufacturing techniques for polymer matrix composites (PMCs), Woodhead Publishing, 2012, pp. 414–432.

[14] P. Robinson, E. Greenhalgh, and S. Pinho, "Out-of-autoclave curing process in polymer matrix composites," in Manufacturing techniques for polymer matrix composites (PMCs), Woodhead Publishing, 2012, pp. 435–479.

[15] S. Carosella, S. Hügle, F. Helber, and P. Middendorf, "A short review on recent advances in automated fiber placement and filament winding technologies," Compos B Eng, vol. 287, 2024, doi: 10.1016/j.compositesb.2024.111843.

[16] Z. August, G. Ostrander, J. Michasiow, and D. Hauber, "Recent Developments in Automated Fiber Placement of Thermoplastic Composites," Sampe Journal, no. 50, no.6, 2014, pp. 30–37.

[17] F. Sacchetti, W. J. B. Grouve, L. L. Warnet, and I. F. Villegas, "Effect of cooling rate on the interlaminar fracture toughness of unidirectional Carbon/PPS laminates," Eng Fract Mech, vol. 203, pp. 126–136, 2018, doi: 10.1016/j.engfracmech.2018.02.022.

[18] L. Raps, A. R. Chadwick, I. Schiel, and I. Schmidt, "CF/LM-PAEK: Characterisation and sensitivity to critical process parameters for automated fibre placement," Compos Struct, vol. 284, p. 115087, 2022, doi: 10.1016/J.COMPSTRUCT.2021.115087.

[19] M. D. Hoang, "Procedure for making flat thermoplastic composite plates by Automated Fiber Placement and their mechanical properties," Master of Applied Science, Concordia University, Montreal, Quebec, Canada, 2015. doi: 10.1145/3132847.3132886.

[20] X. Cai, "Determination of Process Parameters for the Manufacturing of Thermoplastic Composite Cones Using Automated Fiber Placement," Master of Applied Science, Concordia University, Montreal, Quebec, Canada, 2012.

[21] S. K. Kim, H. J. Kim, and W. Il Lee, "Characterization of boundary conditions during thermoplastic composite tape lay-up process using an inverse method," Model Simul Mat Sci Eng, vol. 11, no. 4, pp. 417–426, 2003, doi: 10.1088/0965-0393/11/4/301.

[22] Z. Qureshi, T. Swait, R. Scaife, and H. M. El-Dessouky, "In situ consolidation of thermoplastic prepreg tape using automated tape placement technology: Potential and possibilities," Compos B Eng, vol. 66, pp. 255–267, 2014, doi: 10.1016/j.compositesb.2014.05.025.

[23] F. O. Sonmez and M. Akbulut, "Process optimization of tape placement for thermoplastic composites," Compos Part A Appl Sci Manuf, vol. 38, no. 9, pp. 2013–2023, 2007, doi: 10.1016/j.compositesa.2007.05.003.

[24] R. Schledjewski and M. Latrille, "Processing of unidirectional fiber reinforced tapes - fundamentals on the way to a process simulation tool (ProSimFRT),"

Compos Sci Technol, vol. 63, no. 14, pp. 2111–2118, 2003, doi: 10.1016/S0266-3538(03)00108-8.

[25] D. Maurer and P. Mitschang, “Laser-powered tape placement process–simulation and optimization,” Advanced Manufacturing: Polymer and Composites Science, vol. 1, no. 3, pp. 129–137, 2015, doi: 10.1080/20550340.2015.1114798.

[26] M. A. Khan, P. Mitschang, and R. Schledjewski, “Parametric study on processing parameters and resulting part quality through thermoplastic tape placement process,” J Compos Mater, vol. 47, no. 4, pp. 485–499, 2013, doi: 10.1177/0021998312441810.

[27] W. J. B. Grouve, L. L. Warnet, B. Rietman, H. A. Visser, and R. Akkerman, “Optimization of the tape placement process parameters for carbon-PPS composites,” Compos Part A Appl Sci Manuf, vol. 50, pp. 44–53, 2013, doi: 10.1016/j.compositesa.2013.03.003.

[28] A. J. Comer et al., “Mechanical characterisation of carbon fibre-PEEK manufactured by laser-assisted automated-tape-placement and autoclave,” Compos Part A Appl Sci Manuf, vol. 69, pp. 10–20, 2015, doi: 10.1016/j.compositesa.2014.10.003.

[29] Paul. Robinson, E. S. . Greenhalgh, and Silvestre. Pinho, “Filament winding process in thermoplastics,” in Manufacturing techniques for polymer matrix composites (PMCs), Woodhead Publishing, 2012, p. 450.

[30] A. Rajasekaran and F. Shadmehri, “Steering of carbon fiber/PEEK tapes using Hot Gas Torch-assisted automated fiber placement,” Journal of Thermoplastic Composite Materials, vol. 36, no. 4, pp. 1651–1679, Apr. 2023, doi: 10.1177/08927057211067962.

[31] J. Mack and R. Schledjewski, “Filament winding process in thermoplastics,” in Manufacturing Techniques for Polymer Matrix Composites (PMCs), Woodhead Publishing, 2012, pp. 182–208. doi: 10.1533/9780857096258.2.182.

[32] X. Song, “Modeling of Thermoplastic Composite Filament Winding,” Master of Science, Virginia Polytechnic Institute and State University, 2000.

[33] S. Khan, “Thermal Control System Design for Automated Fiber Placement Process,” Master of Applied Science, Concordia University, Montreal, Quebec, Canada, 2011.

[34] R. H. Rizzolo and D. F. Walczyk, “Ultrasonic consolidation of thermoplastic composite prepreg for automated fiber placement,” Journal of Thermoplastic Composite Materials, vol. 29, no. 11, pp. 1480–1497, 2016, doi: 10.1177/0892705714565705.

[35] P.-E. Bourban, N. Bernet, J.-E. Zanetto, and J.-A. E. M. Ênson, “Material phenomena controlling rapid processing of thermoplastic composites.” Compos Part A Appl Sci Manuf, vol.32, no.8, pp.1045-1057, 2001.

[36] R. Funck and M. Neitzel, “Improved thermoplastic tape winding using laser or direct-flame heating,” Composites Manufacfuring, vol. 6, no. 3–4, pp. 189–192, 1995, doi: https://doi.org/10.1016/0956-7143(95)95010-V.

[37] F. Henninger, J. Hoffmann, and K. Friedrich, “Thermoplastic filament winding with online-impregnation. Part B. Experimental study of processing parameters,” Compos Part A Appl Sci Manuf, vol. 33, no. 12, pp. 1684–1695, 2002, doi: 10.1016/S1359-835X(02)00186-0.

[38] P. Mindermann, M. U. Witt, and G. T. Gresser, “Pultrusion-winding: A novel fabrication method for coreless wound fiber-reinforced thermoset composites with distinct cross-section,” Compos Part A Appl Sci Manuf, vol. 154, p. 106763, 2022, doi: 10.1016/J.COMPOSITESA.2021.106763.

[39] P. Mindermann and G. T. Gresser, “Adaptive winding pin and hooking capacity model for coreless filament winding,” Journal of Reinforced Plastics and Composites, vol. 42, no. 1–2, pp. 26–38, 2023, doi: 10.1177/07316844221094777.

[40] C. Duan, J. Huang, L. Wu, and X. Luo, “Fine modeling of reinforced thermoplastic filament winding container,” in 6th International Conference on Computer-Aided Design, Manufacturing, Modeling and Simulation (CDMMS 2018), 2018. doi: 10.1063/1.5039127.

[41] J. C. H. Wong, J. M. Blanco, and P. Ermanni, “Filament winding of aramid/PA6 commingled yarns with in situ consolidation,” Journal of Thermoplastic Composite Materials, vol. 31, no. 4, pp. 465–482, 2018, doi: 10.1177/0892705717706528.

[42] B. Deng, Y. Shi, T. Yu, and P. Zhao, “Influence mechanism and optimization analysis of technological parameters for the composite prepreg tape winding process,” Polymers, vol. 12, no. 8, 2020, doi: 10.3390/POLYM12081843.

[43] P. Mindermann et al., “Design of Fiber-Composite/Metal–Hybrid Structures Made by Multi-Stage Coreless Filament Winding,” Applied Sciences, vol. 12, no. 5, 2022, doi: 10.3390/app12052296.

[44] R. Gennaro, F. Montagna, A. Maffezzoli, F. Fracasso, and S. Fracasso, “On-line consolidation of commingled polypropylene/glass roving during filament winding,” Journal of Thermoplastic Composite Materials, vol. 24, no. 6, pp. 789–804, 2011, doi: 10.1177/0892705711401849.

[45] F. Lionetto, R. Dell’Anna, F. Montagna, and A. Maffezzoli, “Ultrasonic Assisted Consolidation of Commingled Thermoplastic/Glass Fiber Rovings,” Front Mater, vol. 2, no. 5 pp. 1–9, 2015, doi: 10.3389/fmats.2015.00032.

[46] R. Dell’Anna, F. Lionetto, F. Montagna, and A. Maffezzoli, “Lay-up and consolidation of a composite pipe by in situ ultrasonic welding of a thermoplastic matrix composite tape,” Materials, vol. 11, no. 5, 2018, doi: 10.3390/ma11050786.

[47] F. Lionetto, R. Dell’Anna, F. Montagna, and A. Maffezzoli, “Ultrasonic assisted consolidation of commingled thermoplastic/glass fiber rovings,” Front Mater, vol. 2, no. April, pp. 1–9, 2015, doi: 10.3389/fmats.2015.00032.

[48] P. Karbuz, M. Dogu, and B. Ozbek, “Manufacturing of hexagonal cross-section thermoplastic matrix composite parts with automatic filament winding system,” J Manuf Process, vol. 129, pp. 62–76, 2024, doi: 10.1016/j.jmapro.2024.08.051.

[49] H. Geng et al., “The Effects of Laser-Assisted Winding Process Parameters on the Tensile Properties of Carbon Fiber/Polyphenylene Sulfide Composites,” Materials, vol. 17, no. 18, 2024, doi: 10.3390/ma17184664.

[50] A. Vedernikov et al., “Effects of the Pre-Consolidated Materials Manufacturing Method on the Mechanical Properties of Pultruded Thermoplastic Composites,” Polymers, vol. 14, no. 11, 2022, doi: 10.3390/polym14112246.

[51] L. Ye, K. Friedrich, J. Kästel, and Y. W. Mai, “Consolidation of unidirectional CF/PEEK composites from commingled yarn prepreg,” Compos Sci Technol, vol. 54, no. 4, pp. 349–358, 1995, doi: 10.1016/0266-3538(95)00061-5.

[52] G. Xian et al., “Design, preparation and mechanical properties of novel glass fiber reinforced polypropylene bending bars,” Constr Build Mater, vol. 429, 2024, doi: 10.1016/j.conbuildmat.2024.136455.

[53] X. Chen, Y. Wang, M. Liu, S. Qu, Q. Zhang, and S. Chen, “Preparation and Process Parameter Optimization of Continuous Carbon Fiber-Reinforced Polycarbonate Prepreg Filament,” Polymers, vol. 15, no. 3, 2023, doi: 10.3390/polym15030607.

[54] Y. Mo, S. Ye, Z. Qaiser, and S. Johnson, “Structural and winding sequence optimization of coreless filament wound composite lattice structures,” International Journal of Advanced Manufacturing Technology, vol. 127, no. 9–10, pp. 4903–4914, 2023, doi: 10.1007/s00170-023-11761-y.

[55] T. V. Lisbôa, J. H. S. Almeida, I. H. Dalibor, A. Spickenheuer, R. J. Marczak, and S. C. Amico, “The role of winding pattern on filament wound composite cylinders under radial compression,” Polym Compos, vol. 41, no. 6, pp. 2446–2454, 2020, doi: 10.1002/pc.25548.

[56] R. Mishra, B. K. Behera, S. Mukherjee, M. Petru, and M. Muller, “Axial and radial compression behavior of composite rocket launcher developed by robotized filament winding: Simulation and experimental validation,” Polymers, vol. 13, no. 4, pp. 1–18, 2021, doi: 10.3390/polym13040517.

[57] M. A. Bezerra, R. E. Santelli, E. P. Oliveira, L. S. Villar, and L. A. Escaleira, “Response surface methodology (RSM) as a tool for optimization in analytical chemistry,” Talanta, vol. 76, no. 5, pp. 965–977, 2008, doi: 10.1016/j.talanta.2008.05.019.

[58] D. C. Baird, “Experiment Planning”, in An Introduction to Measurement Theory and Experiment Design. Prentice-Hall Inc., pp. 88–123, 1962.

[59] J. Antony, “Fundamentals of Design of Experiments,” in Design of Experiments for Engineers and Scientists, Elsevier, pp. 7–17, 2014, doi: 10.1016/b978-0-08-099417-8.00002-x.

[60] R. H. Myers, D. C. Montgomery, G. Geoffrey Vining, C. M. Borror, and S. M. Kowalski, “Response Surface Methodology: A Retrospective and Literature Survey,” Journal of Quality Technology, vol. 36, no.1, pp. 53–77, 2004, doi: 10.1080/00224065.2004.11980252.

[61] D. C. Montgomery, “Response Surface Methods and Designs” in Design and analysis of experiments. John Wiley & Sons, Inc., pp. 478-554, 2013.

[62] L. A. Sarabia and M. C. Ortiz, “Response Surface Methodology,” in Comprehensive Chemometrics, Elsevier, pp. 345–390, 2009, doi: https://doi.org/10.1016/B978-044452701-1.00083-1.

[63] D. Bas and I. H. Boyaci, “Modeling and optimization I: Usability of response surface methodology,” J Food Eng, vol. 78, no. 3, pp. 836–845, 2007, doi: 10.1016/j.jfoodeng.2005.11.024.

[64] M. A. Bezerra, R. E. Santelli, E. P. Oliveira, L. S. Villar, and L. A. Escaleira, “Response surface methodology (RSM) as a tool for optimization in analytical chemistry,” Talanta, vol. 76, no. 5, pp. 965–977, 2008, doi: 10.1016/j.talanta.2008.05.019.

[65] S. L. C. Ferreira, R. E. Bruns, H. S. Ferreira, G. D. Matos, J. M. David, G. C. Brandão, E. G. P. da Silva, L. A. Portugal, P. S. dos Reis, A. S. Souza, and W. N. L. dos Santos, "Box-Behnken design: An alternative for the optimization of analytical methods," *Analytica Chimica Acta*, vol. 597, pp. 179–186, 2007, doi: 10.1016/j.aca.2007.07.015.

[66] O. C. Zienkiewicz, R. L. Taylor, and J. Z. Zhu, “Problems in linear elasticity” in The Finite Element Method: Its Basis and Fundamentals, McGraw-Hill, pp.187-229, 2005.

[67] S. D. Müzel, E. P. Bonhin, N. M. Guimarães, and E. S. Guidi, “Application of the finite element method in the analysis of composite materials: A review,” Polymers, 2020, doi: 10.3390/POLYM12040818.

[68] N. Cummings, Z. Hashin. “Analysis of Composite Materials-A Survey,” J Appl Mech, vol. 50, pp. 481–505, 1983.

[69] A. Köllner, “Predicting buckling-driven delamination propagation in composite laminates: An analytical modeling approach,” Compos Struct, vol. 266, 2021, doi: 10.1016/j.compstruct.2021.113776.

[70] F. Islam, M. J. Donough, E. Oromiehie, A. W. Phillips, N. A. St John, and B. G. Prusty, “Data-driven optimization of additive composite manufacturing using automated fibre placement: A study on process parameters effects and interactions,” Compos Part A Appl Sci Manuf, vol. 190, 2025, doi: 10.1016/j.compositesa.2024.108599.

[71] S. Behseresht and Y. H. Park, “Additive Manufacturing of Composite Polymers: Thermomechanical FEA and Experimental Study,” Materials, vol. 17, no. 8, 2024, doi: 10.3390/ma17081912.

[72] ASTM, “ASTM:D792 − 20 Standard Test Methods for Density and Specific Gravity (Relative Density) of Plastics by Displacement,” ASTM International, 2020, doi: 10.1520/D0792-20.

[73] J. N. Hay and D. A. Luck, “The conformation of crystalline poly(phenylene sulfide),” Polymer, vol. 42, no. 19, pp. 8297–8301, 2001.

[74] J. E. Mark, “Polypropylene, isotactic” in Polymer Data Handbook. Oxford University Press, Inc., pp. 782, 1999.

[75] M. Mehdikhani, L. Gorbatikh, I. Verpoest, and S. V. Lomov, “Voids in fiber-reinforced polymer composites: A review on their formation, characteristics, and effects on mechanical performance,” J Compos Mater, vol. 53, no. 12, pp. 1579–1669, 2019, doi: 10.1177/0021998318772152.

[76] TS EN ISO 527-5, “Plastics - Determination of tensile properties - Part 5: Test conditions for unidirectional fibre-reinforced plastic composites,” 2007.

[77] ISO 14125:1998, “Fibre-reinforced plastic composites — Determination of flexural properties,” 1998.

[78] “DIN EN 2377:1989-10, Luft- und Raumfahrt; Glasfaserverstärkte Kunststoffe; Prüfverfahren zur Bestimmung der scheinbaren interlaminaren Scherfestigkeit; Deutsche Fassung EN_2377:1989,” DIN Media GmbH, 1989, doi: 10.31030/2341031.

[79] ISO 179-1:2023, “Plastics-Determination of Charpy impact properties-Part 1: Non-instrumented impact test,” 2023.

[80] J. P. Jog, N. Bulakh, and V. M. Nadkarni, “Crystallization of polyphenylene sulfide,” Bull. Mater. Sci., vol. 17, no. 6, pp. 1079-1089, 1994.

[81] H. Zheng, X. Zeng, J. Zhang, and H. Sun, “The Application of Carbon Fiber Composites in Cryotank,” in Solidification, InTech, pp.111-128, 2018. doi: 10.5772/intechopen.73127.

PUBLICATIONS FROM THE THESIS

Conference Papers

1. S. Orman, M. Doğu, and B. Özbek, "Process optimization of glass fiber reinforced PPS composites produced by automated fiber placement," *7th International Technical Textiles Congress*, oral presentation, İzmir, Turkey, 10-12 October 2018.

Papers

1. S. Orman, M. Doğu, and B. Özbek, "Optimization of the filament winding process for glass fiber-reinforced PPS and PP composites using Box-Behnken design," *Polymers*, vol. 16, no. 24, p. 3488, 2024, doi: 10.3390/polym16243488.